Université d'Ottawa · University of Ottawa

Université d'Ottawa · University of Ottawa

FACULTÉ DES ÉTUDES SUPÉRIEURES ET POSTDOCTORALES

FACULTY OF GRADUATE AND POSTDOCTORAL STUDIES

DUBIEN, Danielle

AUTEUR DE LA THÈSE - AUTHOR OF THESIS

M.Sc. (Chemistry)

GRADE - DEGREE

Department of Chemistry

FACULTÉ, ÉCOLE, DÉPARTEMENT - FACULTY, SCHOOL, DEPARTMENT

TITRE DE LA THÈSE - TITLE OF THE THESIS

Thermodynamics of Negative Sulfuric Acid and Nitric Acid Clusters by Electrospray Tandem Mass Spectrometry

P. Mayer

DIRECTEUR DE LA THÈSE - THESIS SUPERVISOR

EXAMINATEURS DE LA THÈSE - THESIS EXAMINERS

R. Burk

A. St-Amant

J.-M. De Koninck, Ph.D.

LE DOYEN DE LA FACULTÉ DES ÉTUDES SUPÉRIEURES ET POSTDOCTORALES

SIGNATURE

DEAN OF THE FACULTY OF GRADUATE AND POSTDOCTORAL STUDIES

THERMODYNAMICS OF NEGATIVE SULFURIC ACID AND NITRIC ACID CLUSTERS BY ELECTROSPRAY TANDEM MASS SPECTROMETRY

Danielle Dubien

Thesis submitted to the
School of Graduate Studies and Research
University of Ottawa
In partial fulfillment of the requirements for the
M.Sc. degree in the

Ottawa-Carleton Chemistry Institute

Thèse soumise à
L'École des études supérieures et de la recherche
Université d'Ottawa
En vue de l'obtention de la maîtrise ès sciences à

L'Institut de chimie d'Ottawa-Carleton

July 2003

Candidate	Supervisor
Danielle Dubien	Paul M. Mayer

Your file Votre référence
ISBN: 0-612-90062-2
Our file Notre référence
ISBN: 0-612-90062-2

Abstract

Electrospray-ionization tandem mass spectrometry was used to determine the binding energy of $HSO_4^-(H_2SO_4)_n$ ions for n up to 4 and $NO_3^-(HNO_3)_n$ ions for n up to 3. The binding energies obtained experimentally are substantially lower than those in the literature except for the values for $NO_3^-(HNO_3)$ and $HSO_4^-(H_2SO_4)$.

The geometries of $HSO_4^-(H_2SO_4)_n$ and $NO_3^-(HNO_3)_n$ for n up to 3 were optimized using the following levels of theory: AM1, HF/3-21G, HF/6-31+G(d) B3LYP/6-31+G(d), and B3LYP/6-311+G(d,p). The values calculated at B3LYP/6-311+G(d,p) are in fair agreement with those in the literature. For the same order of clustering, sulfuric acid clusters are bound more strongly than the nitric acid analogues. Neutral acid molecules form clusters with core ions via hydrogen bonds. As the number of neutrals increases, the binding energy decreases.

Acknowledgments

I would like to thank my supervisor, Paul Mayer for his advice and immense support. Thanks for your infinite patience and for the opportunities you provided me over the course of this program. I would also like to thank John Holmes for his informative discussions. Thank you to Sander Mommers and Clem Kazakoff for their help with the electrospray.

To all the girls in the lab (Janeen Auld, Marie-Soleil Giguère, Julie McCormack, Emma Rennie, Xian Wang) and Clem for your constant support and for the good times. To everyone in the lab, I wish you all the best.

To my friends and family, thank you for your love and support throughout the past two years.

Table of Contents

List of Figures

List of Tables

List of Abbreviations

AC	Alternating current
AM1	Austin Model 1
B3-LYP	Becke-Lee, Yang and Parr
BE	Binding energy
DC	Direct current
DFT	Density functional theory
DMS	Dimethyl sulfide
DMSO	Dimethyl sulfoxide
$DMSO_2$	Dimethyl sulfone
ESI	Electrospray ionisation
FAB	Fast-atom bombardment
COS	Carbonyl sulfide
CID	Collision-induced dissociation
c-o-m	Center-of-mass
HF	Hartree-Fock
MS	Mass spectrometry
MSA	Methyl sulphonic acid
NDDO	Neglect of diatomic differential overlap
PEPICO	Photoelectron photoion coincidence
PES	Potential energy surface
RF	Radio frequency
SCF	Self-consistent field

STO-3G	Slater type orbital and that 3 Gaussian functions were used for each orbital.
TIC	Total ion current
VWN	Vosko, Wilk and Nusair
ZPC	Zero-point-correction

Chapter 1: Introduction

1.1 Occurrance and formation of H_2SO_4 and HNO_3 clusters in the atmosphere

For the past twenty years or more there has been an increased interest in studying the atmospheric chemistry of nitric and sulfuric acids. The reason is that the serious environmental problems caused by compounds containing nitrogen and sulfur have come to the attention of scientists. Acid rain and ozone depletion catalyzed by polar stratospheric clouds (PSCs) are cases in point. Acid rain and PSCs are partly the result of the clustering of gas phase molecules. Water, sulfuric and nitric acid and their derivatives form clusters, occasionally with the help of microscopic particles. These clusters accumulate more water and other molecules until droplets and/or crystals are formed.

An understanding of the role of HNO_3 and H_2SO_4 in environmental chemistry requires an explanation of atmospheric composition. Figure 1.1[1] illustrates the various layers above the earth's surface.[2] Called the thermosphere, stratosphere, mesosphere and the troposphere, these layers are separated by thinner layers which mark the beginning of a change in temperature gradient. For example, the troposphere is characterized by a decrease in temperature with altitude. In the next layer above, the stratosphere, the temperature increases with altitude. At the temperature gradient transition the layers are separated by the tropopause.

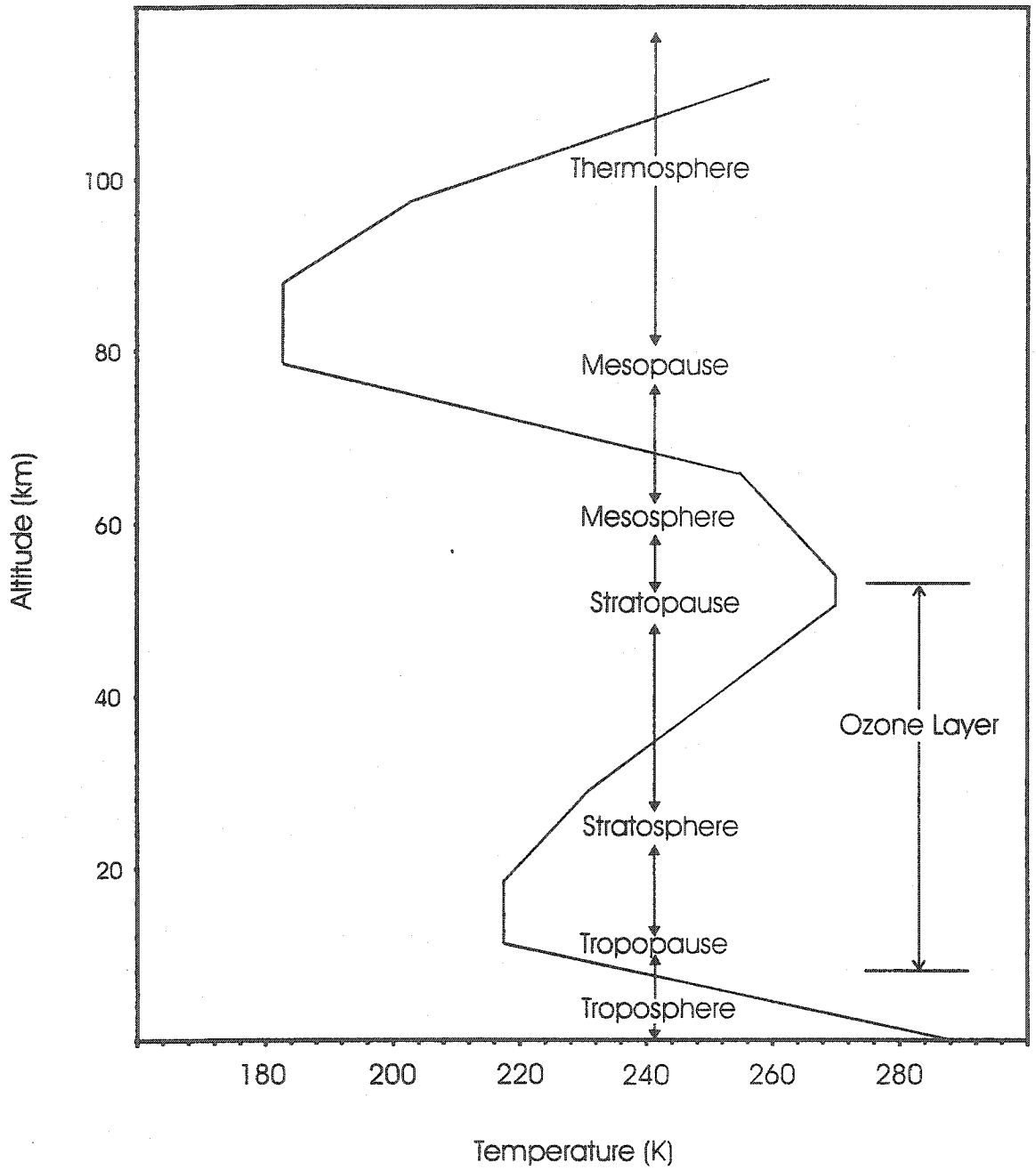

Figure 1.1. Vertical profile of the temperature between the surface of the Earth and 100 km in altitude. This diagram is based on one created by Brasseur et al. [ref. 1]

Atmospheric chemistry is in great part driven by ionization. In the upper atmosphere (the thermosphere), the ionization source is solar and stellar UV and X-Ray radiation. In the lower atmosphere (mesosphere, stratosphere, and troposphere), it is radioactive rocks, galactic cosmic rays and lightning which act as a source of ionization. This ionization begins a chain of reactions starting with the most abundant gases in the atmosphere, nitrogen and oxygen. N_2^+ and O_2^+ are formed and in turn react with other molecules in the atmosphere. The details of a selection of these reactions are shown in Figure 1.2. In Figure 1.2[3] the cluster ion $NO_3^-(H_2O)_n$ is shown as one of the final products. HNO_3 reacts with it, displacing the water molecule and forming $NO_3^-(HNO_3)_n$. This cluster then reacts with sulfuric acid, which replaces the nitrate core ion, giving $HSO_4^-(HNO_3)_n$.[4] H_2SO_4 frequently replaces NO_3^- and H_2O in negative-ion clusters. This was interpreted as a strong affinity of H_2SO_4 for negative charge centers and as a tendency of this acid to undergo displacement reactions with clustered negative ions. In areas of higher concentration of sulfuric acid there is formation of $HSO_4^-(H_2SO_4)_l(HNO_3)_n$, and ultimately of $HSO_4^-(H_2SO_4)_n$.[4] The final products (clusters around nitrate and sulfate ions) are logical since these are highly stable products and because there is a high abundance of nitric and sulfuric acid in the atmosphere.

Analysis of the negative-ion composition of the atmosphere has revealed that two ion families predominate in the stratosphere: $NO_3^-(HNO_3)_n$ and $HSO_4^-(H_2SO_4)_l(HNO_3)_m$.[5,6] In the troposphere $NO_3^-(HNO_3)_n$ and $NO_3^-(HNO_3)(H_2O)$ constitute the majority of the ions. In fact, the most abundant cluster ions at these two levels have

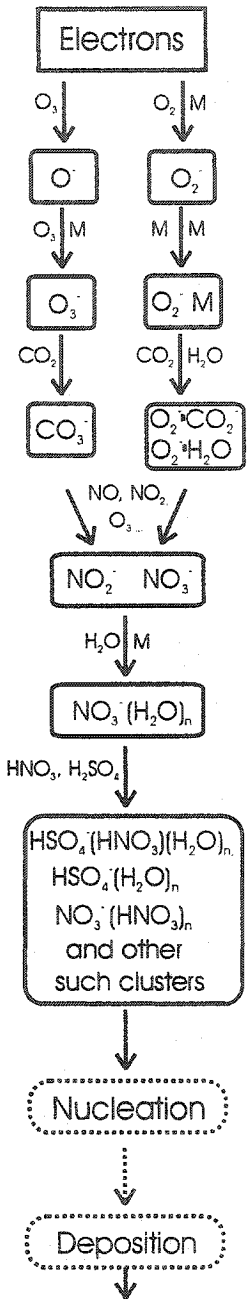

Figure 1.2. Reactions occurring in the atmosphere. This diagram is based on one published by Smith and Spanel. [ref. 3]

NO_3^- and HSO_4^- at their core.[7] CO_3^--core ions are also abundant in the troposphere.

Detailed breakdowns of the abundance of the $NO_3^-(HNO_3)_n$ and $HSO_4^-(H_2SO_4)_n$ species have been produced either as a result of direct measurement (29-40 km)[4,5] or as a calculated model of the region (0- 15 km).[7] The general trend is that nitrate-core ions dominate up to ca. 33 km, with nearly 100% abundance. At this point, the high sulfuric acid vapor concentration (due to the lower temperature) affects the distribution of negative ions such that sulfate-core ions dominate. Within the $NO_3^-(HNO_3)_n$ family, it is n=2 that is most abundant for all heights up to 38 km. In the $HSO_4^-(H_2SO_4)_n$ group, sulfate is by far the most abundant ion until an altitude of 33 km is reached. Above this height, the higher-order clusters increase in abundance, and n=3 dominates.[5]

1.2 Reactions of Sulfur and Nitrogen Compounds in the atmosphere

The chemistry of sulphur in the atmosphere is not fully defined. Anthropogenic and biogenic sources inject sulphur compounds into the atmosphere and various reactions occur. When studying atmospheric clusters, it simplifies the situation to focus on sulphuric acid, for this is the single most important gas phase precursor to particle nucleation and growth. Eisele and McMurry[2] propose the following reactions. Sulphuric acid can be formed from the oxidation of SO_2 by OH radicals and subsequent reactions with oxygen and water. The production rate of sulfuric acid in this series of reactions is easily predicted. A more poorly understood reaction is the oxidation of dimethyl sulfide (DMS). This compound is significant for it is released by the oceans into the atmosphere

in great quantities. The oxidation of DMS by OH radicals is known to give sulfuric acid, methane sulphonic acid (MSA), dimethyl sulphoxide (DMSO), $DMSO_2$ and other products, all at unknown rates and yields. These reactions are shown in Figure 1.3 for a marine atmosphere.

Richard Wayne[8] also described reactions which lead to the formation of sulphuric acid. Briefly, carbonyl sulfide (COS), H_2S, CS_2, CH_3SH, DMS and CH_3SSCH_3 are oxidized by OH radicals. The products, in turn, are oxidized by O_2 until SO_2 is obtained. SO_2 then follows an unknown path to conversion to H_2SO_4. Wayne suggested that SO_2 reacts with a hydroxyl radical:

$$SO_2 + OH + M \rightarrow HSO_3 + M \qquad (1.1)$$

Daniel Jacob[9] also provided that reaction, as well as these:

$$HSO_3 + O_2 \rightarrow SO_3 + HO_2 \qquad (1.2)$$

$$SO_3 + H_2O + M \rightarrow H_2SO_4 + M \qquad (1.3)$$

where M is a third body (O_2 or N_2) which carries away excess kinetic energy.

One source of HNO_3 is indirectly through a positive ion-negative ion combination as in these examples:

$$H^+(H_2O) + NO_3^-(HNO_3)_m \rightarrow (m+1)(HNO_3) + n(H_2O) \qquad (1.4)$$

where m=0 to 3, and

$$H^+(H_2O) + HSO_4^-(HNO_3)_k \rightarrow k(HNO_3) + n(H_2O) + H_2SO_4 \qquad (1.5)$$

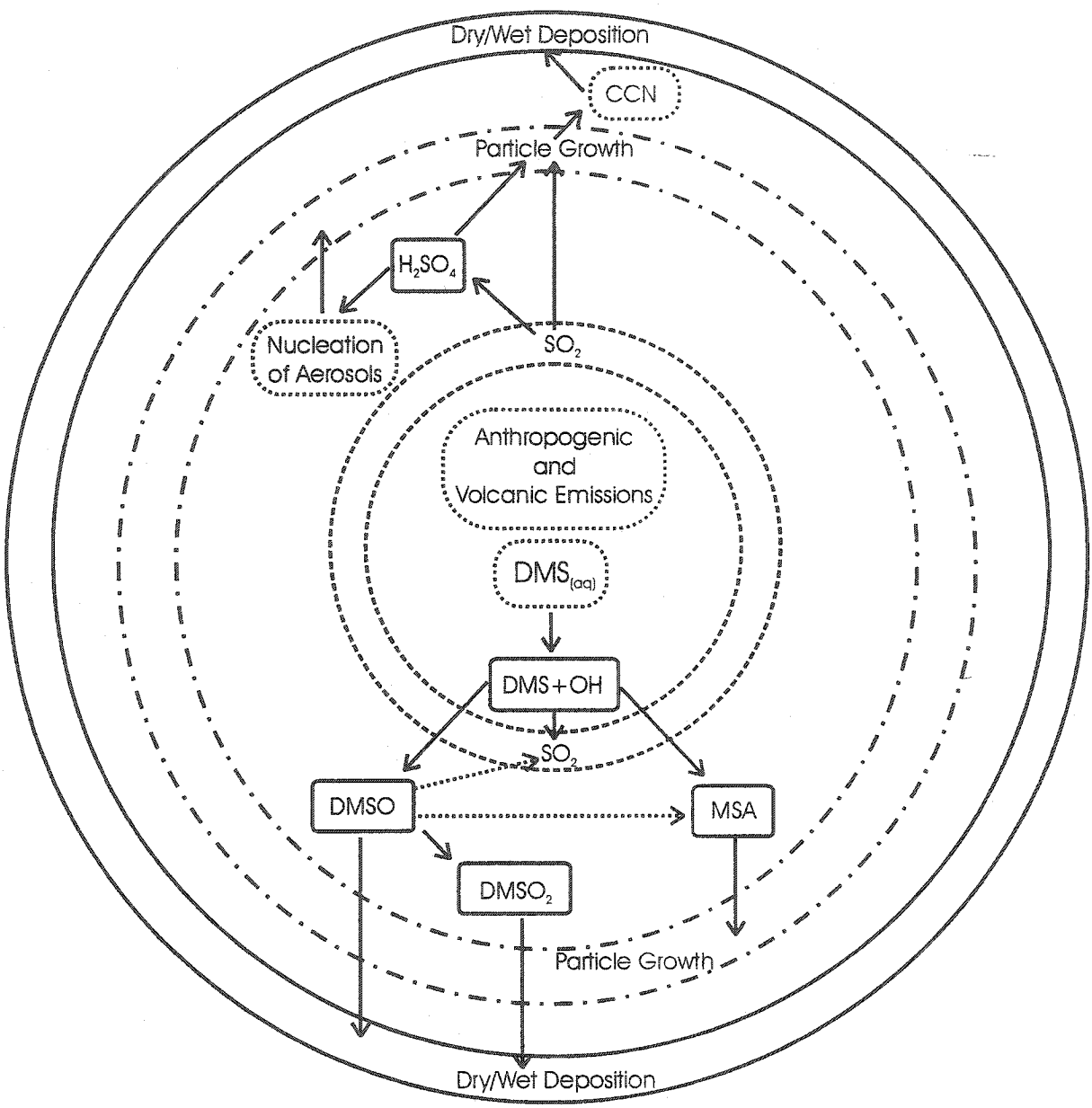

Figure1.3. Tropospheric reactions involving sulfur in the remote marine atmosphere

The formation of HNO_3 based on these reactions depends on the clustering reaction rate of negative ions with HNO_3 versus ion-ion recombination (its rate, in turn, is a function of pressure) and it is a function of the surrounding ion density. Some may suggest that OH will react with different species to form HNO_3, but Aikin showed that this is highly unlikely.[10]

In daylight, nitrogen oxide radicals NO and NO_2 (NOx) are oxidized to form HNO_3

$$NO + O_3 \rightarrow NO_2 + O_2 \quad (1.6)$$

$$NO_2 + OH + M \rightarrow HNO_3 + M \quad (1.7)$$

At night, HNO_3 is formed via this mechanism:

$$NO_2 + O_3 \rightarrow NO_3 + O_2 \quad (1.8)$$

$$NO_3 + NO_2 + M \rightarrow N_2O_5 + M \quad (1.9)$$

$$N_2O_5 + H_2O \xrightarrow{aerosol} 2HNO_3 \quad (1.10)$$

Nitric acid is very stable in the face of photochemical destruction. As a result, it will remain in the atmosphere for weeks before being reconverted back into NO_x or before it travels to the troposphere. It is then deposited from the atmosphere in the form of wet or dry precipitation. This loss is the main sink of NO_y. NO_y is the ensemble of NO_x and its reservoirs (NO, NO_2, NO_3, HNO_3, HNO_4, N_2O_5, $ClONO_2$, peroxyacetyl nitrate (PAN), and organic and inorganic nitrates.)

1.3 Brief review of thermodynamic studies of cluster ions

1.3.1 van't Hoff Method

The binding energies of cluster ions can be determined by the van't Hoff method which involves the use of a mass spectrometer in which ions achieve equilibrium in a high-pressure ion source. This occurs on the μs time-scale. An example of a reaction is given below:

$$(A)_n^- + A \Leftrightarrow (A)_{n+1}^- \qquad (1.11)$$

The pressure is controlled such that A_n^- and A_{n+1}^- are the principal species. The equilibrium constant is:

$$K = \frac{[A_{n+1}^-]}{[A_n^-][A]} \qquad (1.12)$$

The pressure of the neutral molecule [A] is known and the ratio of the ion concentrations in this equation is given by the relative peak heights in the mass spectrum. The equilibrium constant is determined at several temperatures. The van't Hoff relationship relates these two values:

$$\frac{d\ln K}{d(1/T)} = -\frac{\Delta H^\circ}{R} \qquad (1.13)$$

and allows the determination of the enthalpy of reaction, ΔH°.

1.3.2 Kinetic Method

In this method, an electrostatically bound pair is formed in the ion source of a mass spectrometer and the competitive dissociation into two monomers is monitored. An example is shown below for the dissociation of ion complex A_2B^-:

$$A_2^- + B \xleftarrow{k_1} A_2B^- \xrightarrow{k_2} AB^- + A \tag{1.14}$$

A mass spectrum is produced, in which the intensities of A_2^- and AB^- are measured. The statistical thermodynamics version of transition-state theory for the above reactions are:

$$\ln k_1 = \ln\left(\frac{Q_1^{\ddagger}}{Q}\right) - \frac{E_1^{\circ}}{RT} \tag{1.15}$$

and

$$\ln k_2 = \ln\left(\frac{Q_2^{\ddagger}}{Q}\right) - \frac{E_2^{\circ}}{RT} \tag{1.16}$$

Assuming that the peak height of A_2^- reflects k_1 and that AB^- reflects k_2, and subtracting equation 1.16 from 1.15, we have

$$\ln\left(\frac{[AB^-]}{[A_2^-]}\right) = \ln\left(\frac{Q_1^{\ddagger}}{Q_2^{\ddagger}}\right) - \frac{\Delta E^{\circ}}{RT} \tag{1.17}$$

As such, the ratio of partition functions is dependent on the relative entropies of activation of the reactant ion and transition state leading to products. In most cases, this ratio is taken as 1 and the $\ln(Q^{\ddagger}/Q^{\ddagger})$ term assumed to be zero. In addition, the difference in activation energies of the two channels is taken to reflect the difference in enthalpy of the two affinity reactions in question (for example, see Figure 1.4)

For this method to be used properly, there must be no additional decomposition channels and no reverse activation barriers. An example of a reaction involving these

barriers is shown in Figure 1.5. There is no way of knowing that these barriers exist unless an accurate equilibrium constant can be used as a reference. In addition, the products obtained in each channel must be sufficiently similar that entropic effects are negligible. Thus, there is difficulty in making proper conclusions from experiments involving doubly-bonded or chelating compounds.

1.3.3 CID Threshold Measurements

In this method, molecules are ionized and undergo collision-induced dissociation in a mass spectrometer. The CID process excites the precursor ion, elevating its Boltzmann-internal energy distribution to a high energy level. This level is at such a height that the higher-energy tail of the distribution crosses the dissociation limit. The ions in energy states below the limit remain stable. Thus, the CID threshold method measures the minimum energy required for the dissociation of an ion into fragments (Figure 1.6).

The ion intensities from the mass spectra undergo mathematical treatment[11] for conversion into cross-sections, which represent the probability of reaction. The cross-section is plotted as a function of center-of-mass collision energy (E_{cm}) (Figure 1.7). The threshold (E_o) is determined as the part of the function where the cross-section attains a value above zero. This value is then converted into a bond dissociation energy (BDE) using the following formula:

$$E_o = D_o(A_{n-1}B+ - A) \qquad (1.18)$$

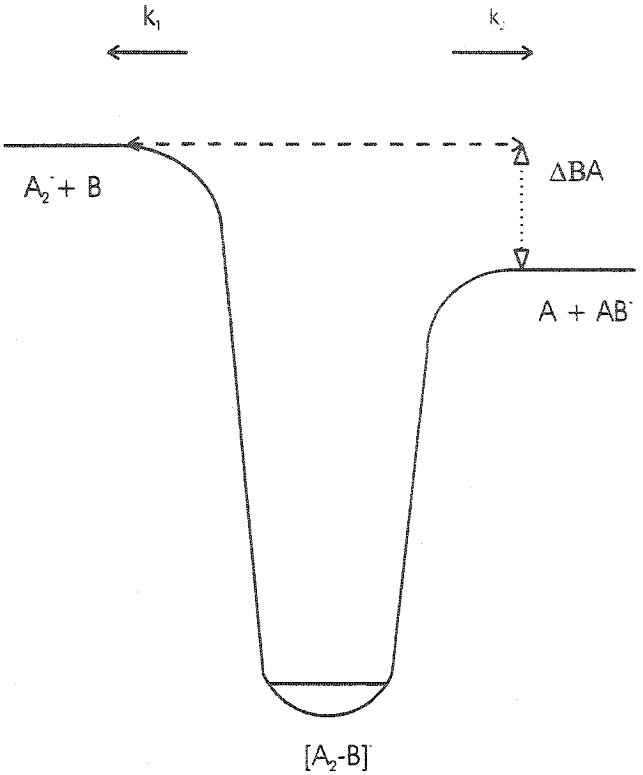

Figure 1.4. Potential energy well for a system whose binding affinity (BA) can be properly measured by the kinetic method

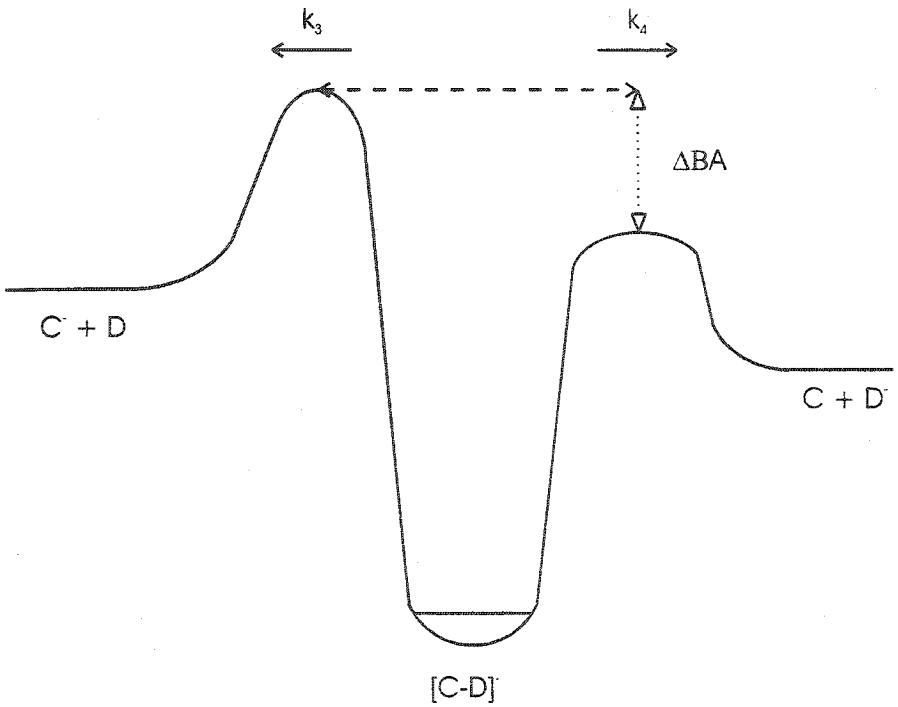

Figure 1.5. Potential energy well for a system whose BA can not be properly measured by the kinetic method

Where D_o is the BDE of the species in question, A_{n-1} B^+ is the cluster, and A is a fragment. This formula applies to clusters where there is no reverse activation barrier, meaning that there is no activation energy in excess of the reaction's endothermicity.[12] Since the dissociation of the acid cluster ions presented in this thesis are all simple-bond cleavage reactions it is expected that there will be no reverse energy barrier.

The accuracy of the results in this type of experiment require certain conditions. The collision energies must be well-defined. An octapole produces an RF field which is less perturbing to the kinetic energy distribution of the ions than the collision cell in a triple quadrupole. The internal energy distribution of the ions must be known. The collision gas must transfer its kinetic energy to the ion in question in the form of internal energy in the most efficient way possible. Xenon fills this role well since, being monoatomic, it does not carry away energy in internal modes. Its large mass also results in long reaction times.[13] Cross-sections must be obtained from single-collision conditions. An ion undergoing two collisions would seem to have dissociated at half its true thermodynamic threshold. The lifetime of the ion must also be shorter than the travel time through the collision area. Otherwise the threshold for the reaction shifts to higher translational energies; a "kinetic shift" occurs. These and other problems are discussed in great detail elsewhere.[12,13]

One advantage of the CID threshold method is that it only requires the observation of the behaviour of one molecule. This is in contrast to the crossover point method where two ions must be considered, as will be seen in the next section.

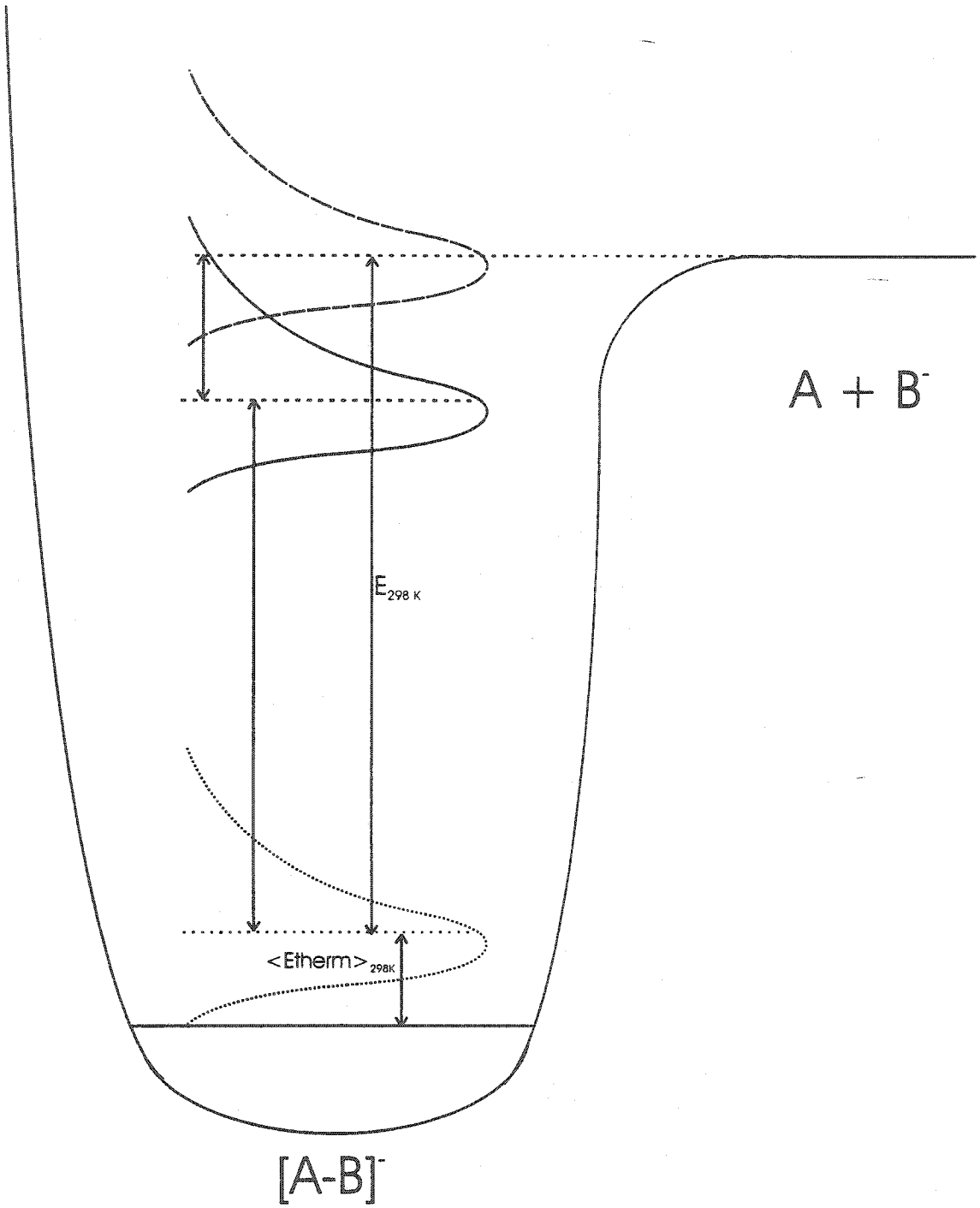

Figure 1.6. Boltzmann distribution of ground-state and excited precursor ions at 298 K. The dotted distribution represents the ground state of the precursor. The distribution drawn in a solid line has a tail that crosses the appearance energy measured by Threshold CID. The distribution drawn in a dashed line has an average energy which is determined by measuring the crossover energy.

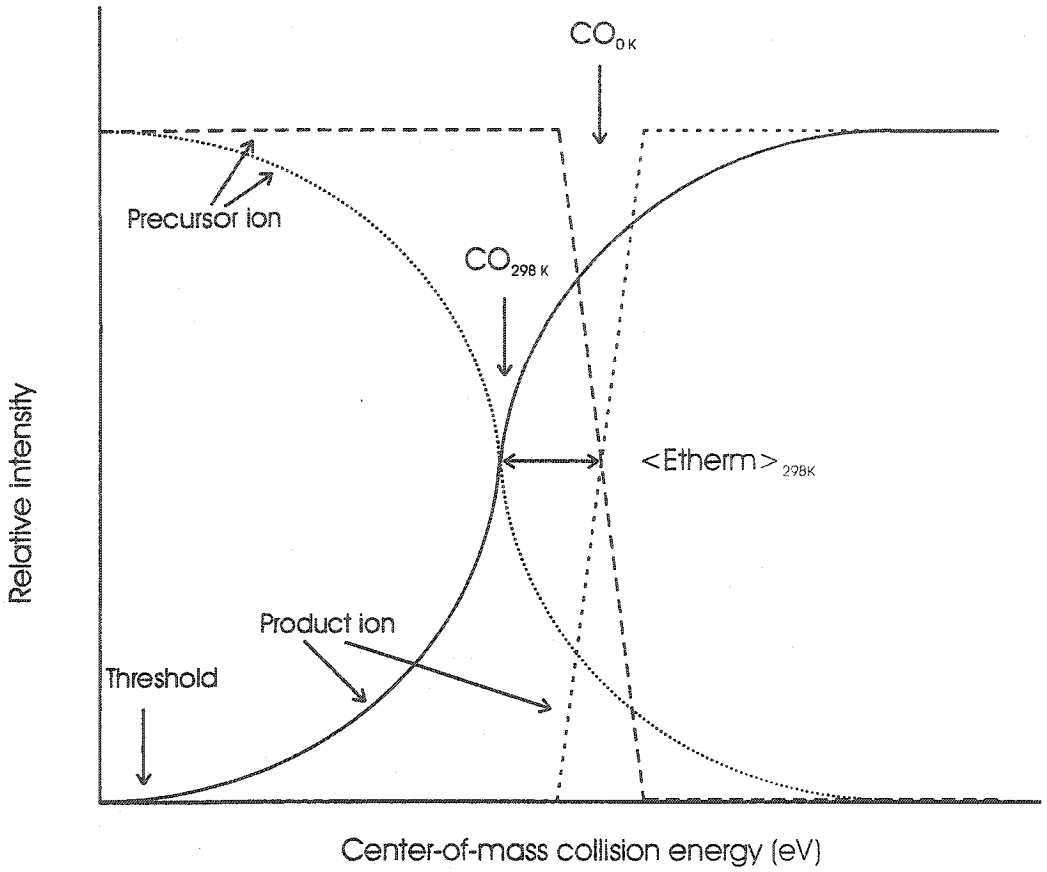

Figure 1.7. Breakdown diagram. At 0 K, the dissociation of a precursor is represented by a step funct At room temperature, the precursor has a Boltzmann distribution of internal energies. The precursors at higher energies require less collision energy to dissociate than those at lower energies. The crossover energy at 298 K corresponds to the average of the Boltzmann energy distribution.

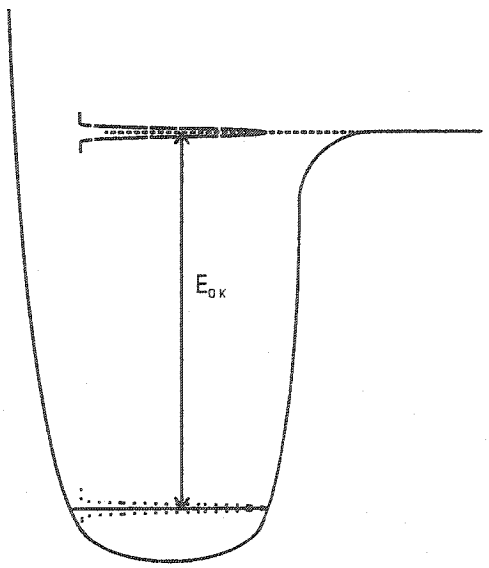

Figure 1.8. Boltzmann distribution of ground-state and excited precursor ions at 0 K. The average of these distributions is equal to their "50 % mark"

1.4 Crossover Energy Using ESI-MS/MS

The crossover-energy method is very similar to the CID threshold method. As above, an ion undergoes collision-induced excitation in a mass spectrometer. However, in this method, the excitation is greater, bringing the distribution higher in energy. The average energy of the excited Boltzmann distribution is determined.

In this study, breakdown graphs are used to determine the appearance energy of fragment ions. To create a breakdown graph, the intensities of the precursor and fragment ions are measured from mass spectra produced as mentioned earlier. The fragmentation occurs over a range of known centre-of-mass (c-o-m) energies. The relative intensities of the two ions are plotted against c-o-m energy.

Such a graph shows the decrease in intensity of a precursor ion with energy, and simultaneously, an increase in intensity of fragment ions (Figure 1.7). The point at which they cross gives the appearance energy of the fragment. This corresponds to the average appearance energy of the fragment ion at the experimental temperature, taken as 298 K.

In the simplest case, where the temperature is 0 K, the energy distribution of the precursor ion is small and symmetrical. The distribution would be excited to a level where its average energy is equal to the dissociation energy. Being at 0 K, the average and the mid-point of the distribution are the same. A breakdown diagram would show 100% abundance of the precursor ion (Figure 1.8). There is a small range of energies at

which both fragment and precursor ions are present, which reflects the extent of the energy distributions. Beyond this range, the fragment ion has 100% abundance. This is a step-function, and it would give the bond-dissociation energy directly at 0K.

In practice, it is difficult to obtain such a cold temperature. As a result, the functions representing the precursor and fragment ions are continuously decreasing and increasing, respectively. The functions reflect the distribution of internal energies corresponding to the experimental temperature.[14] The continuity in these functions results in an underestimation of the precursor's abundance (and an overestimation of the fragment ions' abundance). The difference between the 298 K and 0 K cross over energies is just the average thermal energy of the ion at 298 K (Figures 1.6 and 1.7)

One of the best methods for obtaining breakdown graphs is photoelectron photoion coincidence (PEPICO) spectroscopy. In this method, molecules are subject to UV ionization. The electron travels in the direction opposite that of the ion, carrying a known translational energy (KE_e). Using the formula:

$$E_{M+} = h\nu - IE_M - KE_e, \qquad (1.19)$$

one may determine very accurately the energy of the ion (E_{M+}) formed coincidentally with the electron. A molecule that is ionized at its ionization energy (IE_M) emits an electron with no kinetic energy and becomes an ion in its ground state. Higher energy light increases the internal energy of the ion. By measuring the relative abundance of precursor and fragment ions, a breakdown graph can be plotted.[15] It is assumed in this type of photoionization experiment that the fragment ions are formed in conjunction with

zero kinetic energy electrons.[16] The advantage of using PEPICO for this type of analysis is that the internal energies of the ions are known precisely and can be varied over a continuum of values. In our experiments, a single-collision event is used in place of the photon in PEPICO.

One factor which can affect the accuracy of the measurement is the timescale of the experiment. For fragment ions to be observed, a sufficient number of precursor ions must disociate in the time given them prior to mass analysis (kinetic shift). Thus, the internal energy content of the precursor ion must be high enough for the dissociation to have a rate constant that is sufficiently large for observation. In our experiment, the precursor ions spend on the order of 1 ms in the central, collision hexapole (1.44 ms for m/z 200 at lab frame kinetic energy of 5 eV). So, as long as the rate constant is greater than $10^3 s^{-1}$, observations will be made. This means that kinetic shift will not be a problem.

1.5 Goal

The aim of this project was to determine the bond-dissociation energies of nitric and sulfuric acid clusters using the crossover energy method for these reactions:

$$NO_3^-(HNO_3)_n \rightarrow NO_3^-(HNO_3)_{n-1} + HNO_3 \qquad (1.20)$$

$$HSO_4^-(H_2SO_4)_n \rightarrow HSO_4^-(H_2SO_4)_n + H_2SO_4 \qquad (1.21)$$

The energies obtained were compared to those obtained by other groups. Experimentation was carried out on a Quattro LC tandem quadrupole analyzer fitted with an electrospray ionization source. Optimization and frequency calculations were done on HSO_4^-, H_2SO_4, NO_3^-, HNO_3, $HSO_4^-(H_2SO_4)$, $NO_3^-(HNO_3)$, $HSO_4^-(H_2SO_4)_2$, and $NO_3^-(HNO_3)_2$, $NO_3^-(HNO_3)_3$ using the following methods: AM1, HF/3-21G, HF/6-31+G(d), B3-LYP/6-31+G(d), and B3-LYP/6-311+G(d,p).

Chapter 2: Experimental Procedures and Techniques

2.1 Experimental Techniques

2.1.1 Electrospray ionization

Electrospray ionization (ESI) involves forming a charged species in solution and then desolvating the ion into the gas phase. Thus, unlike most other MS ionization methods such as electron impact ionisation, chemical ionisation and field ionisation, the formation of an ion is determined by solution chemistry. In ESI a solution of the sample is pumped through a stainless steel capillary needle at atmospheric pressure. The needle is maintained at two to four kilovolts with respect to a cylindrical electrode that surrounds the needle. In this manner, an electric field is created around the capillary.

The positive field causes an accumulation of positive charges at the tip of the capillary. These charges are drawn down the potential gradient in the form of a "Taylor cone". The analyte then undergoes desorption (Figure 2.1).

The Ion Evaporation theory of ESI stipulates that the ion desorption process depends on the balance of lifting forces (repulsion between charged molecules and the charged surface of the droplet) and solvation forces (attractive forces, surface tension, and van der Waals forces). Lifting forces must be greater than solvation forces for an ion to desorb from the droplet surface, and therefore the ability of an ion to escape the droplet

is increased by its ability to carry a charge (i.e. the strength of interaction with the cation) and decreased by the solvation forces.[17]

Simply put, the energy of the field must be greater than the solvation energy of the molecule in solution to nebulize and charge the liquid. This occurs in practice when a sufficiently high field causes droplets to break off of the tip of the cone one at a time in "buds". At this moment, the electrostatic energy has surpassed the surface tension.

Once the liquid is transformed into a charged spray of fine droplets it passes through a desolvating zone where evaporation of the solvent occurs. The aerosol is desolvated by a combination of heat, gas flow and vacuum pumping. Evaporation reduces the size of the droplets, increasing the charge density on the solute. Eventually, fission, termed Coulomb explosion, occurs at the Rayleigh limit (Figure 2.2). At this point, the charge on the ion is so great that the associated electrostatic energy surpasses the surface tension of the droplet. The result is separation into finer droplets. Continued separation in this manner leads to the production of many droplets, each containing a single ion.

In the first stages of the ion source-to-vacuum interface, a beam of sample-related ions is accelerated across a potential created relative to the sampling cone. This potential differential sends the ions into the mass spectrometer. The potential applied to the cone can be varied over the range of 1 to 200 V, and it deposits internal energy onto the

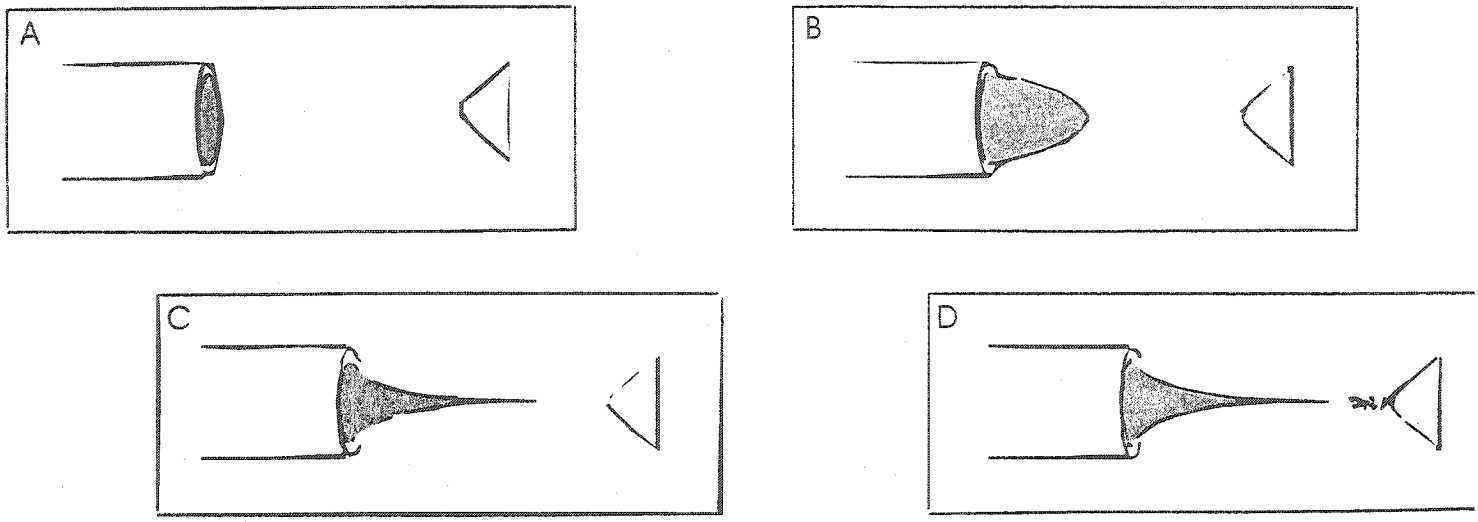

Figure 2.1. The Electrospray Ionization process. The sample solution in the metal capillary of the ion source *(A)* is unaffected in the absence of a potential difference (B). Then, the capillary is held at a potential of 3.5 kV with respect to the entrance to the analyzer. Consequently, charges concentrate and are attracted to the entrance. Maintenance of the potential difference (C) causes the formation of a Taylor Cone, where increasingly charged droplets advance toward the entry slit. Eventually, ions experience Coulombic explosion and a budding process occurs, where drops each containing one ion are formed (D).

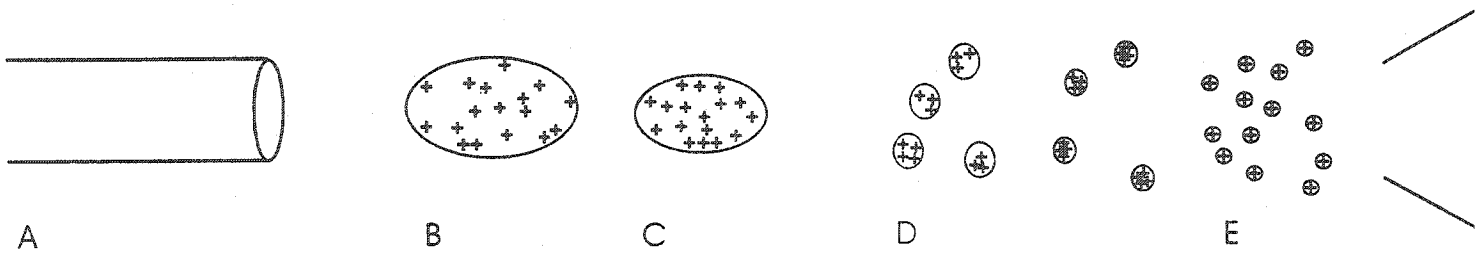

Figure 2.2. Coulombic explosion. From the tip of a Taylor cone (A) a charged droplet (B) emerges. As it desolvates, its charge density increases (C). Eventually, Coulombic repulsion overcomes the surface tension of the solvent, and there is the formation of smaller charged droplets (D). The process repeats, and eventually, droplets are formed which contain single ions (E).

analyte. For small molecules, the cone voltage need only to go up to 30 V. On the other hand, polymers require a greater cone voltage (up to 150 V) to be guided along the path into the MS. In each case, sample ions can undergo collisions with the solvent and/or drying gas prior to passing into the MS. This phenomenon is referred to as "skimmer-cone collision-induced dissociation" and can result in the fragmentation of molecular ions into fragment ions.

The Micromass Quattro-LC uses the Z-Spray ^{TM} ESI source. In this variation, cone voltage is used to control the entry of analytes into the mass analyzer. As the molecules make their way from the capillary to the first skimmer, their path is curved. As the cone voltage increases, the path of the heavier ions is curved increasingly toward the skimmer, at the expense of the lighter ones, and vice versa at lower cone voltages.

As the ion travels through the first skimmer, or sample cone, it enters a chamber maintained at lower-than-atmospheric pressure. Then its path is curved towards a second skimmer, or extraction cone, into an area that is further evacuated. This trajectory is in the form of the letter z. Such an assembly, with two pressure differentials, is very efficient at clearing a path for the ions.

Before the advent of the z-conformation ESI, the ion path was linear and there was only one pressure differential. As a result, large vacuum pumps were necessary for lowering the pressure in the instrument. To minimize the amount of solvent molecules entering the analyser, the skimmer opening had to be small. This meant that the capillary

delivering the sample had to be aligned very accurately with the skimmer slit. Also, because the capillary faced the skimmer, the bulk of the flow accumulated on the skimmer causing frequent blockages. The modern conformation avoids these problems greatly: the pumps are smaller, the skimmer openings are larger, the capillary need not be placed with extreme position near the skimmer, and the bulk of the flow is sprayed on to a metal plate facing the capillary.

2.1.2 Quadrupole Mass Spectrometry

The MS analyzer used in this research is a quadrupole mass filter. This is the most common type of analyzer, popular because of its fast scanning capability, linear mass scale, programmability, compactness, ruggedness and low cost. In this instrument, ions travel along an axis parallel to four rods, made of molybdenum. The rods are ideally hyperbolically shaped. However, cylindrical rods are easier to manufacture and provide approximately the same results when the radius of the individual rods r is related to the distance between the rods $2r_o$, by $r = 1.16\ r_o$.

Two opposing rods are connected to the positive side of a variable DC source. The other two are attached to the negative terminal. The four rods are also connected to a variable radio-frequency AC source in a similar manner. The rf voltage of the two pairs of rods are 180 degrees out of phase. The RF and DC voltages (represented by $V\cos \omega t$ and U, respectively) form a potential field ϕ that acts on the ions passing through. The relation is shown by

$$\phi = U + V \cos \omega t \qquad (2.1)$$

ω is the angular frequency measured in rad/s and is 2π times the frequency in Hertz ($\omega = 2\pi f$)

This equation demonstrates that the total field oscillates periodically with time. Also, the field distribution is symmetric with respect to the axis of an ion beam. By altering the potential field, ions of a certain mass-to-charge ratio (m/z) can be selected for detection. As the total field increases, ions of higher masses are transmitted. The ions of improper mass are deflected away from the axis. These unwanted ions will be neutralized by one of the poles and carried away. By plotting a graph of U vs. V showing the values where a molecule of mass m is stable in the total field (giving a stability diagram for that molecule) and superimposing stability graphs for many molecules, it is shown that there are great regions of overlap, and small regions where only one molecule has a stable trajectory (Figure 2.3). In these small areas, U:V is approximately 1:6. To draw a line from the origin through the graph gives an operating line. Only ions above the operating line are transmitted to the detector. Masses are selected by varying the total field while maintaining the U:V ratio at 1:6. When the line has a slope of ~ 1/6, the ions each appear as an individual peak. Thus, resolution of the analyzer is high. However, high resolution comes at the expense of sensitivity; the peaks can be well distinguished, but the abundance of the corresponding ions is fairly low.

2.1.3 Tandem Mass Spectrometry

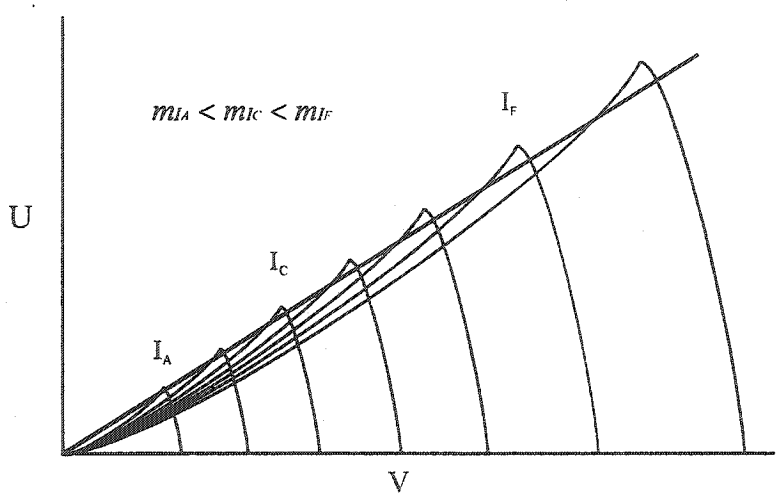

Figure 2.3. Superimposed stability diagram for ions (I) of masses m_{In}.

Quadrupole instruments can be used for tandem mass spectrometric analyses (Figure 2.4). As the sample goes through the first quadrupole, a single ion (parent or precursor ion) is selected for further analysis. It enters a collision-only chamber consisting of a hexapole (six poles arranged in alternating polarity) where there exists only a radio-frequency field. This area is filled with an inert inorganic gas such as He, Ar, O_2 or Xe at variable pressures. The ion collides with the gas at energies up to 200 eV and gradually dissociates into daughter ions. These ions travel through the hexapole slowly, providing time for further collisions and fragmentation. Since there is no dc voltage, the precursor and fragment ions have stable trajectory through the chamber and a single ion can not be selected from all those present. Then the second quadrupole analyses all the ions, providing a mass spectrum. ESI is well suited to tandem mass spectrometry since it provides molecular ions, rather than fragments for analysis.

The results of preliminary experiments showed that a variation in cone voltage produces little effect on the appearance of the CID mass spectra. On the other hand, CID experiments where the collision gas pressure was altered showed patterns in the fragmentation of the precursor ion. These series were developed into a set of experiments where the collision energy was varied at each of several gas pressures (see section 4.2).

2.2. Experimental Procedures

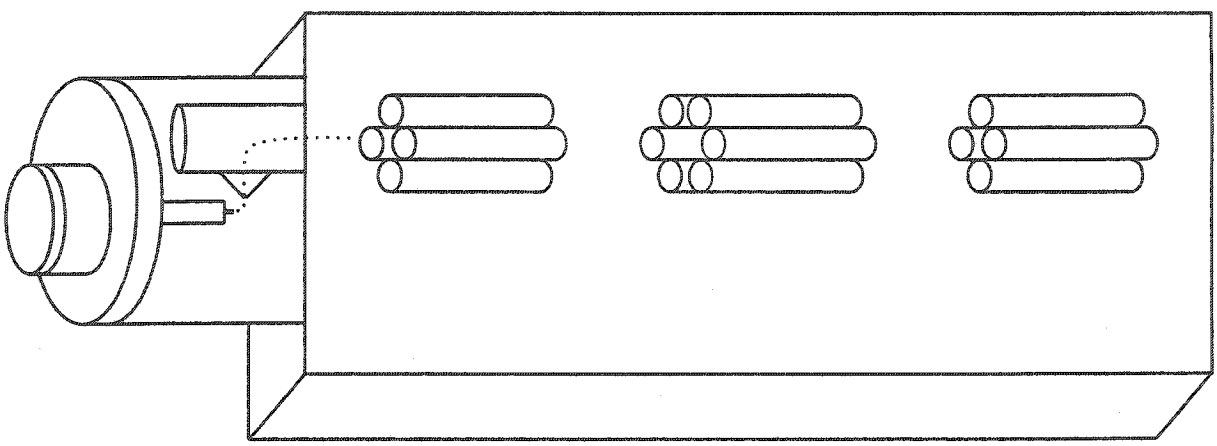

Figure 2.4. Schematic of the ESI/MS instrument. The ions follow a z-shaped path from the ion source into the analyzer. A hexapole collision cell sits between two quadrupoles.

All experiments were carried out on a Quattro LC tandem quadrupole analyser (Q1qQ2, where q is a hexapole collision cell) fitted with an electrospray ionization source (Micromass, Manchester, UK). All data were processed by means of the MassLynx 3.3 program. The sampling cone potential was held at 80 V. The capillary voltage was between 3.5 and 4.20 kV. For tandem mass spectrometry analyses, the collision energy was varied between 0 and 30 eV. This was done to determine the cross-over energy of each ion. There was no potential applied to the entry and exit slits of the hexapole so as to eliminate interference with the voltage of the collision slit. The series of collisions were repeated at some or all of several pressures of the collision gas (Argon), which were 0, 1, 2, 2.5, 3, 4, 8 and 10 $x10^{-4}$ mBar. 25 μL of 1% HNO_3 or 1% H_2SO_4 (in distilled and deionized water) were injected into a flow of CH_3CN. The flow rate was 0.1 mL/min.

Chapter 3: Computational Procedures and Techniques

There are several types of computational methods. *Ab initio* methods generate results from quantum mechanics. Semi-empirical methods are a cruder form of calculation and are generally used for bigger molecules - those containing hundreds of atoms. These methods can also be used as a first step in calculations for molecules to be further analyzed using *ab initio* methods. Semi-empirical methods are derived from ab initio methods which are simplified by replacing key integrals with experimental data.

3.1 Computational Methods

3.1.1 AM1

The AM1[18] (Austin Model 1) method is one which is based on the neglect of diatomic differential overlap (NDDO). The overlap of atomic orbitals on different atoms is ignored, so many integrals in a system are set to zero. So that meaningful results could be obtained from this method, experimental values are included in the calculations. AM1 is an improvement on this method; repulsive and attractive Gaussians were used to better approximate core-core interactions. The goal of this method is to perform calculations rapidly, and sufficiently accurately to produce a reasonable geometry. This geometry can then be submitted as an initial guess for calculations by more rigorous methods.

3.1.2 Hartree-Fock Theory

The Hartree-Fock energy is determined by the Schrödinger equation for molecules:

$$E\Psi = -\frac{\hbar^2}{2\mu}\nabla^2\Psi + U(r)\Psi \qquad (3.1)$$

where U(r) is made up of terms representing electron-electron repulsion, nucleus-nucleus repulsion and electron-nucleus attraction. Since this cannot be solved for any system other than hydrogen, Hartree-Fock makes an important assumption.

In the Hartree-Fock method, electrons are seen as interacting with the average of the field generated by the remaining electrons. The difference between the exact electronic energy and the HF energy is therefore due to the instantaneous positions of electrons:

$$E_{correlation} = E_{exact} - E_{Hartree-Fock} \qquad (3.2)$$

3.1.3 DFT

Density functional theory (DFT) is based on the electron density of a system rather than its wavefunction. While the electron density is the square of the wavefunction, Hohenberg and Kohn showed that only the density need be specified - not the wavefunction - to predict the properties of a system. [19]

Density functional theory attempts to determine the correlation energy as well as the exchange energy, as seen in this equation:

$$E_{HF} = V + < h\rho > + 1/2 < \rho J(\rho) > + E_X[\rho] + E_C[\rho] \qquad (3.3)$$

where V is the nuclear repulsion energy, ρ is the density matrix, <hρ> is the one-electron (kinetic plus potential) energy, ½ <ρJ(ρ)> is the classical Coulomb repulsion of the electrons, $E_X[\rho]$ is the exchange functional (given in the Hartree-Fock method as ½ < Ψ J(Ψ)>) and $E_C[\rho]$ is the correlation functional.

Several methods have been developed to approximate both of these functionals. There is the Slater exchange functional, and Becke 88, which is an improvement on Slater. As for correlation functionals, there are VWN (Vosko, Wilk, and Nusair), Perdew/Wang 91 and LYP (Lee, Yang and Parr). These functionals are denoted as S, B, VWN, and PW91. Any correlation functional can be combined with any exchange functional to give a unique method. The density functional method used in this work is B3-LYP, (a hybrid method due to the use of Hartree-Fock theory for the exchange functional) where the Becke functional contains three parameters.

3.2 Basis Sets

A basis set consists of atomic orbitals employed in a given approximation. A set of one-electron functions (basis functions), each representative of an orbital in a molecule, is called a basis set. A linear combination of these atomic orbitals is a wavefunction. An *ab initio* method will determine, as best it can given the

approximations used, the coefficients of these orbitals, giving the wavefunction of the molecule in question.

Several types of basis sets exist. The split valence basis set is one type, in which less importance is accorded to the inner shell electrons of the atoms. In considering the 3-21G basis set, there are three functions used to describe the inner shells. Two contracted functions and one diffuse function are associated with each valence electron.

In the 6-31G(d) basis set, a set of d-orbitals has been added to non-hydrogen atoms. These are called "polarization functions" as they give direction to the resulting atomic orbital.

Diffuse functions are essential to obtaining accurate results where anions are concerned. In going from a neutral atom to an ion the additional electron is weakly bound (it resides in an orbital that has a large radius from the nucleus). In consideration of this condition, the basis functions must be allowed to become highly diffuse (α becomes very small). The notation for a diffuse function is +. In 6-31+G, the + signifies that highly diffuse s and p orbitals have been added to non-hydrogen atoms.

3.3 Optimization and Frequency Calculations

The calculation methods discussed above are used to determine the optimal geometry of a molecule. To begin this process, a reasonable geometry of a molecule is

submitted for calculation. The wavefunction and energy for the system are calculated. The geometry is changed slightly and the process is repeated until a structure of minimum energy is obtained. It is not possible to distinguish between local and global minima.

Vibrational frequencies of a system are calculated for optimized structures. These can be used to determine the vibrational energy, but more often, they are an indication of the position of a system on a potential energy surface (PES). If all the frequencies are positive ("real"), the system is at a local or global minimum. If one frequency is negative ("imaginary") the system is at a transition state. In the case that two or more frequencies are negative, an N-dimensional saddle-point has been reached.

3.4 Computational Procedures

The Gaussian 98[20] suite was used for the present project. Semi-empirical, *ab initio*, and density functional theory (DFT) calculations were performed using AM1, HF/3-21G, HF/6-31+G(d), B3-LYP/6-31+G(d) and B3-LYP/6-311+G(d,p). Optimization and frequency calculations were performed on HSO_4^-, H_2SO_4 trans, $HSO_4^-(H_2SO_4)$, $HSO_4^-(H_2SO_4)_2$, $HSO_4^-(H_2SO_4)_3$, NO_3^-, HNO_3, $NO_3^-(HNO_3)$, $NO_3^-(HNO_3)_2$ and $O_3^-(HNO_3)_3$. Scaling factors were used to correct the zero-point energies. The scaling factors for AM1, HF/3-21G, HF/6-31+G(d), B3-LYP/6-31+G(d), B3-LYP/6-311+G(d,p) are 0.9532, 0.9085, 0.8970, 0.9614, 0.9986, respectively.[21] The energies calculated were used to determine the bond strengths of each cluster. (See section 4.4.2)

Chapter 4: Results/Discussion

4.1 Cluster Distribution

Samples of sulfuric acid and nitric acid in water were injected into a Quattro LC ESI triple quadrupole mass spectrometer. Mass spectra revealed the formation of various clusters of the formulae $HSO_4^-(H_2SO_4)_n$ and $NO_3^-(HNO_3)_n$. Figures 4.1 and 4.2 are spectra representative of those studied in this project. Certain peaks have been magnified for clarification. The intensities indicated are independent of magnification.

As the clusters increase in size, there is an exponential decrease in intensity. Figure 4.1 shows clusters up to n = 4 for $HSO_4^-(H_2SO_4)_n$. Analysis of nitric acid clusters revealed ions including NO_3^- (m/z 62) and clusters with the formula $NO_3^-(HNO_3)_n$. The relative intensity of the cluster peaks was plotted against their mass, as shown in Figure 4.3 for H_2SO_4 and in Figure 4.4 HNO_3. For both acids, there is an exponential decrease in intensity such that cluster ions with $n \geq 3$ are nearly negligible.

Sharp and Futrell[22] studied the behaviour of H_2SO_4 using fast-atom bombardment (FAB) mass spectrometry. In positive ion FAB, they found a series of peaks corresponding to $(H_2SO_4)_nH_3O^+$ with n up to 21. The negative ion FAB spectrum showed almost exclusively a simple cluster series of formula $(H_2SO_4)_nHSO_4^-$ n=1,2,3,... up to about 20 due to the high concentration of the acid. Neat H_2SO_4 gave spectra with peaks corresponding to $HS_2O_7^-$ and HSO_3^-.

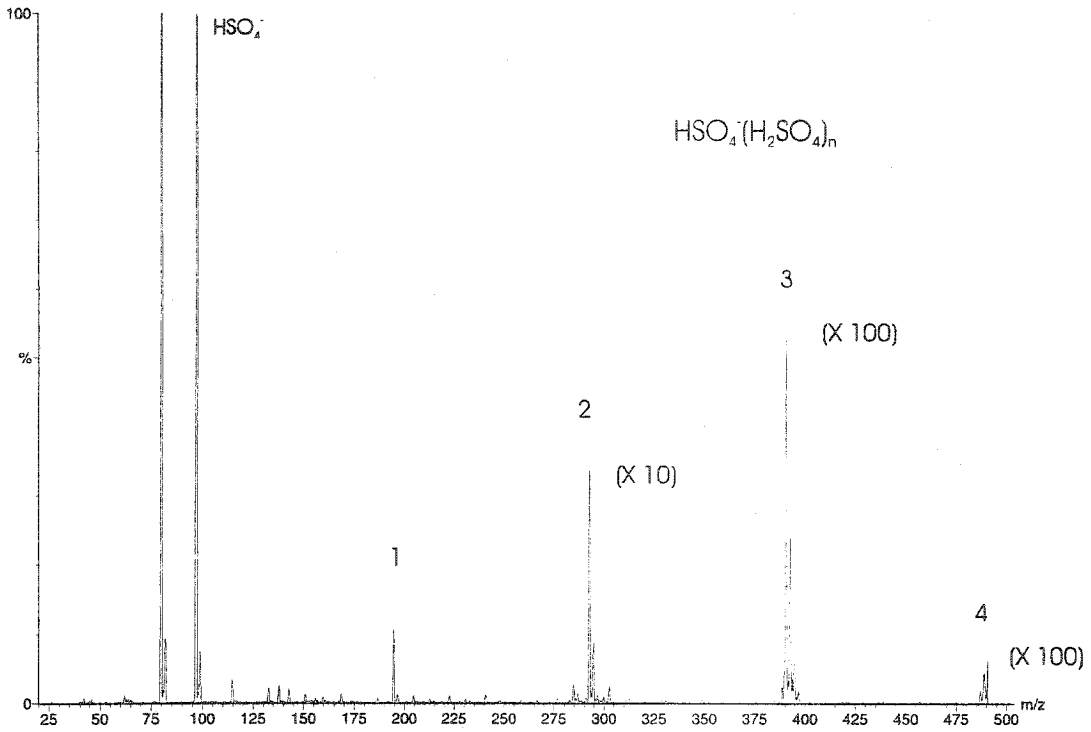

Figure 4.1. Mass spectrum of 1% H_2SO_4. Values in brackets are the magnification factor of each peak.

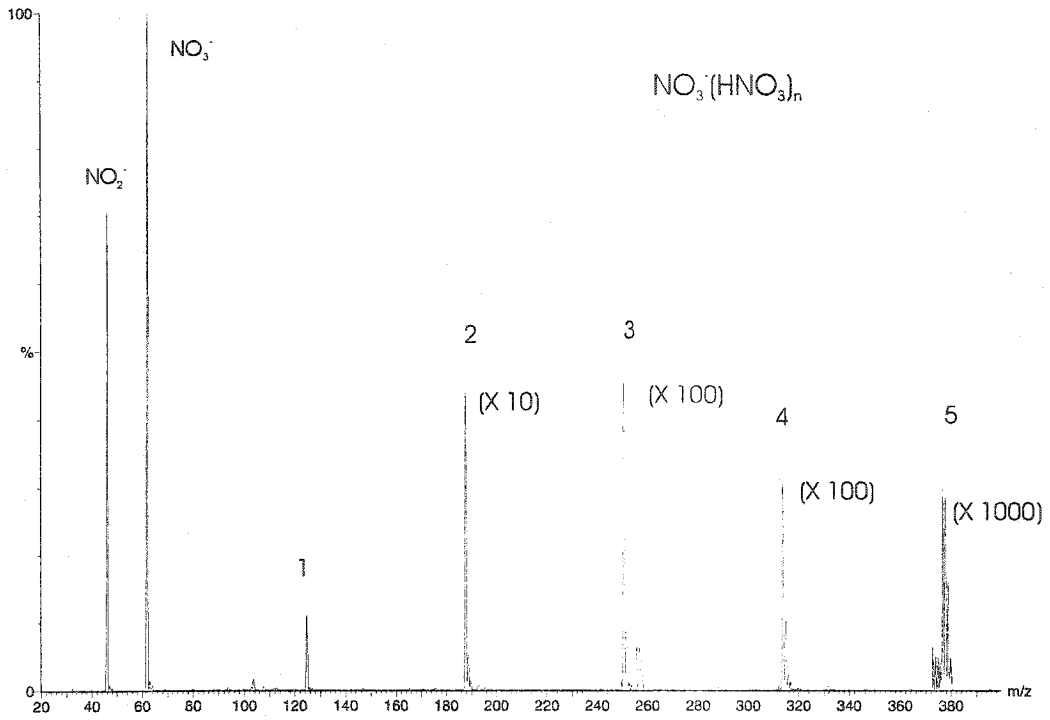

Figure 4.2. Mass spectrum of 1% HNO_3. Peaks for n = 3 and higher contain $NO_3^-(HNO_3)_n(H_2O)_m$ as well as $NO_3^-(HNO_3)_n$.

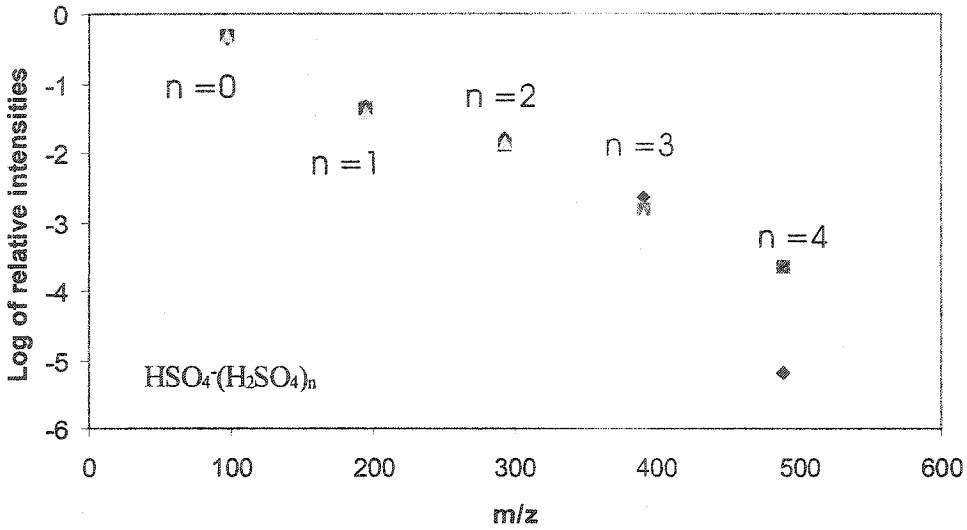

Figure 4.3 : Log of relative intensities of sulfuric acid clusters as a function of mass. Three trials were performed to obtain these results.

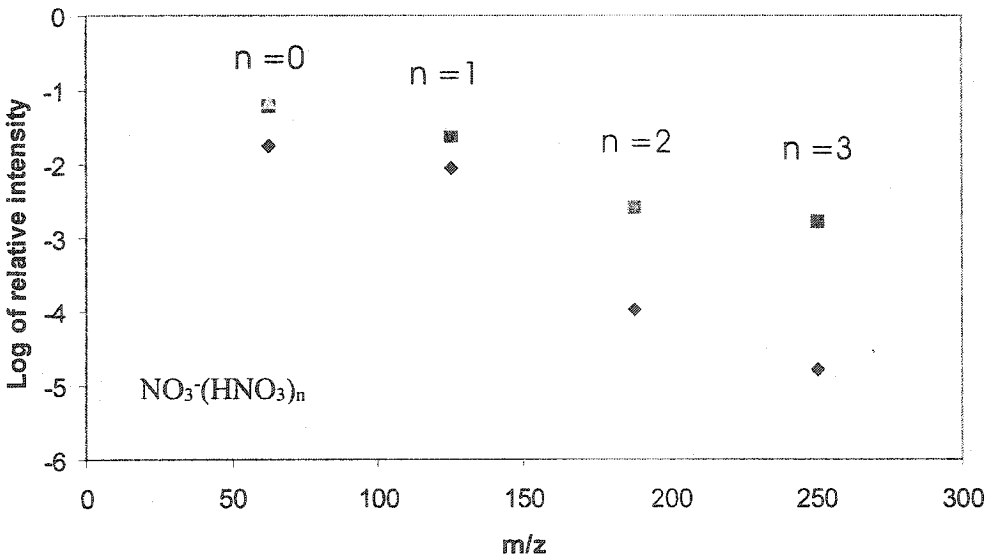

Figure 4.4: Log of relative intensities of nitric acid clusters as a function of mass. Three trials were performed to obtain these results.

There was no evidence of "magic numbers" in Futrell's data or our own. "Magic numbers" signify preferred cluster ion structures (of high stability) and result in a discontinuity in the cluster distribution. The absence of any detectable structure is evidence that sulfuric acid and nitric acid clusters are extended open chains of hydrogen-bonded species.[22]

There was also the formation of water and sulfuric acid clusters. However, their intensity was negligible in comparison to that of the $HSO_4^-(H_2SO_4)_n$ clusters. The clusters containing water appeared randomly. In contrast, Sharp and Futrell's spectra showed that there were signs of the presence of water. Even freshly-opened and rapidly analyzed sulfuric acid showed clusters with water. They compared two solutions with different H_2SO_4:H_2O molar ratios; one with 11:1 and the other, 1:1. It was seen that there was an increase in total water content of about 50% for a 10-fold increase in the bulk concentration of water. This information combined with knowledge of the properties of sulfuric acid solutions led to the hypothesis that a proton-exchange conduction mechanism occurred. Furthermore, it appears that the main effect of adding water was to increase the concentration of H_3O^+ and HSO_4^-. There was an accompanying decrease in $H_3SO_4^+$ and $HS_2O_7^-$. Also, the total ion concentration increased substantially. The ions in solution attach by strong hydrogen bonds, forming hydrates of sulfuric acid; mono and tetrahydrates were particularly stable.

4.2 Tandem MS

Clusters of a given mass were subjected to CID with argon. The collision energy ranged from 0 to 30 eV and the gas pressures ranged from nil to 1.0 x10 $^{-3}$ mBar. In the case where there was no gas present, the mass spectrometer had been pumped down overnight previous to experimentation.

It was found that for nitric acid clusters for n = 3 and higher, the precursor ion dissociated via two channels: The $NO_3^-(HNO_3)_{n-x}$ clusters and $NO_3^-(HNO_3)_{n-x}(H_2O)_{m-y}$ clusters. For example, for n=7, the precursor ion should correspond to $NO_3^-(HNO_3)_7$, but it also appears to consist of $NO_3^-(HNO_3)_5(H_2O)_7$ and more likely, $NO_3^-(HNO_3)_3(H_2O)_{14}$. This is based on the pattern of the fragment ions (Figure 4.5). The height of the n=4 peak shows that few of the ions in the spectra correspond purely to $NO_3^-(HNO_3)_n$. Given all of this evidence, it is reasonable to assume that for precursor ions of mass 566 and higher, we have fragments of $NO_3^-(HNO_3)_{n-x}(H_2O)_{m-y}$ rather than of $NO_3^-(HNO_3)_n$. Even-numbered precursors likely consist of $NO_3^-(HNO_3)_2(H_2O)_{7x}$ and odd-numbered precursors, $NO_3^-(HNO_3)(H_2O)_{7y}$.

As a solution, $H^{15}NO_3$ was used to study the cluster where n = 3. However, with higher-order clusters this increased the complexity of the spectra. For this reason, only clusters up to m/z 251 (n = 3) have been studied further. Similar experiments were done using H_2SO_4. The clusters obtained were of the form $HSO_4^-(H_2SO_4)_n$ with n = 1- 4. (Table 4.1)

Above m/z 251, the precursor ion is not present in the spectrum. Likely, the reason is that high-order clusters, especially those containing water, are not very stable. Between the collision cell and the detector, there is opportunity for water molecules to detach from the precursor.

Table 4.1: Mass of various clusters

N	$HSO_4^-(H_2SO_4)_n$	$NO_3^-(HNO_3)_n$
1	195	125
2	293	188
3	391	251
4	489	---

Representative tandem mass spectra are shown in Figures 4.6 and 4.7 for both acids. For cluster ions where n ≥2, no more than two product ions are formed. In studying HNO_3, the clusters were subject to collision energies from 0 to 20 or to 30 eV. For H_2SO_4, five to seven collision energies were used (see section 4.3). Fragmentation is due to the successive loss of acid molecules until the charged core ion, HSO_4^- or NO_3^- is formed.

In comparison with these experiments, Sharp and Futrell[22] conducted experiments to observe the metastable decay and collision-induced dissociation of small positive-ion clusters. The principal fragments of $(H_2SO_4)(H_3O)^+$ and $(H_2SO_4)_2H^+$ were results of the loss of H_2O and of SO_3, respectively. For $(H_2SO_4)_2(H_3O)^+$, the most important unimolecular and CID processes were losses of H_2O and H_2SO_4, in that order of relative

abundance. The CID mass spectrum showed the successive loss of H_2O and H_2SO_4 as the only additional mechanism. The authors believed that larger clusters would fragment by breakage of hydrogen bonds while smaller clusters would decompose by cleavage of both covalent and hydrogen bonds. The authors attempted to determine mechanisms of ion production. They analyzed solution properties such as surface tension and bulk and surface concentration of preformed ions. They concluded that these properties were irrelevant to the distribution of clusters. After focusing on proton affinities, dipole moments, and elimination products, Sharp and Futrell deduced that gas phase stability was the determinant factor for the observed patterns of cluster ions. Thus, for positive ions, gas phase energetics takes precedence over solution thermodynamics in determining ion production mechanisms.

4.3 Thermochemistry of Clusters

The relative abundances of the ions obtained by tandem mass spectrometry were plotted against collision energy. This gives a breakdown diagram of the precursor ion. The lab-frame energy (E_{LF}) was converted to center-of-mass energies (E_{cm}) using the formula:

$$E_{cm} = E_{LF} \frac{M_{gas}}{M_{gas} + M_{ion}} \qquad (4.1)$$

E_{cm} better reflects the energy which was absorbed by the different sized ions in collisions with the target gas, than does the collision energy delivered by the instrument. CID experiments were undertaken to find the total ion current (TIC) 10 %

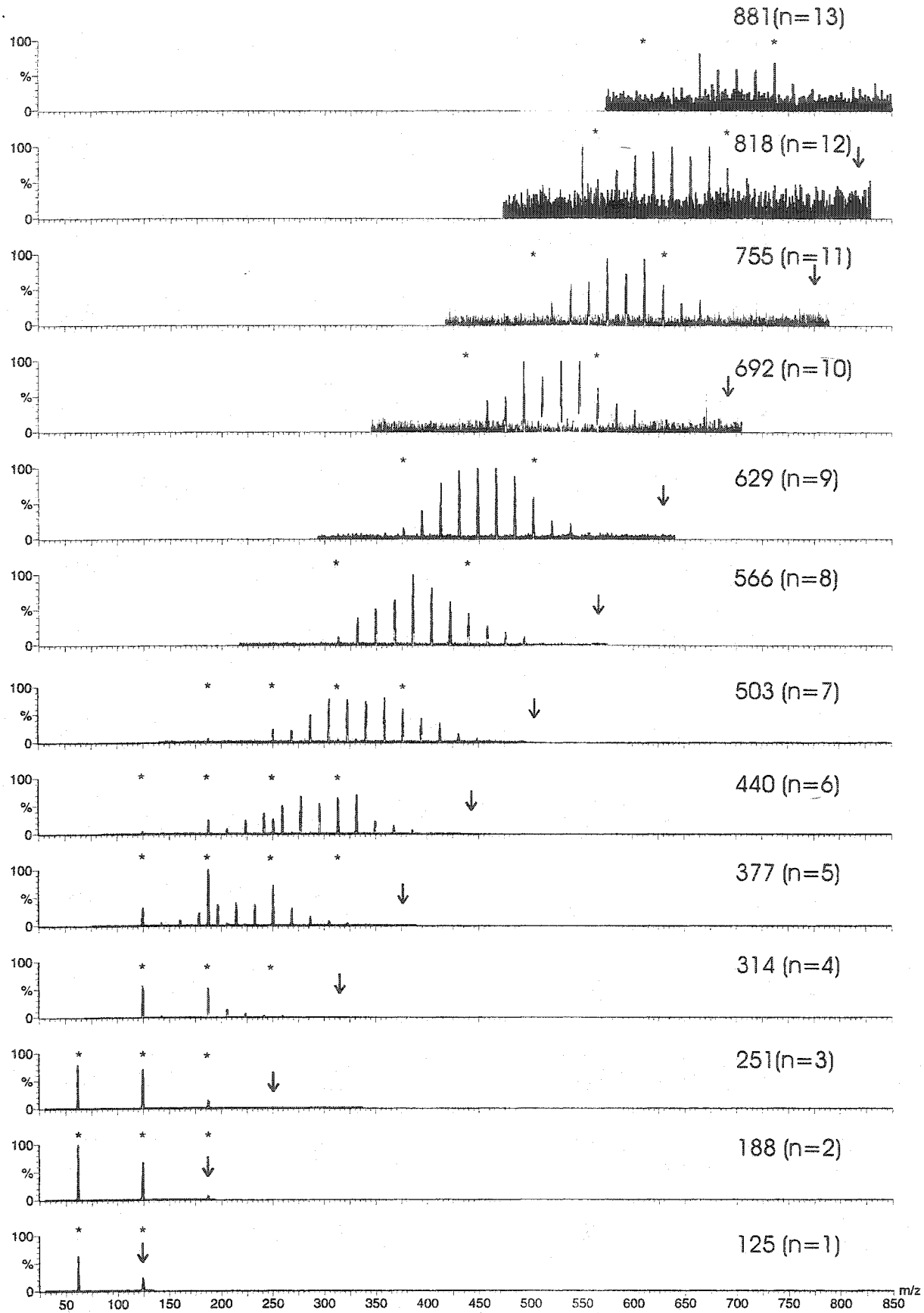

Figure 4.5. Tandem mass spectra of clusters containing nitric acid. The peaks marked with an asterisk can be associated wi $NO_3^-(HNO_3)_n$. Arrows indicate where the precursor ion is/should be for each spectrum. The numbers are the mass of these precursors. Peaks in progressions consist of $NO_3^-(HNO_3)_n(H_2O)_m$. The values of n are associated with the cluster originally thought to be the precursor. CID was performed using 4 x 10 -4 mBar and 15 eV collision energy.

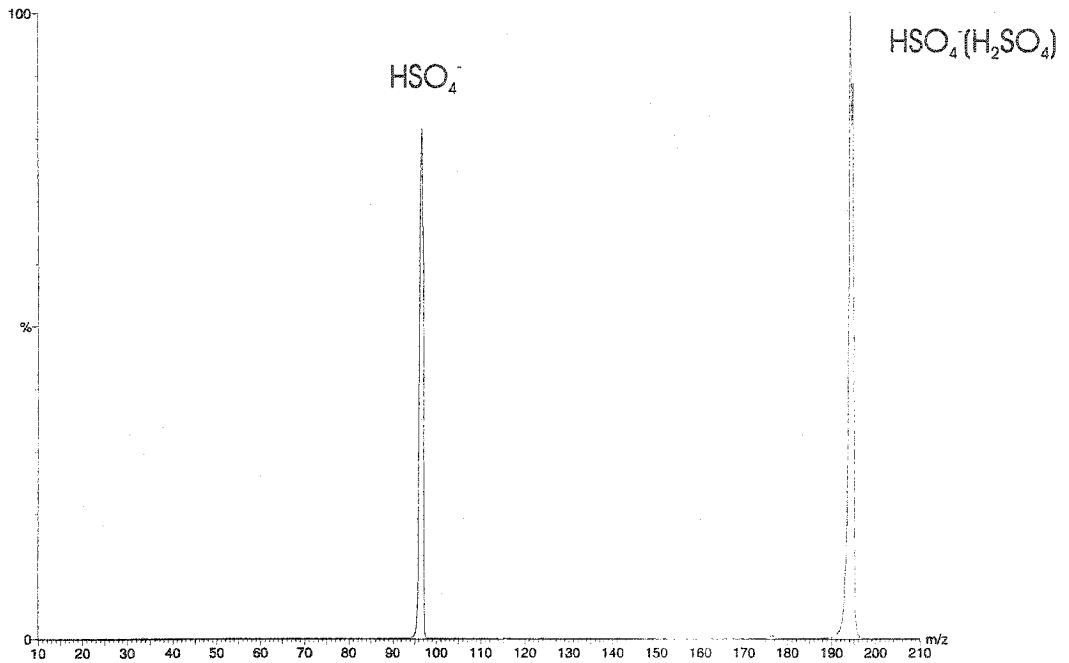

Figure 4.6. Tandem mass spectrum of $HSO_4^-(H_2SO_4)$.

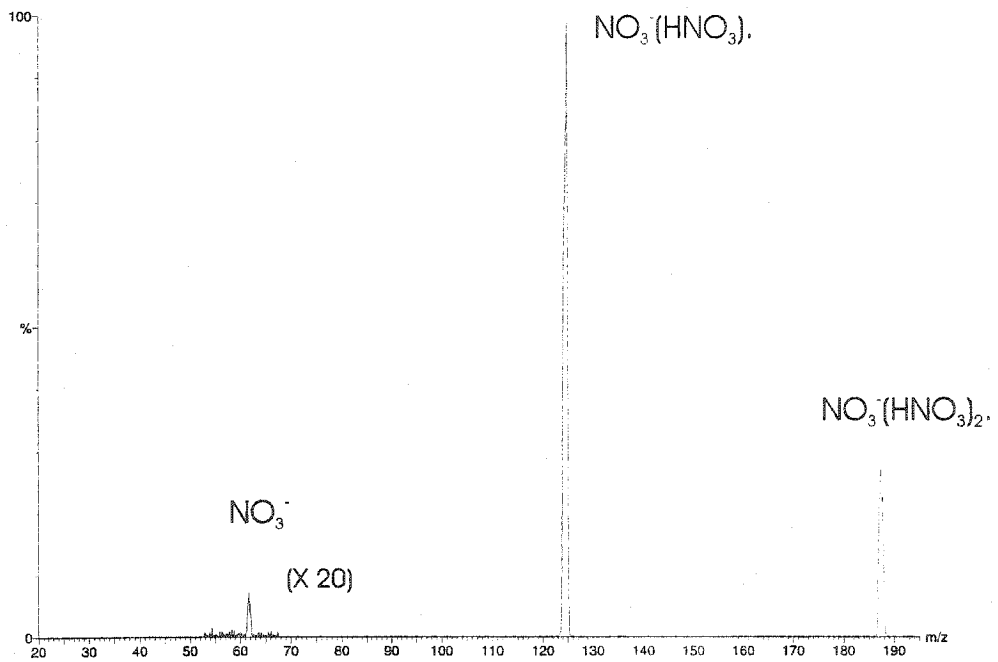

Figure 4.7. Tandem mass spectrum of $NO_3^-(HNO_3)_2$.

reduction. This reduction is a standard chosen in CID experiments. At this value, most ions are experiencing a single collision with the target gas.[23] At higher gas pressures, the ions are likely to undergo more than one collision, in which case the results would show a precursor ion with a lower intensity (and fragment ions with higher intensities) than it would have in a proper experiment. Ultimately, this would lead to a crossover energy occurring at a lower value. It is important to keep this in mind while interpreting the results from this experiment since the gas pressure is very difficult to control. In the case of m/z 188, 10% TIC reduction corresponded to a gas pressure of 2.0×10^{-4} mBar. This pressure has been taken to be the 10 % reduction pressure for all ions.

In some cases it was not possible to obtain a crossover point. In the case of nitric acid clusters with n=1, there was no crossover until at least 3×10^{-4} mBar of collision gas was introduced into the instrument. This will be further discussed in section 4.4.

For the experiments involving cluster precursor ions that were not observed at higher gas pressures, trends in the breakdown diagrams showed that the crossover energy would have been negative. This supports the claim that too great a number of collisions may have occurred. The shape of the larger clusters made them easier targets for collision. This suggestion is based on the concept of collision frequency. Two molecules are said to have collided if they are separated by their collision diameter, d which is the sum of the radii of the molecules in question (supposing that they have a spherical or conical shape). The collision frequency z is the number of collisions per unit time, for a given molecule. It is calculated using:

$$z = \sigma \bar{c}_{rel} \frac{N}{V} \qquad (4.2)$$

where σ is the collision cross-section, $\bar{c}_{rel}$ is the relative mean speed (the mean speed with which two molecules approach each other) and N is the number of molecules in a volume V.[24]

As mentioned before, water and nitric acid form clusters whose masses overlap those of the ions under investigation. When $H^{15}NO_3$ was used, water/cluster peaks were absent or negligible in the CID spectra of clusters for n=3. However, for n=4 and 5, water peaks were once again present, as well as isotopic peaks whose water clusters had the same mass as those of interest.

The crossover energies were determined. One trial is shown for each cluster in Figures 4.8.a to 4.8.g. All of the trials are shown in appendices C and D. All trials were plotted against the logarithm of gas pressure (Figures 4.9 and 4.10). The curve increases dramatically at low pressure, due to insufficient collisions between the target gas and the sample. As the curve decreases, many collisions occur with each sample ion and the results are once again inconclusive.

The c-o-m collision energy corresponding to the crossover point for each cluster ion was equated to the 298 K binding energy for that cluster. The results are summarized in Table 4.2 and are compared to values from the literature and theoretical results from section 4.4.2.

The values for the nitric acid clusters are significantly different from those taken from the literature. Explanations are given below. Despite the difference in absolute values between experiment and literature, certain trends are consistent. The bonding energies decrease with the size of the cluster for nitric acid. This is true for the calculated, experimental and literature values. The same is also true for the experimental values of sulfuric acid. As well, the experimental bond energies of nitric acid clusters are lower than those consisting of sulfuric acid. This result will be confirmed and explained in section 4.4.2.

Lee, Keesee, and Castleman[25] used high-pressure mass spectrometry to determine thermodynamic values for clusters of HNO_3 on NO_3^-. A thermionic source produced ions which underwent reactions in a nearly field-free region. The reactions reached equilibrium at specified temperatures and they were analyzed using a quadrupole mass filter and pulse counting circuitry. Studies on $NO_3^-(HNO_3)_n$ were performed using a mixture of 1-2% HNO_3 and 99-98% N_2O.

$$NO_3^-(HNO_3)_n + HNO_3 \Leftrightarrow NO_3^-(HNO_3)_{n+1} \tag{4.3}$$

The equilibrium for the general reaction (n, n+1) is

$$K_{n,n+1} = \frac{I_{n+1}}{I_n P} \tag{4.4}$$

where $I_{n+1} / I_n P$ is the measured ion ratio and P is the partial pressure of HNO_3. The equilibrium constants were measured as a function of source temperature for each (n, n+1).

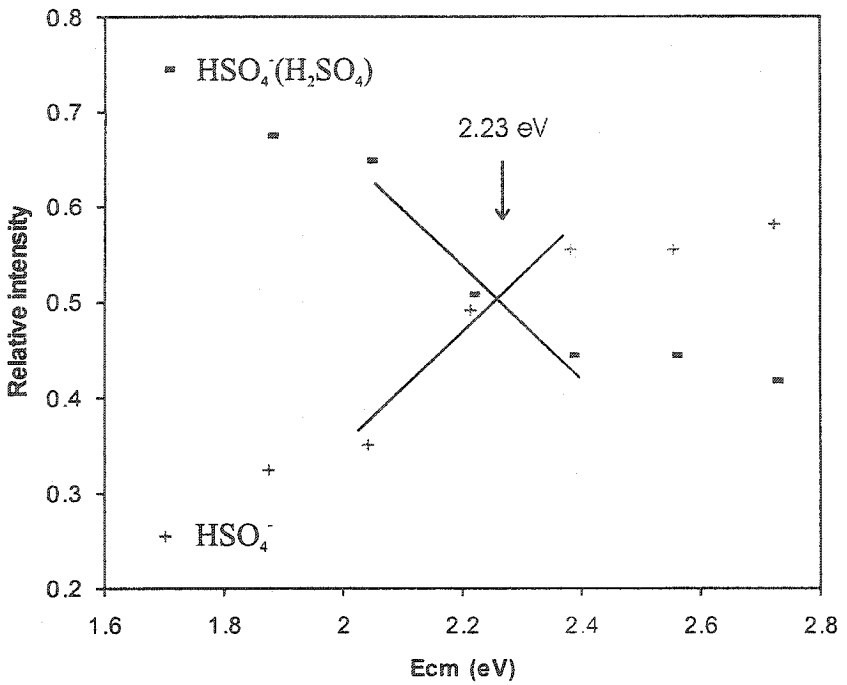

Figures 4.8.a-g. Breakdown diagrams of various species at different pressures.
Figure 4.8.a. $HSO_4^-(H_2SO_4)$ at 2 x 10^{-4} mBar.

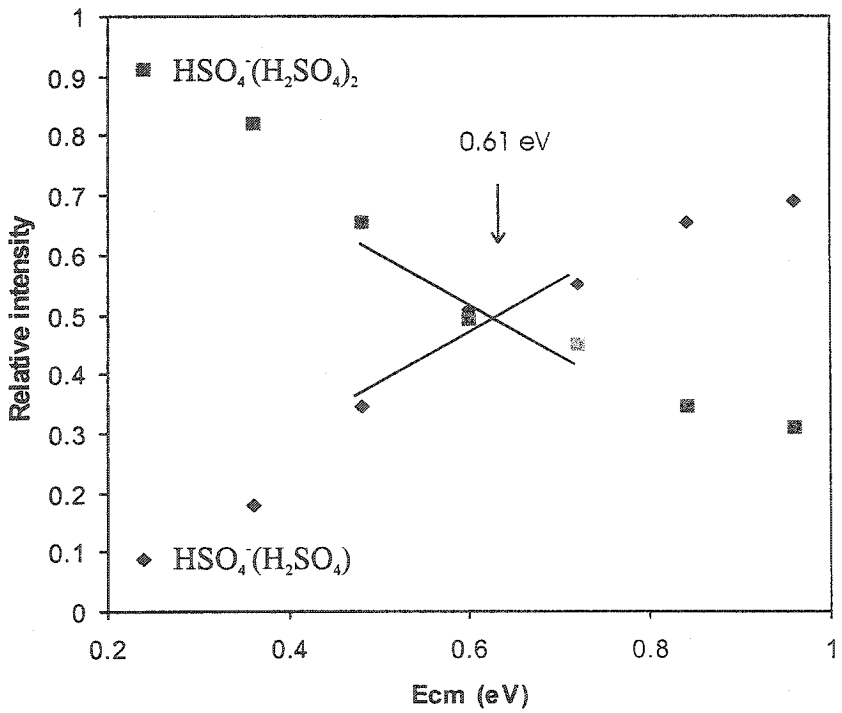

Figure 4.8.b. $HSO_4^-(H_2SO_4)_2$ at 2 x 10^{-4} mBar.

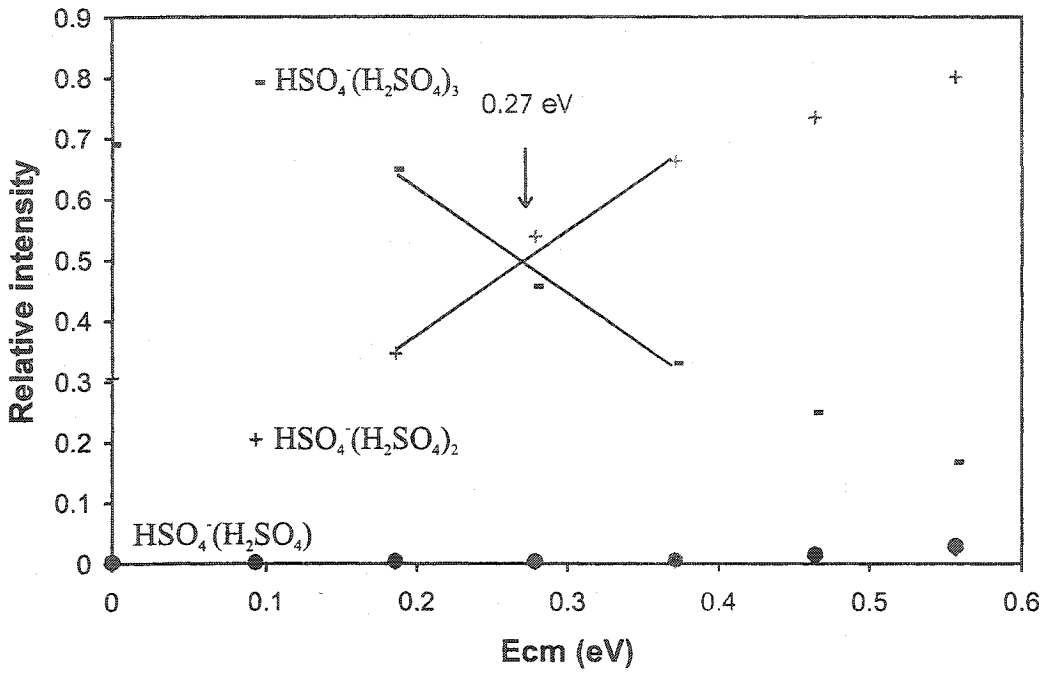

Figure 4.8.c. $HSO_4^-(H_2SO_4)_3$ at 2 x 10^{-4} mBar.

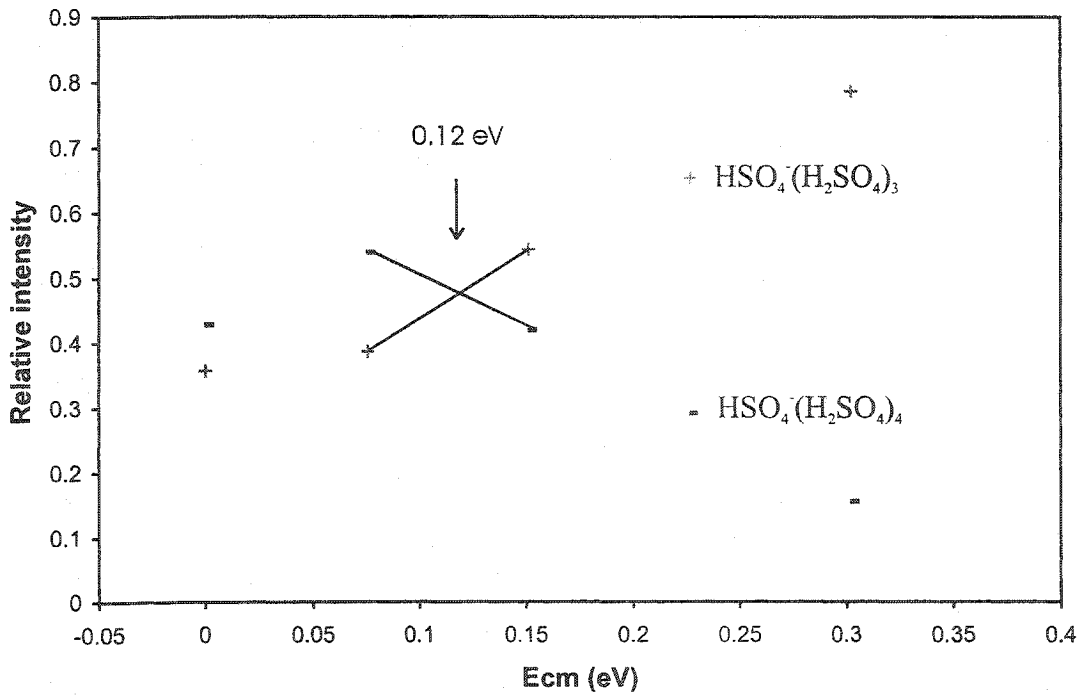

Figure 4.8.d. $HSO_4^-(H_2SO_4)_4$ at 2 x 10^{-4} mBar.

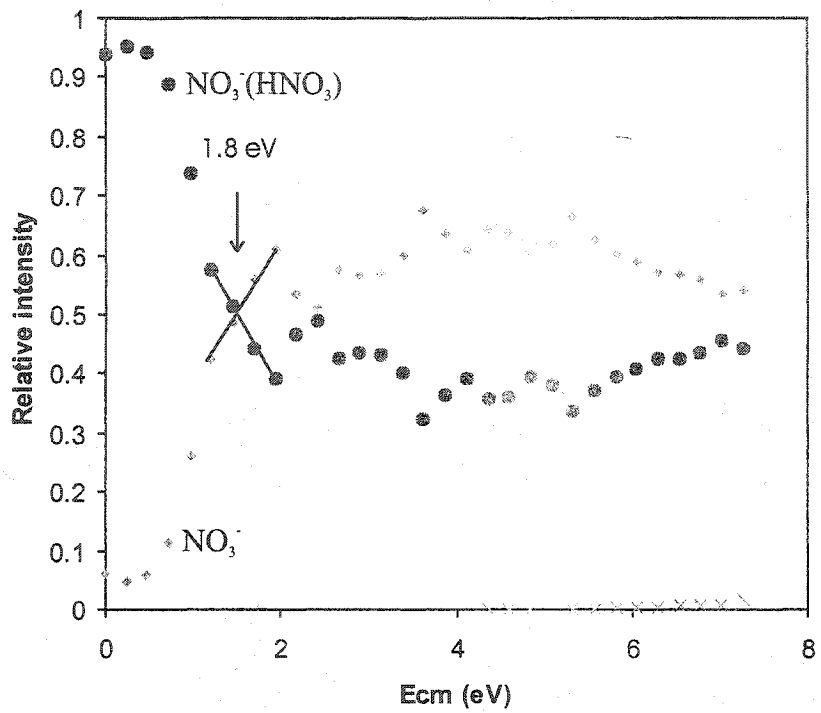

Figure 4.8.e. $NO_3^-(HNO_3)$ at 3 x 10^{-4} mBar.

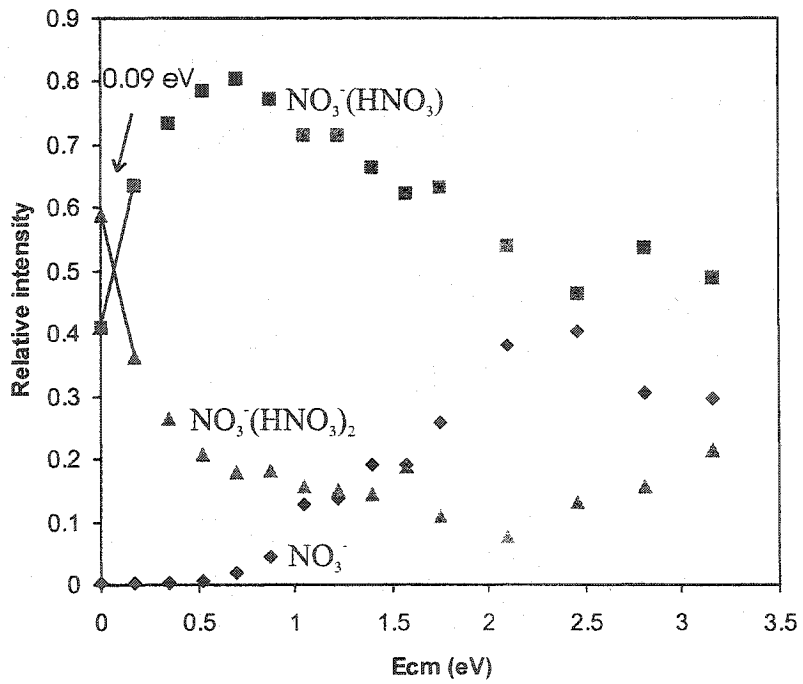

Figure 4.8.f. $NO_3^-(HNO_3)_2$ at 2 x 10^{-4} mBar.

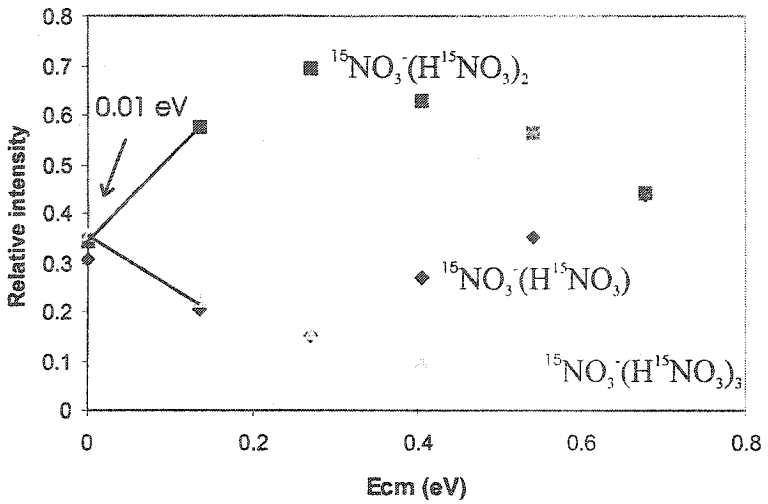

Figure 4.8.g. $^{15}NO_3^-(H^{15}NO_3)_3$ at 2 x 10^{-4} mBar.

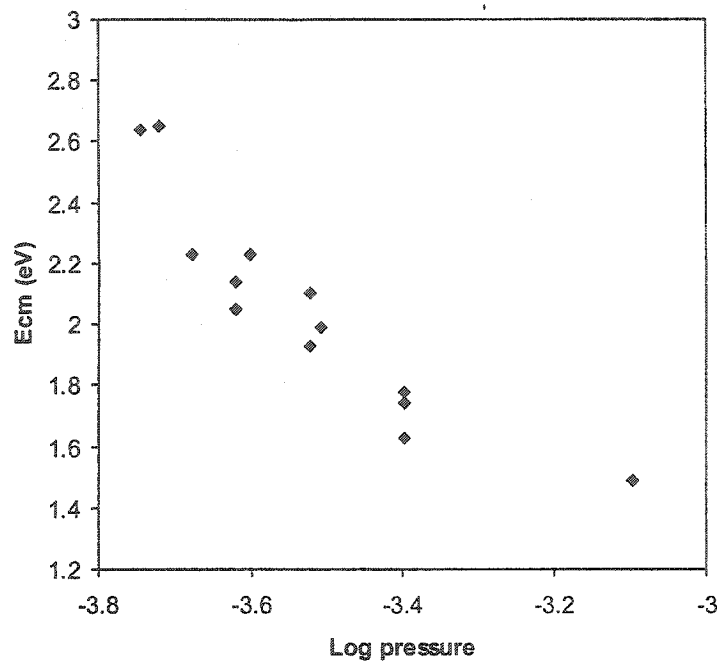

Figure 4.9. Crossover point center-of-mass collision energy as a function of the log of collision gas pressure for $HSO_4^-(H_2SO_4)$.

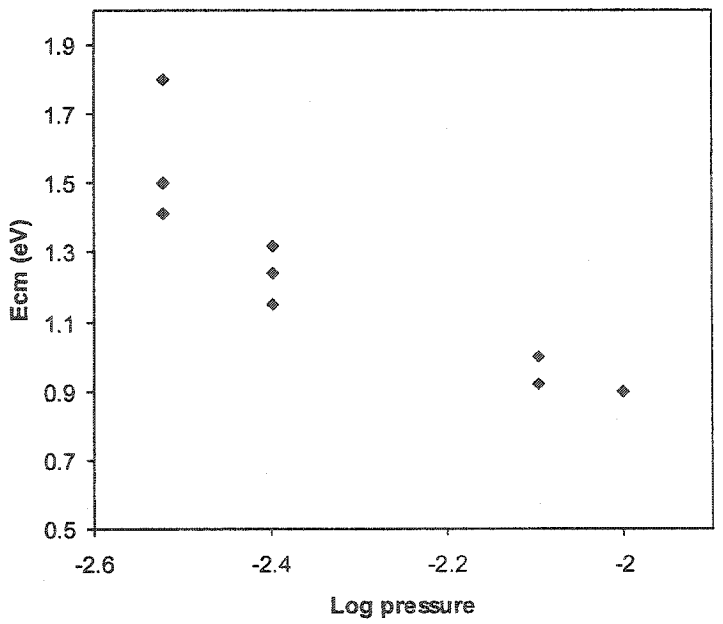

Figure 4.10. Crossover point center-of-mass collision energy as a function of the log of collision gas pressure for $NO_3^-(HNO_3)$.

$$-RT\ln K_{(n,n+1)} = \Delta G^{o}_{n,n+1} = \Delta H^{o}_{n,n+1} - T\Delta S^{o}_{n,n+1} \quad (4.5)$$

The standard state was chosen as 1 atm. Certain source conditions were fixed such as cell pressure, gas mixture and electrical field. The equilibrium ion ratios were measured for $NO_3^-(HNO_3)_n$ and were used in van't Hoff plots to give enthalpy changes.

Thermochemical values of NO_3^- had been determined by other groups. These groups used flowing-after glow and batch reaction cell techniques employing a few keV electron beam.[25]

Table 4.2: Comparison of bonding energies (kJ/mol) at 298 K

Cluster	Calc	Exp	Literature			
$NO_3^-(HNO_3)$	-117*	-151 ± 19		-108.8[b]		
$NO_3^-(HNO_3)_2$	-69*	-32 ± 25	-74.1[a]	-76.6[b]	-66.9[c]	
$NO_3^-(HNO_3)_3$	-59*	-1***	-66.9[a]	-67.4[b]	-58.2[c]	
$HSO_4^-(H_2SO_4)$	-180*	-242 ± 20	-174.9[d]	-197[e]		
$HSO_4^-(H_2SO_4)_2$	-184**	-61 ± 1	-114.6[d]	>-103.8[e]		
$HSO_4^-(H_2SO_4)_3$	-132**	-26 ± 2	-99.6[d]	-94.6[e]	-99.6[e]	-99.2[e]
$HSO_4^-(H_2SO_4)_4$		-13 ± 5	-90.4[d]	-90.4[e]	-92.5[e]	

a (Lee et al.)[25]

b (Davidson et al.)[26]

c (Wlodek et al.)[27]

d (Lovejoy and Curtius. Experimental values.)[28]

e (Jeffrey and Saenger)[29]

f (Lovejoy and Curtius. Values are derived from atmospheric ion measurements.)[28]

* Optimized at the B3-LYP/6311+G(d,p) level

** Optimized at the HF/3-21G level

*** This is very rough estimate, since dissociation of the product ion interfered with the crossover point.

The experimental values in this work are significantly lower than those in the literature and those which are calculated except for the values for $NO_3^-(HNO_3)$ and in one case, $HSO_4^-(H_2SO_4)$. All literature and calculated values are beyond the range of experimental error for the values reported here. There are several reasons for obtaining low BDEs as compared to the calculated and literature values. Several breakdown diagrams (see Appendices C and D) showed the formation of more than two product ions. The unwanted ion usually had a low relative abundance, but the interference is present nonetheless. The higher the abundance of the secondary product ion, the lower the experimental binding energy will be. Schultz et al.[13] suggest that the internal energy of the parent ion may be in excess. However, the process of ESI/MS involves the cooling of ions as they desolvate. Therefore, there should be little or no problems of this nature. Another suggestion referred to the efficiency of the target gas in transferring energy. Rodgers and Armentrout[12] and Schultz et al.[13] recommend using Xenon, since it is heavy, giving a long interaction time. Also, it is monoatomic so it doesn't carry away energy in internal modes, and it is polarizable, giving a better interaction for energy transfer. It is necessary that experiments of this nature be undertaken under single-collision conditions. The pressure in the collision cell of the triple quadrupole can not be measured specifically. Instead, single-collision conditions were assumed to occur when the total ion current was reduced by 10%. This reduction was relative to the precursor ion's abundance in CID experiments when no gas was present in the instrument. This may

have been an inaccurate method. Collision energies need to be well known. Rodgers and Armentrout are of the opinion that octapoles create the more stable ion trajectories than quadrupoles, and likely, also hexapoles. A change in the instrumentation could then be beneficial to this type of experiment. As well, it would be ideal to perform collisions using decimal values of collision energies. The instrument used for the present work allows only the use of whole-number energies. Also, the gas pressure was very difficult to control; it decreased with time and required frequent tuning.

4.4 Calculations

4.4.1 Structure of Acids and Clusters

The optimized structures discussed above are presented as Figures 4.11.a-d. Bond angles and lengths are shown for AM1, HF/3-21G, HF/6-31+G(d), B3-LYP/6-31+G(d) and B3-LYP/6-311+G(d,p). Tables 4.3.a to 4.3.j give the values of all bonds and angles, except where symmetry leads to redundant values.

HSO_4^- almost has a tetrahedral form, but it is not entirely symmetrical. The hydrogen atom could either be staggered (shown) with **O2** and **O4** (notation corresponds with that in Tables 4.3.a-j. and in Figures 4.11.a-d.), or eclipsed with **O3** (not shown). The **S-O1** bond is the same length in both B3-LYP/6-31+G(d), and B3-LYP/6-311+G(d,p).

For H_2SO_4, there were two options of structures: cis and trans. The cis conformation was ignored because it is higher in energy. The trans conformer is highly symmetrical.

The covalent O-H bonds in H_2SO_4 and HSO_4^- have become H-bridges in forming $HSO_4^-(H_2SO_4)$. The H_2SO_4 structure remains symmetrical in the dimer but it haschanged to a cis conformer. This allows for the formation of more H-bridges than if H_2SO_4 had remained trans. Concerning the O-S-O angles nearest the H-bridges, that of H_2SO_4 has decreased in forming the dimer cluster, while that of HSO_4^- has increased. The results from HF/6-31+G(d) show that the H-bridges **O3-H2** and **O7-H2** are of equal length whereas the B3-LYP/6-31+G(d), and B3-LYP/6-311+G(d,p) results have the two hydrogen atoms therein closer to the sulfuric acid than to HSO_4^-. AM1 optimization produces a structure in which one hydrogen simultaneously interacts with two oxygen atoms on the accompanying molecule. One oxygen and one hydrogen form a weak bridge, and one hydrogen atom faces the direction opposite to HSO_4^-. HF/3-21G optimization results in a structure where the geometry of HSO_4^- (b) is retained. There are two H-bridges formed. This structure makes more sense than that of AM1, however, it is still not ideal.

A trimeric form of sulfuric acid was optimized with HF/3-21G, and was not successfully calculated with other methods. In this structure, H_2SO_4 (with **S1**) is attached to two oxygen atoms from HSO_4^-. HSO_4^- has formed three H-bridges with H_2SO_4 (with **S3**). No symmetry exists in this molecule, however the H bridges between H_2SO_4 (**S1**)

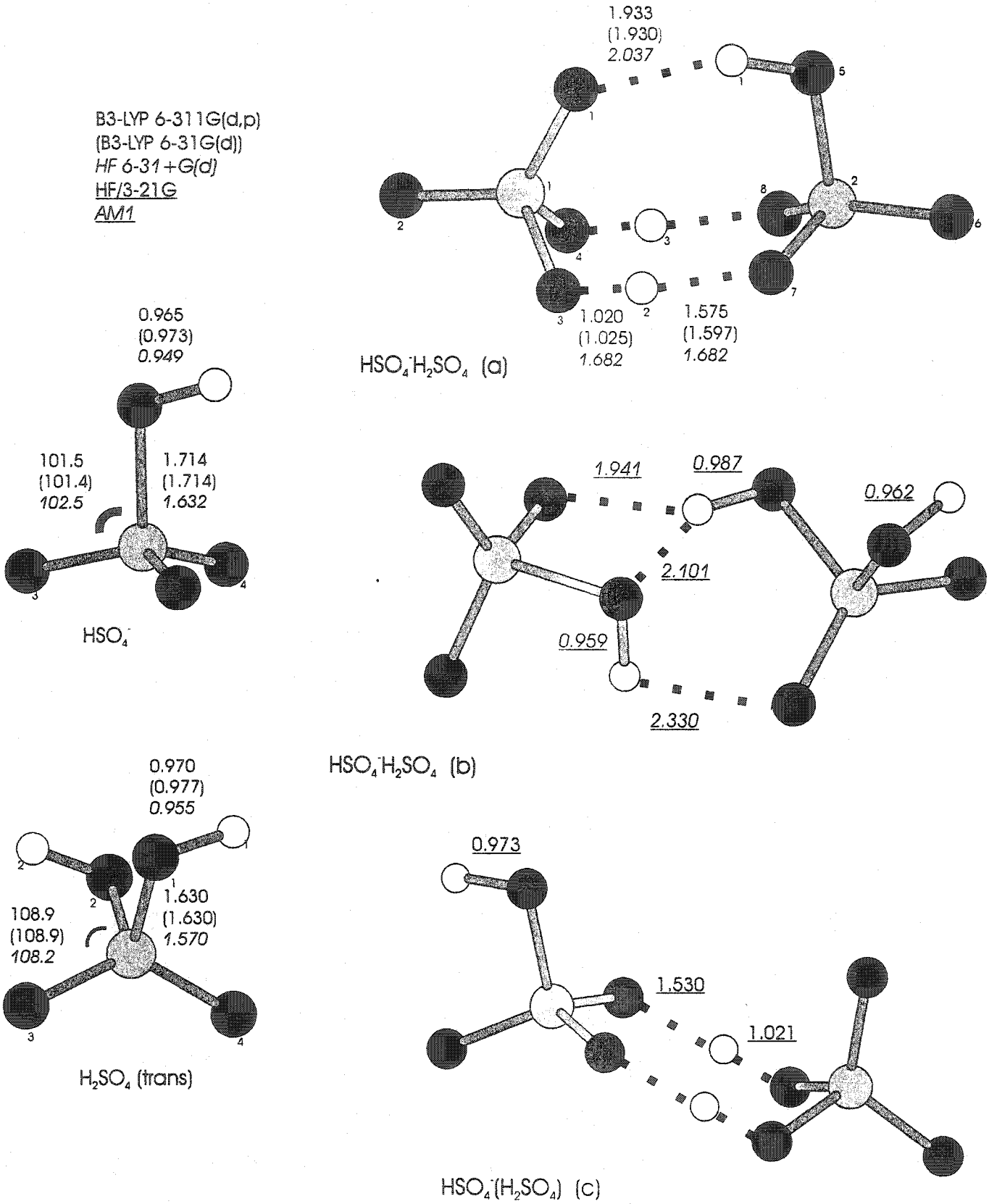

Figure 4.11.a. Selected geometric parameters for HSO_4^-, H_2SO_4 (trans) and $HSO_4^-(H_2SO_4)$. Values in regular font were obtained at the B3-LYP6311+G(d,p) level of theory; values in parentheses, at B3-LYP/6-31+G(d); values in italics, at HF/6-31+G(d); values underlined and in italics at AM1; and values underlined at HF/3-21G. Bond lengths are in Angstroms, bond angles in degrees.

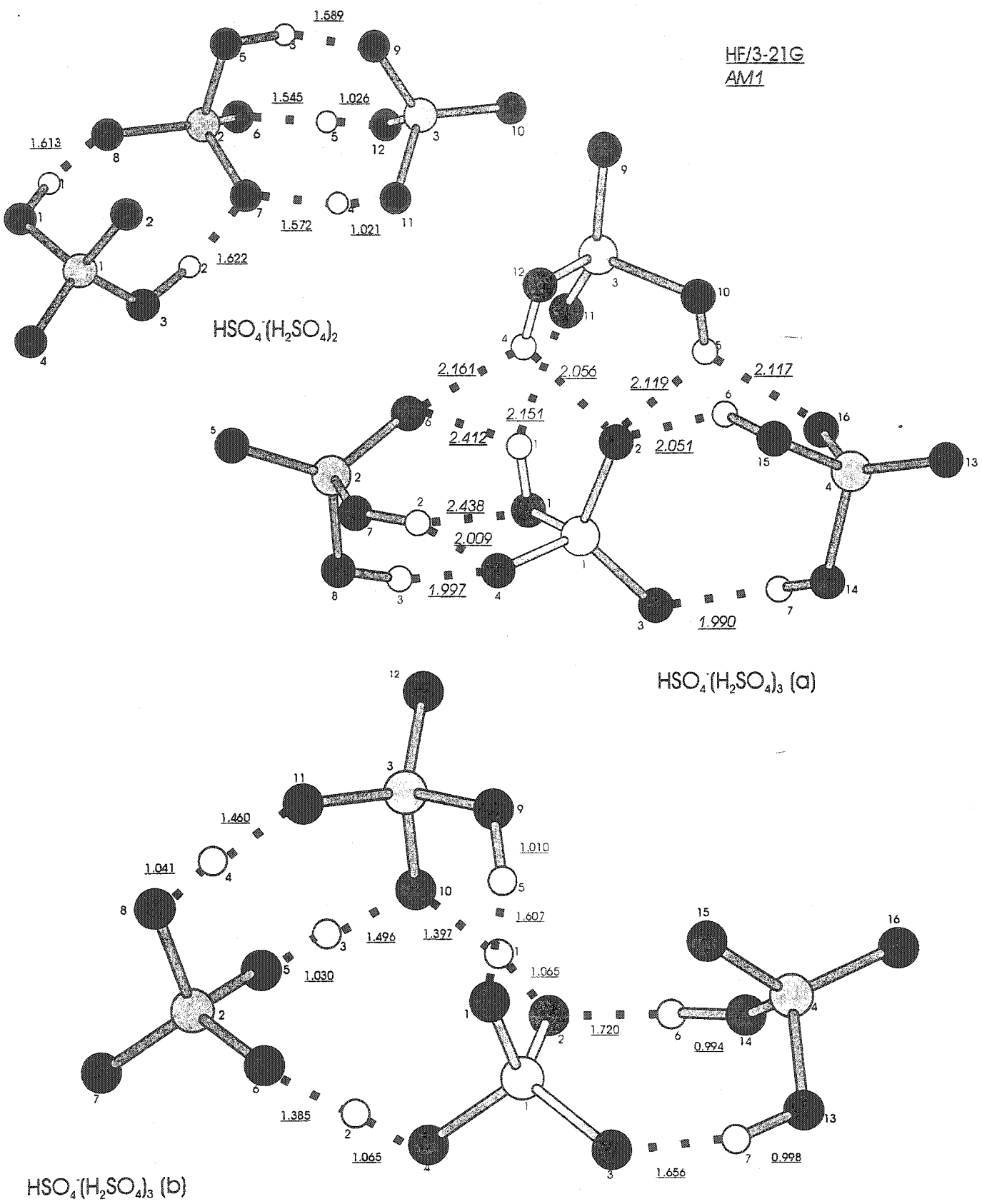

Figure 4.11.b. Selected geometric parameters for $HSO_4^-(H_2SO_4)_2$, and $HSO_4^-(H_2SO_4)_3$.

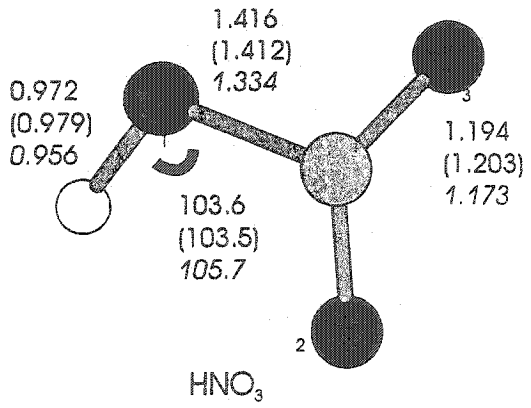

HNO_3

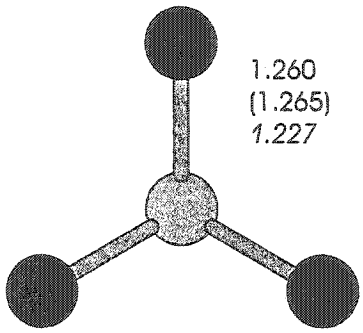

NO_3-

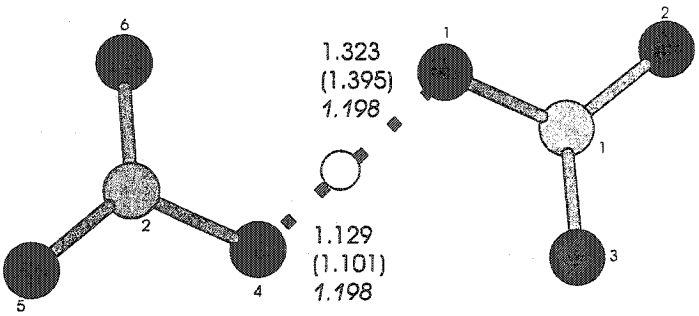

$NO_3^-(HNO_3)$ (a)

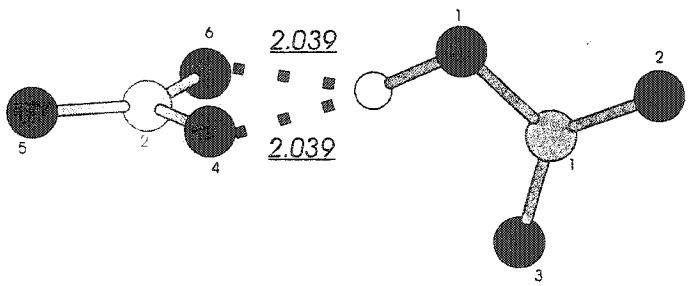

B3-LYP 6-311G(d,p)
(B3-LYP 6-31G(d))
HF 6-31+G(d)
AM1

$NO_3^-(HNO_3)$ (b)

Figure 4.11.c. Selected geometric parameters for HNO_3, NO_3^- and $NO_3^-HNO_3$.

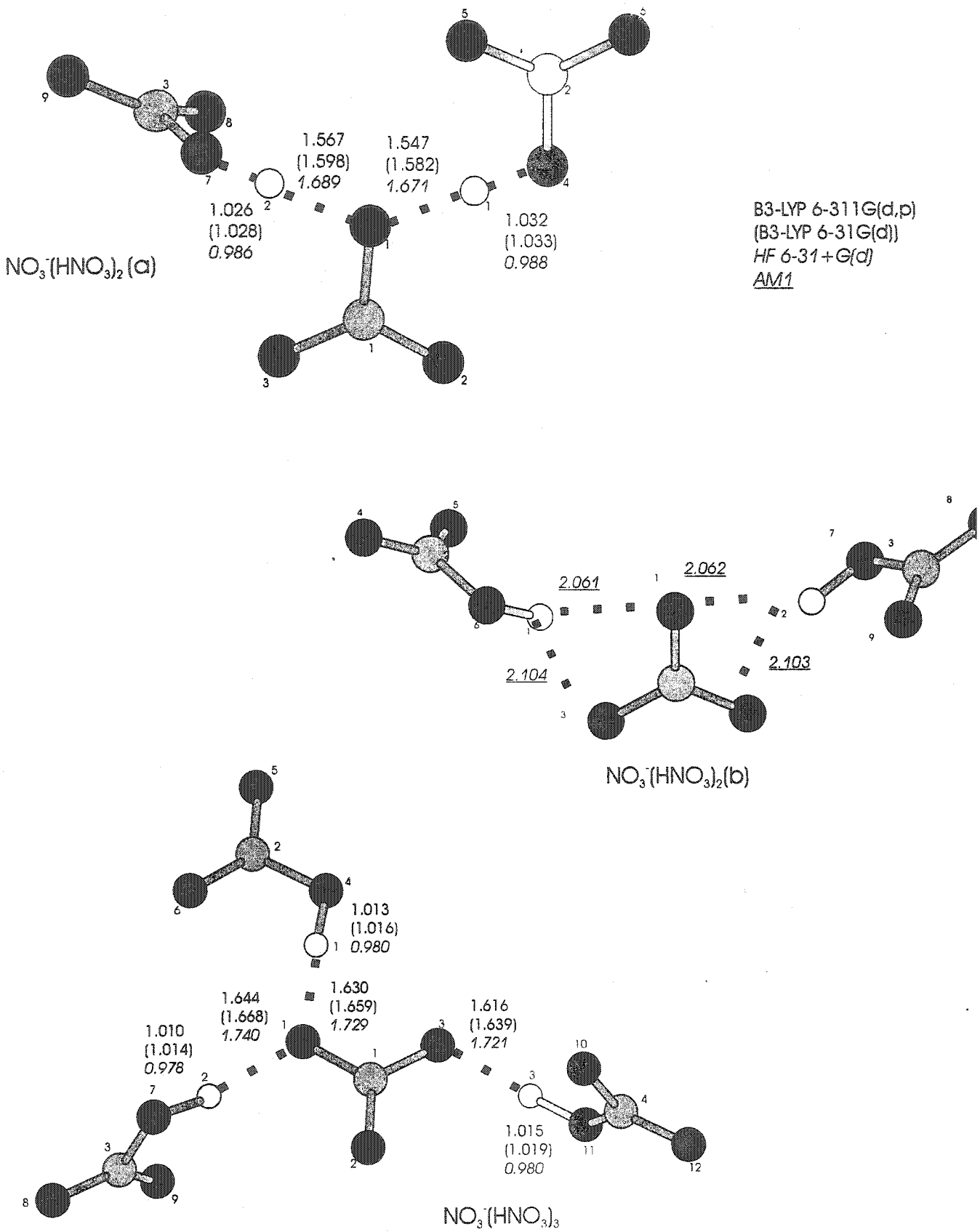

Figure 4.11.d. Selected geometric parameters for $NO_3^-(HNO_3)_2$ and $NO_3^-(HNO_3)_3$.

Table 4.3.a. Geometric parameters for HSO_4^-

Bond/Angle	HF/6-31+G(d)	B3-LYP/6-31+G(d)	B3-LYP/6-311+G(d,p)
O-H	0.949	0.973	0.965
S-O1	1.632	1.714	1.714
S-O2	1.448	1.487	1.480
S-O3	1.439	1.487	1.480
S-O4	1.448	1.477	1.470
S-O1-H	107.2	104.7	105.1
O1-S-O2	104.1	103.9	103.9
O1-S-O3	102.5	101.4	101.5
O1-S-O4	104.1	103.9	103.9
O2-S-O3	115.3	115.7	115.7
O2-S-O4	113.3	113.6	113.8
O3-S-O4	115.3	115.7	115.7

Table 4.3.b. Geometric parameters for H_2SO_4 (trans)

Bond/Angle	HF/6-31+G(d)	B3-LYP/6-31+G(d)	B3-LYP/6-311+G(d,p)
O1-H1	0.955	0.977	0.970
S-O1	1.570	1.630	1.630
S-O3	1.411	1.447	1.439
O1-S-O4	108.2	108.9	108.9
O1-S-O3	106.4	105.2	105.3
O1-S-O2	101.9	101.6	101.6
O3-S-O4	123.6	124.7	124.6
S-O1-H1	110.9	108.8	109.5

Table 4.3.c. Geometric parameters for $HSO_4^-H_2SO_4$

Bond/Angle	HF/6-31+G(d)	B3-LYP/6-31+G(d)	B3-LYP/6-311+G(d,p)
S1-O1	1.433	1.474	1.468
S1-O2	1.416	1.451	1.444
S1-O3	1.549	1.597	1.591
S1-O4	1.549	1.597	1.591
S2-O5	1.592	1.650	1.645
S2-O6	1.427	1.461	1.453
S2-O7	1.463	1.505	1.499
S2-O8	1.463	1.505	1.499
O1-H1	2.037	1.930	1.933
O5-H1	0.958	0.985	0.979
O3-H2	0.985	1.025	1.02
O7-H2	1.682	1.597	1.575
O4-H3	0.984	1.025	1.020
O8-H3	1.683	1.598	1.575
O1-S1-O2	119.4	119.4	119.4
O1-S1-O3	108.5	108.6	108.6
O1-S1-O4	108.5	108.6	108.6
O2-S1-O3	107.7	107.6	107.6
O2-S1-O4	107.7	107.6	107.6
O3-S1-O4	103.9	103.8	104
O5-S2-O6	104.8	104.3	104.4
O5-S2-O7	105.1	105.3	105.3
O5-S2-O8	105.1	105.3	105.3
O6-S2-O7	115.1	115.0	115.1
O6-S2-O8	115.1	115.0	115.1
O7-S2-O8	110.4	110.7	110.3
S1-O1-H1	128.6	129.2	129.1
S2-O5-H1	108.8	106.4	106.9
S1-O3-H2	111.3	108.7	109.3
S2-O7-H2	123.4	122	122.8
S1-O4-H3	111.2	108.7	109.3
S2-O8-H3	123.6	122.0	122.8

Table 4.3.d. Geometric parameters for $HSO_4^-(H_2SO_4)$ determined by HF/3-21G

Bond		Angle	
S1-O1	1.628	O1-S1-O2	109.7
S1-O2	1.552	O1-S1-O3	101.1
S1-O3	1.630	O1-S1-O4	108.1
S1-O4	1.549		
		O5-S2-O6	107.5
S2-O5	1.623	O5-S2-O7	105.8
S2-O6	1.568	O5-S2-O8	107.2
S2-O7	1.586		
S2-O8	1.555	O2-S1-O3	108.1
		O2-S1-O4	119.8
S3-O9	1.562	O3-S1-O4	108.4
S3-O10	1.549		
S3-O11	1.621	O6-S2-O7	108.9
S3-O12	1.620	O6-S2-O8	115.1
		O7-S2-O8	111.8
O1-H1	1.003		
O8-H1	1.613	O9-S3-O10	118.0
		O9-S3-O11	107.0
O3-H2	1.005	O9-S3-O12	107.3
O7-H2	1.622		
		O10-S3-O11	110.0
O5-H3	1.011	O10-S3-O12	109.9
O9-H3	1.589	O11-S3-O12	103.6
O11-H4	1.021	S1-O1-H3	113.9
O7-H4	1.572	S1-O3-H2	115.0
O12-H5	1.026	S2-O5-H3	111.1
O6-H5	1.545		
		S3-O11-H4	114.2
		S3-O12-H5	114.0

Table 4.3.e. Geometric parameters for $HSO_4^-(H_2SO_4)_3$ determined by HF/3-21G

Bond		Angle		Angle	
S1-O1	1.560	O1-S1-O2	108.4	S2-O8-H4	114.7
S1-O2	1.628	O1-S1-O3	119.2	S3-O11-H4	131.4
S1-O3	1.551	O1-S1-O4	109.5		
S1-O4	1.600			S1-O1-H5	123.3
		O2-S1-O3	107.2	S3-O9-H5	115.1
S2-O5	1.618	O2-S1-O4	103.7		
S2-O6	1.564	O3-S1-O4	107.8	S1-O2-H6	118.8
S2-O7	1.548			S4-O14-H6	111.9
S2-O8	1.609	O5-S2-O6	107.1		
		O5-S2-O7	109.8	S1-O3-H7	135.6
S3-O9	1.617	O5-S2-O8	104.1	S4-O13-H7	110.3
S3-O10	1.604				
S3-O11	1.562	O6-S2-O7	117.3		
S3-O12	1.548	O6-S2-O8	107.0		
		O7-S2-O8	110.7		
S4-O13	1.630				
S4-O14	1.635	O9-S3-O10	103.2		
S4-O15	1.559	O9-S3-O11	108.4		
S4-O16	1.549	O9-S3-O12	109.2		
O2-H1	1.065	O10-S3-O11	105.9		
O10-H1	1.397	O10-S3-O12	112.7		
		O11-S3-O12	116.6		
O4-H2	1.065				
O6-H2	1.385	O13-S4-O14	101.9		
		O13-S4-O15	108		
O5-H3	1.030	O13-S4-O16	108.9		
O10-H3	1.496				
		O14-S4-O16	109.2		
O8-H4	1.041	O14-S4-O15	106.5		
O11-H4	1.460	O15-S4-O16	120.8		
O1-H5	1.607	S1-O2-H1	111.4		
O9-H5	1.010	S3-O10-H1	126.4		
O2-H6	1.720	S1-O4-H2	117.6		
O14-H6	0.994	S2-O6-H2	132.3		
O3-H7	1.656	S2-O5-H3	115.0		
O13-H7	0.998	S3-O10-H3	121.1		

Table 4.3.f. Geometric parameters for NO_3^-

	HF/6-31+G(d)	B3-LYP/6-31+G(d)	B3-LYP/6-311+G(d,p)
NO bond length	1.227	1.265	1.260

Table 4.3.g. Geometric parameters for HNO_3

Bond/Angle	HF/6-31+G(d)	B3-LYP/6-31+G(d)	B3-LYP/6-311+G(d,p)
N-O1	1.334	1.412	1.416
N-O2	1.189	1.218	1.21
N-O3	1.173	1.203	1.194
O-H	0.956	0.979	0.972
N-O1-H	105.7	103.5	103.6
O1-N-O2	116.1	115.8	115.8
O1-N-O3	114.8	113.9	113.8
O2-N-O3	129	130.3	130.4

Table 4.3.h. Geometric parameters for $NO_3^-(HNO_3)$

Bond/Angle	HF/6-31+G(d)	B3-LYP/6-31+G(d)	B3-LYP/6-311+G(d,p)
N1-O1	1.275	1.303	1.305
N1-O2	1.200	1.242	1.233
N1-O3	1.204	1.247	1.238
N2-O4	1.275	1.38	1.331
N2-O5	1.200	1.230	1.225
N2-O6	1.204	1.231	1.227
O1-H	1.198	1.395	1.323
O4-H	1.198	1.101	1.129
N1-O1-H	114.3	113.4	114.5
N2-O4-H	114.3	110.5	111.8
O1-N1-O2	117.4	118.0	117.7
O1-N1-O3	118.8	119.0	119.0
O2-N1-O3	123.8	123.0	123.4
O4-N2-O5	117.4	115.8	116.1
O4-N2-O6	118.8	118.8	118.9
O5-N2-O6	123.8	125.4	125.1

Table 4.3.i. Geometric parameters for $NO_3^-(HNO_3)_2$

Bond/Angle	HF/6-31+G(d)	B3-LYP/6-31+G(d)	B3-LYP/6-311+G(d,p)
N1-O1	1.265	1.317	1.318
N1-O2	1.206	1.239	1.231
N1-O3	1.205	1.237	1.230
N2-O4	1.307	1.359	1.358
N2-O5	1.191	1.225	1.218
N2-O6	1.187	1.222	1.215
N3-O7	1.307	1.359	1.358
N3-O8	1.189	1.224	1.217
N3-O9	1.188	1.222	1.215
O1-H1	1.671	1.582	1.547
O4-H1	0.988	1.033	1.032
O1-H2	1.689	1.598	1.567
O7-H2	0.986	1.028	1.026
N1-O1-H1	114.3	113.3	115.0
N2-O4-H1	109.2	108.1	108.5
N1-O1-H2	114.6	114.0	115.2
N3-O7-H2	109.5	108.4	108.7
O1-N1-O2	118.3	117.8	117.8
O1-N1-O3	118.4	118.0	117.8
O2-N1-O3	123.3	124.2	124.4
O4-N2-O5	118.1	118.2	118.2
O4-N2-O6	115.3	114.9	115.0
O5-N2-O6	126.5	126.9	126.8
O7-N3-O8	118.2	118.3	118.2
O7-N3-O9	115.2	114.8	114.9
O8-N3-O9	126.6	126.9	126.9

Table 4.3.j. Geometric parameters for $NO_3^-(HNO_3)_3$

Bond/Angle	RHF/6-31+G(d)	B3-LYP/6-31+G(d)	B3-LYP/6-311+G(d,p)
N1-O1	1.248	1.291	1.288
N1-O2	1.198	1.231	1.223
N1-O3	1.226	1.262	1.257
N2-O4	1.312	1.367	1.368
N2-O5	1.185	1.218	1.211
N2-O6	1.190	1.224	1.216
N3-O7	1.311	1.367	1.367
N3-O8	1.185	1.219	1.211
N3-O9	1.189	1.227	1.216
N4-O10	1.189	1.228	1.216
N4-O11	1.311	1.366	1.367
N4-O12	1.186	1.219	1.211
O1-H1	1.729	1.659	1.630
O4-H1	0.980	1.016	1.013
O1-H2	1.740	1.668	1.644
O7-H2	0.978	1.014	1.01
O3-H3	1.721	1.639	1.616
O11-H3	0.980	1.019	1.015
N1-O1-H1	115.0	114.0	115.8
N2-O4-H1	108.6	107.2	107.5
N1-O1-H2	116.1	114.4	115.9
N3-O7-H2	108.9	107.4	107.6
N1-O3-H3	117.5	115.4	117.2
N4-O11-H3	109.1	107.7	108.0
O1-N1-O2	120.1	120.1	120.1
O1-N1-O3	117.9	117.1	117.0
O2-N1-O3	122.0	122.8	122.9
O4-N2-O5	115.2	114.7	114.7
O4-N2-O6	117.8	117.8	117.8
O5-N2-O6	126.9	127.5	127.5
O7-N3-O8	115.2	114.6	114.7
O7-N3-O9	117.9	117.9	117.8
O8-N3-O9	127.0	127.5	127.5
O10-N4-O11	117.9	117.9	117.8
O10-N4-O12	127.0	127.4	127.5
O11-N4-O12	115.2	114.7	114.7

and HSO_4^- are more similar to each other than the H bridges between H_2SO_4 (S3) and HSO_4^-. A geometry for $HSO_4^-(H_2SO_4)_2$ could not be optimized using AM1.

$HSO_4^-(H_2SO_4)_3$ was optimized using AM1 and HF/3-21G. The geometries are very different. Once again, the AM1 structure has many hydrogen atoms interacting with two oxygen atoms simultaneously, and generally at longer distances than in $HSO_4^-(H_2SO_4)$. On the other hand, the HF/3-21G structure shows interaction between single atoms only, and the H-bridges have much more reasonable lengths (Table 4.3.5).

Within the sulfuric acid group of molecules, the covalent O-H bond gets longer from structure to structure in this order : HSO_4^-, H_2SO_4, $HSO_4^-(H_2SO_4)$, $HSO_4^-(H_2SO_4)_2$. The S-O bonds where O is covalently bound to a hydrogen atom get longer in each molecule in the same order, except for the trimer; the values for this cluster fall in the range of those for the dimer. Given that the bond lengths were calculated with HF/3-21G, it could be assumed that for the higher methods, the bond length does increase. In the case of the S-O bonds where O is part of a H-bridge, there is a significant increase in length from the dimer to the trimer. The S-O bonds where the O does not interact with a hydrogen atom, increase in this order: H_2SO_4, $HSO_4^-(H_2SO_4)$, HSO_4^-, $HSO_4^-(H_2SO_4)_2$. In general, bonds increase in length with the size of the molecule. This explains the higher susceptibility of larger clusters to fragmentation as the bond will also be weaker.

NO_3^- is symmetrical and planar. HNO_3 is also planar. As such, the hydrogen atom interacts slightly with **O2**. The **N-O2** bond is thus longer than the **N-O3** bond,

rendering the molecule less symmetric. The **N-O1** bond is shorter in B3-LYP/6-31+G(d) than in B3-LYP/6-311+G(d,p). $NO_3^-(HNO_3)$ is also planar. With the HF/6-31+G(d) method, the hydrogen atom in the H bridge is equidistant from **O1** and **O4**. As a result, there is a high degree of symmetry in the molecule; all analogous bonds and angles are the same. When using B3-LYP/6-31+G(d) and B3-LYP/6-311+G(d,p), the hydrogen atom is closer to one nitrogen atom than to the other. The N1-O1 bond is shorter in B3-LYP/6-31+G(d) than in B3-LYP/6-311+G(d,p). $NO_3^-(HNO_3)$ has a non-planar form in AM1, which could not be reproduced using the other levels of theory. The hydrogen atom of HNO_3 interacts with two oxygen atoms in NO_3^-.

In comparing $NO_3^-(HNO_3)$ to $NO_3^-(HNO_3)_2$, the dimer retains its structure in the trimer. The additional HNO_3 is in such a position as to minimize repulsion between oxygen atoms, and to reduce steric hindrance. No H-bridges in the trimer are symmetrical. They are all longer than in the dimer, with all methods of calculation. To compare the results of the calculations on the trimer, all bonds are longer in B3-LYP/6-31+G(d) than in B3-LYP/6-311+G(d,p) and HF/6-31+G(d) except for **O1-H1** and **O1-H2** as calculated by HF/6-31+G(d). In $NO_3^-(HNO_3)_2$ as optimized by AM1, neither HNO_3 lies in the same plane as NO_3^-. The two HNO_3 molecules are positioned such that steric hindrance is limited. Once again, the hydrogen atoms each interact with two oxygen atoms.

The structure of $NO_3^-(HNO_3)_3$ shows that the structure of $NO_3^-(HNO_3)_2$ within it has been retained. The O-H bonds are all shorter in the tetramer than they are for the

corresponding O-H interactions in the trimer. As well, the H-bonds between the oxygen and hydrogen atoms are longer in the tetramer than in the trimer. Once again, the HNO_3 molecules are positioned such that they reduce steric hindrance. $NO_3^-(HNO_3)_3$ could not be optimized at the AM1 level. Based on the smaller structures, it would be necessary to design a structure which is counter-intuitive.

The total energies for the nitric acid clusters and sulfuric acid clusters are listed in Tables 4.4 and 4.5

Table 4.4 Optimized energies for nitric acid and its derivatives (in Hartrees)

Level of theory	NO_3^-	HNO_3	$NO_3^-(HNO_3)$	$NO_3^-(HNO_3)_2$	$NO_3^-(HNO_3)_3$
AM1	-0.124970706	-0.032397602	-0.1835390	-0.244653097	
HF/3-21G	-277.2760434	-277.8071678	-555.1536275	-833.0047301	-1110.848303
HF/6-31+G(d)	-278.9239038	-279.4269531	-558.3927021	-837.8523271	-1117.306450
B3-LYP/6-31+G(d)	-280.3674192	-280.8700762	-561.284101	-842.1880447	-1123.080460
B3-LYP/6-311+G(d,p)	-280.4437453	-280.9523515	-561.4433439	-842.4247705	-1123.402132
HF/6-31G*			-558.4049238506[a]	-837.8857584438[a]	

a (Lovejoy and Bianco)[30]

Table 4.5 Optimized energies for sulfuric acid and its derivatives (in Hartrees)

Level of theory	HSO_4^-	H_2SO_4	$HSO_4^-(H_2SO_4)$	$HSO_4^-(H_2SO_4)_2$	$HSO_4^-(H_2SO_4)_3$
AM1	0.018887104	-0.068881432	-0.073414973		-0.10350663
HF/3-21G	-694.2243484	-693.7146006	-1388.029451	-2082.33636	-2776.623349
HF/6-31+G(d)	-698.0106164	-697.5195686	-1395.594843		
B3-LYP/6-31+G(d)	-700.1854303	-699.6995004	-1399.951707		
B3-LYP/6-311+G(d,p)	-700.3008321	-699.8105776	-1400.178873		

It has been reported that, of the two geometries of $NO_3^-(HNO_3)$ discussed here, "$NO_3^-HNO_3$ b" was found to be more stable. Wlodek et al[27] determined this using STO-3G. This result is clearly basis set dependent with respect to structure b being disfavored at larger basis sets.

Lovejoy and Bianco[30] showed structures for $NO_3^-(HNO_3)$ and $NO_3^-(HNO_3)_2$ which were optimized at HF/6-31G*. These structures are similar to those optimized in this work at AM1.

Curtius et al.[31] reported structures and energies for HSO_4^-, H_2SO_4, HNO_3 and $HSO_4^-(H_2SO_4)$ optimized at HF/6-31+G(d). They are all the same as those found in this work. The energies of the three sulphur compounds just mentioned are within 0.08 J/mol of those optimized by Evleth[32] at the same level of theory. Curtius et al.[31] reported energies for $HSO_4^-(H_2SO_4)_n$ n=2 to 5, also optimized at HF/6-31G*, however they did not give the geometries of these structures. They are to be submitted by Bianco.[31]

Lee et al[25] performed CNDO/2 semiempirical molecular calculations on NO_3^-. A bond length of 1.239 A was obtained, whereas in this work, values of 1.227, 1.265 and 1.260 were calculated with HF/6-31+G(d), B3-LYP/6-31+G(d), and B3-LYP/6-311+G(d,p) methods.

4.4.2 Cluster Ion Binding Energies

Binding energies were determined for $HSO_4^-(H_2SO_4)$, $NO_3^-(HNO_3)$, and $NO_3^-(HNO_3)_2$ and $NO_3^-(HNO_3)_3$ using AM1, HF/3-21G, HF/6-31+G(d), B3-LYP/6-31+G(d), and B3-LYP/6-311+G(d,p). Binding energies for $HSO_4^-(H_2SO_4)_2$ and $HSO_4^-(H_2SO_4)_3$ were determined using HF/3-21G in both cases, and AM1 for the latter only.

The total energies shown in Tables 4.4 and 4.5 were used to calculate the binding energy at 0 K (Table 4.6) for the cluster anions according to the relationship shown below for $NO_3^-(HNO_3)$:

$$BE = E_{NO_3^-(HNO_3)} - \left(E_{NO_3^-} + E_{HNO_3}\right) \tag{4.6}$$

Once the structures were optimized, the energy value was modified by the addition of a zero-point-correction (ZPC) which was multiplied by a scaling factor. To the resulting value were added the vibrational and rotational energies at 298 K. Using the frequencies in wavenumbers provided in the output of the calculations, and this equation:

$$E_{rot,vib(T)} = \frac{3}{2}RT + \sum \frac{h\nu}{e^{h\nu/k_BT} - 1} \tag{4.7}$$

where R is the gas constant, T is the temperature h is Planck's constant, ν is a vibrational frequency, and k_B is Boltzmann's constant.

Table 4.6 Binding energies for nitric acid and sulfuric acid dimers at 0 K (in kJ/mol)

Level of theory	Binding energy					
	$NO_3^-(HNO_3)$	$NO_3^-(HNO_3)_2$	$NO_3^-(HNO_3)_3$	$HSO_4^-(H_2SO_4)$	$HSO_4^-(H_2SO_4)_2$	$HSO_4^-(H_2SO_4)_3$
AM1	-78	-66		-62		
HF/3-21G	-185	-115	-96	-238	-217	-164
HF/6-31+G(d)	-110	-86	-71	-170		
B3-LYP/6-31+G(d)	-122	-80	-68	-175		
B3-LYP/6-311+G(d,p)	-124	-76	-66	-177		

Table 4.7 Binding energies for nitric acid and sulfuric acid dimers at 298 K (in kJ/mol)

Level of theory	Binding energy					
	$NO_3^-(HNO_3)$	$NO_3^-(HNO_3)_2$	$NO_3^-(HNO_3)_3$	$HSO_4^-(H_2SO_4)$	$HSO_4^-(H_2SO_4)_2$	$HSO_4^-(H_2SO_4)_3$
AM1	-71	-58		-70		
HF/3-21G	-178	-108	-88	-246	-184	-132
HF/6-31+G(d)	-103	-78	-63	-178		
B3-LYP/6-31+G(d)	-115	-72	-60	-183		
B3-LYP/6-311+G(d,p)	-117	-69	-58	-185		

It remains consistent that the AM1 values differ greatly from the rest. The HF/3-21G values are also very different from the values given by higher methods of calculation. However, from HF/6-31+G(d) to B3-LYP/6-311+G(d,p), the binding energy lowers. As a whole, this table shows that values calculated using both AM1 and HF/3-21G should be questioned, for binding energies as well as for geometries.

For the sulfuric acid ions which have crossover energies only at low pressures, the reason is probably that the attraction between the neutral acid and the ion (for example, H_2SO_4 and $HSO_4^-(H_2SO_4)_{n-1}$ to form $HSO_4^-(H_2SO_4)_n$ diminishes with size. The charge density diminishes with size, and the interaction between neutral and ion likens itself to the interaction of two neutrals. This reasoning applies to nitric acid as well.

The calculated binding energies follow the same trends as those in the literature. That is, the energies decrease with the size of the cluster. Wlodek et al.[27] suggested that the reason for decreasing difference between successive binding energies is the formation of a neutral shell around the core ion. As the cluster size increases, the total negative charge decreases slightly, and the charge dispersion among outer oxygen atoms increases. As mentioned above, the cluster's behaviour approaches that of a neutral molecule. Wlodek related this effect to that of the solvation of NH_4^+ by NH_3 molecules. In that case, there was the formation of a quasi-spherical structure, as opposed to the branching structure of H_3O^+. Caldwell and Kebarle[5] studied proton-bound bihalide ions of the form XHY^-. They found that these ions increased in stability with the acidity of XH and the basicity of Y^-. This is another expression of the explanation given above.

4.5 Conclusion

Negative-mode electrospray mass spectrometry revealed the presence of $HSO_4^-(H_2SO_4)_n$, and $NO_3^-(HNO_3)_n$ clusters. Tandem mass spectrometry was used to determine the relative abundance of precursor and product ions. Breakdown diagrams were created,

yielding binding energies which were all low in comparison with literature values except for $HSO_4^-(H_2SO_4)$ and $NO_3^-(HNO_3)$. This occurs even when considering the experimental error. Possible reasons are the further breakdown of a product ion before reaching the crossover point and the inefficient transfer of collision energy from the target gas (Argon) to the precursor ion. Precursor ions may have been subject to multiple collisions despite efforts to control the gas pressure and total ion current. Ideally, collision energies would have been measured to at least one decimal place, but the present instrument allows only integer values.

Calculations were performed on the clusters mentioned above at these levels of theory: AM1, HF/3-21G, HF/6-31+G(d) B3LYP/6-31+G(d), and B3LYP/6-311+G(d,p). Absolute energies and binding energies were calculated. Sulfuric acid clusters bind more strongly than nitric acid clusters for the same number of neutral molecules since they are capable of forming more hydrogen bonds. AM1 and HF/3-21G values were found to deviate substantially from the values determined at higher levels of theory. At AM1, individual hydrogen atoms usually interacted with two oxygen atoms. HF/3-21G also produced geometries which were counter-intuitive, although less so. At HF/6-31+G(d), B3LYP/6-31+G(d), and B3LYP/6-311+G(d,p) bonds were formed between single hydrogen and oxygen atoms. Differences between these three levels of theory lay in the bond lengths and angles, but not in the general structure. Clusters seem to grow until the core ion is surrounded by neutrals and is rendered incapable of forming more hydrogen bonds.

References

(1) Brasseur, G.; Orlando, J.; Tyndall, G. *Atmospheric Chemistry and Global Change*; Oxford University Press: New York, 1999.

(2) Eisele, F.; McMurry, P. *Philosophical Transactions of the Royal Society of London B* **1997**, *352*, 191-201.

(3) Smith, D.; Spanel, P. *Mass Spectrometry Reviews* **1995**, *14*, 255-278.

(4) Viggiano, A. A.; Sclager, H.; Arnold, F. *Planetary and Space Science* **1983**, *31*, 813-820.

(5) Schlager, H.; Arnold, F. *Planetary and Space Science* **1986**, *35*, 693-701.

(6) Arijs, E.; Nevejans, D.; Ingels, J.; Fussen, D. *Physicalia Magasine* **1990**, *12*, 109-122.

(7) Kawamoto, H.; Ogawa, T. *Planetary and Space Science* **1986**, *34*, 1229-1239.

(8) Wayne, R. *Chemistry of Atmospheres*; 2nd ed.; Clarendon Press: Oxford, 1991.

(9) Jacob, D. J. *Introduction to Atmospheric Chemistry*; Princeton University Press: New Jersey, 1999.

(10) Aikin, A. C. *Journal of Geophysical Research* **1997**, *102*, 12921-12925.

(11) Ervin, K. M.; Armentrout, P. B. *Journal of Chemical Physics* **1984**, *83*, 166-189.

(12) Rodgers, M. T.; Armentrout, P. B. *Mass Spectrometry Reviews* **2000**, *19*, 215-247.

(13) Schultz, R. H.; Crellin, K. C.; Armentrout, P. B. *Journal of the American Chemical Society* **1991**, *113*, 8590-8601.

(14) Baer, T.; Li, Y. *International Journal of Mass Spectrometry* **2002**, *219*, 381-389.

(15) Ferreira, M. A. A., Ed. *Ionic Processes in the Gas Phase*; D. Reidel, 1984; Vol. 118.

(16) Stockbauer, R. *International Journal of Mass Spectrometry and Ion Physics* **1977**, *25*, 401-410.

(17) Nohmi, T.; Fenn, J. *Journal of the American Chemical Society* **1991**, *114*, 3241-3246.

(18) Leach, A. R. *Molecular Modelling: Principles and Applications*; Addison Wesley Longman Limited: London, 1996.

(19) Koch, W.; Holthausen, M. C. *A Chemist's Guide to Density Functional Theory*; Wiley-VCH: Weinheim, 2000.

(20) M. J. Frisch, G. W. T., H. B. Schlegel, G. E. Scuseria,; M. A. Robb, J. R. C., V. G. Zakrzewski, J. A. Montgomery, Jr.,; R. E. Stratmann, J. C. B., S. Dapprich, J. M. Millam,; A. D. Daniels, K. N. K., M. C. Strain, O. Farkas, J. Tomasi,; V. Barone, M. C., R. Cammi, B. Mennucci, C. Pomelli, C. Adamo,; S. Clifford, J. O., G. A. Petersson, P. Y. Ayala, Q. Cui,; K. Morokuma, D. K. M., A. D. Rabuck, K. Raghavachari,; J. B. Foresman, J. C., J. V. Ortiz, A. G. Baboul,; B. B. Stefanov, G. L., A. Liashenko, P.

Piskorz, I. Komaromi,; R. Gomperts, R. L. M., D. J. Fox, T. Keith, M. A. Al-Laham,; C. Y. Peng, A. N., C. Gonzalez, M. Challacombe,; P. M. W. Gill, B. J., W. Chen, M. W. Wong, J. L. Andres,; C. Gonzalez, M. H.-G., E. S. Replogle, and J. A. Pople *Gaussian 98*; Revision A.7 ed.; Gaussian, Inc.: Pittsburgh, 1998.

(21) Scott, A. P.; Radom, L. *Journal of Physical Chemistry* **1996**, *100*, 16502-16513.

(22) Sharp, T. R.; Futrell, J. H. *International Journal of Mass Spectrometry and Ion Processes* **1989**, *90*, 39-54.

(23) Holmes, J. L. *Organic Mass Spectrometry* **1985**, *20*, 169-183.

(24) Atkins, P. *Physical Chemistry*; 6th ed., 1999.

(25) Lee, N.; Keesee, R. G.; A. W. Castleman, J. *Journal of Chemical Physics* **1980**, *72*, 1089-1094.

(26) Davidson, J. A.; Fehsenfeld, F. C.; Howard, C. J. *International Journal of Chemical Kinetics* **1977**, *IX*, 17-29.

(27) Wlodek, S.; Luczynski, Z.; Wincel, H. *International Journal of Mass Spectrometry and Ion Physics* **1980**, *35*, 39-46.

(28) Lovejoy, E. R.; Cutius, J. *Journal of Physical Chemistry* **2001**, *105*, 10874-10883.

(29) Jeffrey, G. A.; Saenger, W.; Springer: Berlin, 1991.

(30) Lovejoy, E. R.; Bianco, R. *Journal of Physical Chemistry* **2000**, *104*, 10280-10287.

(31) Curtius, J.; Froyd, K. D.; Lovejoy, E. R. *Journal of Physical Chemistry* **2001**, *105*, 10867-10873.

(32) Evleth, E. M. *Journal of Molecular Structure: Theochem* **1993**, *307*, 179-185.

Appendices

Appendix A: GAUSSIAN archive entries for AM1, HF/3-21G, HF/6-31+G(d), B3-LYP/6-31+G(d) and B3-LYP/6-311+G(d,p) optimized geometries

(Sulfuric Acid)

HSO_4^- AM1

1\1\GINC-FRED\FOpt\RAM1\ZDO\H1O4S1(1-)\JAULD\17-Jan-2003\0\\# OPT FREQ
=NORAMAN RAM1\\Title Card Required\\-1,1\S,-0.1685697855,-0.0325666358
,0.020451062\O,0.0208278421,0.5025093331,1.5080441291\O,1.4785593009,0
.1784271094,-0.504370959\H,1.9285818097,0.5357147514,0.2603740713\O,-0
.4085979113,-1.5978282529,-0.1239343079\O,-0.9947223868,0.9150607381,-
0.953187745\\Version=SGI-G98RevA.7\HF=-0.0912721\RMSD=0.000e+00\RMSF=3
.891e-06\Dipole=0.7708902,0.2317438,0.1574235\PG=C01 [X(H1O4S1)]\\@

HSO_4^- HF/3-21G

1\1\GINC-MS1\FOpt\RHF\3-21G\H1O4S1(1-)\DAN\15-Mar-2003\0\\# OPT FREQ=N
ORAMAN RHF/3-21G\\HSO4-\\-1,1\S,-0.139241305,-0.0000028797,0.048537383
6\O,-0.2184182814,0.0000152044,1.6021236123\O,1.5240575964,-0.00001271
01,-0.2372551863\H,1.6935557218,0.0000927651,-1.1916720703\O,-0.619443
9719,-1.3053094087,-0.6564765356\O,-0.6194071984,1.3053010781,-0.65650
76489\\Version=x86-Linux-G98RevA.7\HF=-693.7361707\RMSD=6.227e-09\RMSF
=1.653e-04\Dipole=0.9174947,0.0000652,-0.8441477\PG=C01 [X(H1O4S1)]\\@

HSO_4^- HF/6-31+G(d)

1\1\GINC-MS1\FOpt\RHF\6-31+G(d)\H1O4S1(1-)\DAN\07-Mar-2003\0\\# OPT FR
EQ=NORAMAN RHF/6-31+G(D)\\HSO4-\\-1,1\S,-0.1407676196,0.0000005563,-0.
0041651627\O,-0.2272067411,0.0000031902,1.4466066285\O,1.4763436322,0.
0000036802,-0.2448609028\H,1.8728021158,-0.0000322723,0.61684144\O,-0.
6008503355,-1.2123780569,-0.6352563348\O,-0.6008515809,1.2123741081,-0
.6352642455\\Version=x86-Linux-G98RevA.7\HF=-697.5454557\RMSD=6.716e-0
9\RMSF=1.547e-05\Dipole=1.1270006,-0.000023,0.4390812\PG=C01 [X(H1O4S1
)]\\@

HSO_4^- B3-LYP/6-31+G(d)

1\1\GINC-MS4\FOpt\RB3LYP\6-31+G(d)\H1O4S1(1-)\DAN\03-Feb-2003\0\\# OPT
FREQ=NORAMAN B3LYP/6-31+G(D) GEOM=CHECK GUESS=CHECK\\HSO4-\\-1,1\S,0.
1551428523,-0.0237878546,0.0005826788\O,0.2960098217,-0.8267327693,-1.
2426183338\O,-1.4870877148,0.4667679809,-0.0091944536\H,-1.9926207306,
-0.3646175375,-0.0025080607\O,0.2802235871,-0.8261336981,1.2460436533\
O,0.8496461927,1.2792513879,0.0049172841\\Version=x86-Linux-G98RevA.7\

HF=-699.7244958\RMSD=3.087e-09\RMSF=1.207e-04\Dipole=-0.9501754,-0.314
1111,-0.0004115\PG=C01 [X(H1O4S1)]\\@

HSO_4^- B3-LYP/6-311+G(d,p)

1\1\GINC-MS1\FOpt\RB3LYP\6-311+G(d,p)\H1O4S1(1-)\DAN\04-Feb-2003\0\\#
OPT FREQ=NORAMAN RB3LYP/6-311+G(D,P)\\HSO4-\\-1,1\S,-0.1542809655,0.01
83231373,0.0273866783\O,-0.1517711764,0.019502276,1.5070457896\O,1.509
2035478,0.0143034915,-0.3864345022\H,1.8653807053,-0.7880405098,0.0146
928005\O,-0.6715797452,-1.2336774809,-0.5676629108\O,-0.6104632834,1.2
617305026,-0.6095583334\\Version=x86-Linux-G98RevA.7\HF=-699.836671\RM
SD=8.276e-09\RMSF=5.979e-06\Dipole=0.8422336,-0.4814446,0.0832346\PG=C
01 [X(H1O4S1)]\\@

H_2SO_4 AM1

1\1\GINC-FRED\FOpt\RAM1\ZDO\H2O4S1\JAULD\17-Jan-2003\0\\# OPT FREQ=NOR
AMAN RAM1\\Title Card Required\\0,1\S,-0.0134695894,-0.1382949736,-0.1
358487164\O,-0.0888731092,-0.215473032,1.5675532632\H,0.7846104929,-0.
4942441354,1.8669664134\O,1.3391389661,-0.8533332047,-0.504877093\O,-1
.4592641321,-0.3820540033,-0.7080861907\O,0.2185310979,1.5481502824,-0
.2591159526\H,-0.645359644,1.9286433738,-0.4571791663\\Version=SGI-G98
RevA.7\HF=-0.0137314\RMSD=0.000e+00\RMSF=1.521e-05\Dipole=0.0595069,0.
6155052,0.6049831\PG=C01 [X(H2O4S1)]\\@

H_2SO_4 HF/3-21G

1\1\GINC-MS1\FOpt\RHF\3-21G\H2O4S1\DAN\07-Mar-2003\0\\# OPT FREQ=NORAM
AN RHF/3-21G\\H2SO4 trans\\0,1\S,0.0167385154,-0.1047345687,-0.0937935
728\O,0.0761823834,-0.1240320496,1.5467566019\H,0.9638786697,-0.350561
0644,1.8828903951\O,1.4430441517,-0.4389404983,-0.5981968578\O,-1.2322
402086,-0.8800733263,-0.58304389\O,-0.2946328231,1.4908764186,-0.32267
83537\H,-1.1705229445,1.643669808,-0.7248932345\\Version=x86-Linux-G98
RevA.7\HF=-694.2585744\RMSD=5.615e-09\RMSF=5.439e-06\Dipole=-0.1109596
,0.694404,0.6218354\PG=C01 [X(H2O4S1)]\\@

H_2SO_4 HF/6-31+G(d)

1\1\GINC-MS1\FOpt\RHF\6-31+G(d)\H2O4S1\DAN\07-Mar-2003\0\\# OPT FREQ=N
ORAMAN RHF/6-31+G(D)\\H2SO4 trans\\0,1\S,0.0180481464,-0.112946202,-0.
1011055153\O,-0.0085677134,-0.1848142484,1.4671942121\H,0.8599020806,-
0.0257690437,1.8301459404\O,1.3260377161,-0.4173990188,-0.535186528\O,
-1.1321893346,-0.7957007847,-0.5513836246\O,-0.1891172269,1.4219353299
,-0.3591932452\H,-1.1179799536,1.6407380517,-0.3839042097\\Version=x86
-Linux-G98RevA.7\HF=-698.0487585\RMSD=5.902e-09\RMSF=5.866e-05\Dipole=

-0.1647406,1.0308949,0.9234393\PG=C01 [X(H2O4S1)]\\@

H_2SO_4 B3-LYP/6-31+G(d)

1\1\GINC-MS4\FOpt\RB3LYP\6-31+G(d)\H2O4S1\DAN\31-Jan-2003\0\\# OPT FRE
Q=NORAMAN B3LYP/6-31+G(D)\\H2SO4 trans\\0,1\S,-0.0124175026,-0.1196005
292,-0.1171782847\O,-0.1447865198,-0.246235649,1.502909864\H,0.7518836
964,-0.2923664065,1.8885738734\O,1.2069475624,-0.7753613983,-0.5393672
649\O,-1.3310132694,-0.4217496298,-0.6319478098\O,0.2721435272,1.47500
39782,-0.3002392389\H,-0.5795340586,1.9527164649,-0.2645657197\\Versio
n=x86-Linux-G98RevA.7\HF=-700.2219866\RMSD=8.932e-09\RMSF=4.619e-05\Di
pole=0.092586,0.8939571,0.8729997\PG=C01 [X(H2O4S1)]\\@

H_2SO_4 B3-LYP/6-311+G(d,p)

1\1\GINC-MS1\FOpt\RB3LYP\6-311+G(d,p)\H2O4S1\DAN\03-Feb-2003\0\\# OPT
FREQ=NORAMAN RB3LYP/6-311+G(D,P)\\H2SO4 trans\\0,1\S,-0.0189865676,-0.
1295426675,-0.106680091\O,-0.0164101448,-0.1285141683,1.5192672685\H,0
.8984747443,-0.1090314237,1.8411978437\O,1.1704417609,-0.79089868,-0.5
744812929\O,-1.3588477535,-0.4945640435,-0.4841727896\O,0.2096134689,1
.4467056542,-0.4336696433\H,-0.633068315,1.9198840053,-0.3498647294\\V
ersion=x86-Linux-G98RevA.7\HF=-700.3389986\RMSD=3.848e-09\RMSF=1.837e-
05\Dipole=0.1414032,0.9647711,0.7945777\PG=C01 [X(H2O4S1)]\\@

$HSO_4^-(H_2SO_4)$ AM1

1\1\GINC-FRED\FOpt\RAM1\ZDO\H3O8S2(1-)\JAULD\17-Jan-2003\0\\# OPT FREQ
=NORAMAN RAM1\\Title Card Required\\-1,1\S,2.136768555,-0.2502555176,0
.0564282882\O,2.1585342466,-0.6501904899,1.7227622094\H,2.9034864356,-
0.165930749,2.0907363385\O,3.6429705613,0.1593364578,-0.1843400773\O,1
.4050469933,-1.4102713075,-0.7258231189\O,1.2515299572,1.1859097042,0.
1364062493\H,0.3056569712,0.9930177439,-0.0671405535\S,-2.296493955,0.
2858226183,-0.2547465929\O,-2.8146505091,-0.6972237705,-1.3880543192\O
,-0.9518674481,-0.6357882031,0.354348879\H,-0.8676316281,-1.4041545456
,-0.2126542551\O,-1.4297245582,1.5316312791,-0.7489880258\O,-3.2350774
152,0.5175955722,1.0039571218\\Version=SGI-G98RevA.7\HF=-0.1297958\RMS
D=0.000e+00\RMSF=3.640e-06\Dipole=2.8310649,-0.3030236,0.8958623\PG=C0
1 [X(H3O8S2)]\\@

$HSO_4^-(H_2SO_4)$ HF/3-21G

1\1\GINC-FRED\FOpt\RHF\3-21G\H3O8S2(1-)\JAULD\21-Jan-2003\0\\# OPT FRE
Q=NORAMAN RHF/3-21G\\HSO4-(H2SO4)\\-1,1\S,1.9449286791,-0.0334657372,0
.498313427\O,2.281800699,0.4548162426,2.0488747624\H,3.2431729804,0.40
03776554,2.1882333789\O,3.3592464441,-0.3693028899,-0.0606510808\O,0.9

74743061,-1.2502510218,0.6581179307\O,1.22824537,1.1888660423,-0.16481
88484\H,-0.1241789321,1.1289616157,-0.8797019701\S,-2.079458614,0.0227
452945,-0.5726729756\O,-3.3105156283,-0.1628096317,-1.4980571804\O,-1.
2767644979,-1.3871200801,-0.528243112\H,-0.3883363111,-1.3843375412,-0
.0247984784\O,-1.024390933,0.9876913972,-1.3404005952\O,-2.3046368622,
0.5414256106,0.8734306045\\Version=SGI-G98RevA.7\HF=-1388.0904468\RMSD
=4.033e-09\RMSF=2.979e-05\Dipole=1.801774,0.1109564,0.8886874\PG=C01 [
X(H3O8S2)]\\@

$HSO_4^-(H_2SO_4)$ HF/6-31+G(d)

1\1\GINC-MS4\FOpt\RHF\6-31+G(d)\H3O8S2(1-)\DAN\23-Jan-2003\0\\# OPT FR
EQ=NORAMAN RHF/6-31+G(D)\\HSO4-(H2SO4)\\-1,1\S,1.8988458734,0.02707095
54,0.2028183607\O,1.4657037749,0.4296888095,1.6805594461\H,0.508950720
9,0.4534507005,1.7270510616\O,3.3252746386,0.0153392108,0.2321132489\O
,1.271460385,-1.2722672575,-0.0366280937\O,1.3035971126,1.0471062479,-
0.6598862569\H,-0.3252437516,1.075152183,-1.0813495709\S,-1.9062116145
,-0.0309054544,-0.2160987354\O,-3.3019072631,-0.0744369216,-0.44869526
7\O,-1.3189597009,-1.4061958617,-0.618129391\H,-0.3582625911,-1.459519
3317,-0.4094224769\O,-1.2887353087,0.9519909965,-1.2412943563\O,-1.419
8827037,0.3078083301,1.0889865425\\Version=x86-Linux-G98RevA.7\HF=-139
5.6630208\RMSD=7.442e-09\RMSF=3.200e-05\Dipole=-1.0101546,0.0220434,0.
021332\PG=C01 [X(H3O8S2)]\\@

$HSO_4^-(H_2SO_4)$ B3-LYP/6-31+G(d)

1\1\GINC-MS4\FOpt\RB3LYP\6-31+G(d)\H3O8S2(1-)\DAN\24-Jan-2003\0\\# OPT
FREQ=NORAMAN RB3LYP/6-31+G(D)\\HSO4-(H2SO4)\\-1,1\S,-1.8670047489,0.0
016889195,-0.3323969187\O,-1.868638416,0.0019105478,1.317225883\H,-0.9
240179005,0.0013347649,1.5968095569\O,-3.2822545593,0.0028808306,-0.69
34763486\O,-1.1080867566,1.2386972124,-0.7291211337\O,-1.1102623847,-1
.2367468144,-0.7287989085\H,0.4849442776,-1.3061274599,-0.6785646173\S
,1.8802028342,-0.0016183476,0.3212382259\O,3.3205073273,-0.0027451594,
0.5004686393\O,1.5072067097,1.2546672029,-0.5912450269\H,0.4871850751,
1.3040979617,-0.6802685031\O,1.5049875575,-1.2589372242,-0.5889406919\
O,1.0041304199,0.000219102,1.5064579184\\Version=x86-Linux-G98RevA.7\H
F=-1400.0163148\RMSD=9.448e-09\RMSF=3.761e-04\Dipole=0.7156747,-0.0008
4,0.2206537\PG=C01 [X(H3O8S2)]\\@

$HSO_4^-(H_2SO_4)$ B3-LYP/6-311+G(d,p)

1\1\GINC-MS4\FOpt\RB3LYP\6-311+G(d,p)\H3O8S2(1-)\DAN\04-Feb-2003\0\\#
OPT FREQ=NORAMAN RB3LYP/6-311+G(D,P)\\HSO4-(H2SO4)\\-1,1\S,-1.85657039
38,0.0005135037,-0.3285755165\O,-1.8619819672,0.0005311655,1.316194233
\H,-0.9264001405,0.0005560373,1.6038409269\O,-3.2619918483,0.000827889

,-0.6954582052\O,-1.0961995187,1.2307721276,-0.7226336067\O,-1.0967644
893,-1.2300933956,-0.7226093475\H,0.475678984,-1.3139016905,-0.6737519
377\S,1.869196242,-0.000435882,0.3168937788\O,3.3029074454,-0.00066342
36,0.486192961\O,1.4911313367,1.2529568079,-0.5874387648\H,0.476240517
3,1.3127400539,-0.6750875711\O,1.4905398746,-1.2550703724,-0.585493680
2\O,1.0039175504,0.0006596581,1.5027347086\\Version=x86-Linux-G98RevA.
7\HF=-1400.2462681\RMSD=9.314e-09\RMSF=2.615e-04\Dipole=0.650314,-0.00
03472,0.2229288\PG=C01 [X(H3O8S2)]\\@

$HSO_4^-(H_2SO_4)_2$ HF/3-21G

1\1\GINC-MS4\FOpt\RHF\3-21G\H5O12S3(1-)\DAN\07-Mar-2003\0\\# OPT FREQ=
NORAMAN RHF/3-21G\\HSO4-(H2SO4)2\\-1,1\S,-3.0582975823,0.1346424795,-1
.5467391487\O,-2.7529477824,0.4074927562,0.021456904\H,-1.7659189656,0
.33914133,0.2737873498\O,-4.5877791872,0.0717104197,-1.7844498702\O,-2
.4387724542,1.4349226878,-2.2884914893\O,-2.1978685266,-1.0980947498,-
1.9722566868\H,-0.6461496196,-1.4100005399,-1.8323486147\S,0.645806280
4,0.1809274029,-1.0333058669\O,2.1753882897,0.2582200337,-0.7636598169
\O,0.0968468054,1.2321063718,-2.0585578028\H,-1.4136823408,1.469501779
8,-2.282279385\O,0.3391535085,-1.2950788759,-1.6352643453\O,-0.1953539
455,0.2840446553,0.3077526625\O,3.4814203693,-0.1629493284,1.454269696
5\H,3.06521324,-0.0172133323,0.5535240039\O,1.3402930512,0.7988450707,
2.3601590161\H,0.655061093,0.600751915,1.6515817519\S,2.4011491461,-0.
4040962771,2.6482531376\O,1.670092114,-1.7555830362,2.428216322\O,3.10
53966436,-0.1213558596,3.9988760278\\Version=x86-Linux-G98RevA.7\HF=-2
082.4351666\RMSD=3.503e-09\RMSF=2.608e-04\Dipole=-0.5881097,0.4136677,
-1.4194121\PG=C01 [X(H5O12S3)]\\@

$HSO_4^-(H_2SO_4)_3$ AM1

1\1\GINC-MS4\FOpt\RAM1\ZDO\H7O16S4(1-)\DAN\25-Mar-2003\0\\# OPT FREQ=N
ORAMAN RAM1 GEOM=CHECK GUESS=CHECK\\HSO4-(H2SO4)3\\-1,1\S,-0.284832898
9,2.8172450024,0.2147201504\O,0.5724135783,2.1858725836,-1.108959\H,0.
8811727837,1.3011338192,-0.8495093214\O,-0.4827540371,4.3639624288,-0.
0376228739\O,-1.7884826096,2.0503018709,-0.0100241778\O,0.3054889799,2
.2125573859,1.5482942179\H,1.135544986,0.238634643,1.7546052967\S,0.22
33358476,-1.3765320543,0.5827766684\O,1.4670169082,-1.9661304835,-0.22
36589628\O,-0.8492054644,-2.409702122,1.1407084305\H,-1.8235664631,1.3
18181823,0.6299073722\O,1.0523595374,-0.7091850044,1.9287243202\O,-0.4
328356735,-0.0978810099,-0.1129708351\O,3.9585921954,-1.6578318101,0.7
424208363\H,3.0356704217,-1.7974158263,1.0200375263\O,3.537705215,-1.2
303851009,-1.8250060916\H,2.5886668099,-1.4242050855,-1.7846480591\S,3
.9481055762,-0.3977519015,-0.3980389061\O,2.7294104778,0.5361437329,-0
.0309686708\O,5.4306419731,0.116481194,-0.5681682927\S,-3.9867191015,-
0.7902176181,-0.3282925111\O,-3.5280790758,-2.3953793582,-0.0065863429

\H,-2.7602952395,-2.3643917437,0.5906424269\O,-2.9098400165,-0.4345044
457,-1.5977693174\H,-2.1583015828,0.0474019538,-1.2113065382\O,-3.5169
752734,0.077683212,0.9028438147\O,-5.4575970261,-0.8124073786,-0.90230
39455\\Version=x86-Linux-G98RevA.7\HF=-0.230735\RMSD=0.000e+00\RMSF=3.
100e-05\Dipole=0.2119789,-0.5634278,-0.2333138\PG=C01 [X(H7O16S4)]\\@

$HSO_4^-(H_2SO_4)_3$ HF/3-21G

1\1\GINC-MS4\FOpt\RHF\3-21G\H7O16S4(1-)\DAN\28-Mar-2003\0\\# OPT FREQ=
NORAMAN RHF/3-21G GUESS=CHECK GEOM=CHECK\\HSO4-(H2SO4)3\\-1,1\S,-0.796
4589993,-1.3301318677,-0.4890201566\O,0.3793278145,-2.3708820383,-0.18
19949566\H,1.3776713082,-2.0611576258,-0.385140379\O,-2.1078794801,-2.
1377421745,-0.6763266427\O,-0.9405309642,-0.4925610399,0.8996005857\O,
-0.3408446491,-0.3474493567,-1.6122653727\H,-0.3162358446,1.248892882,
-1.4315716544\S,1.2221754028,2.2299388937,-0.1317725059\O,2.5029438025
,1.936434674,-0.9770433573\O,1.2028371858,3.5626014681,0.6553800272\H,
-0.1685361303,0.2352666147,0.996425752\O,-0.061576018,2.172787717,-1.1
14125683\O,1.0181706913,0.9502730462,0.8135862334\O,4.3445024452,0.330
1083793,-0.4764517718\H,3.6325440038,1.0421676553,-0.7404380371\O,3.01
7791297,-0.3660788892,1.5794666455\H,2.1910514203,0.217041634,1.384241
6309\S,3.7540374734,-0.967086064,0.2702420486\O,2.6394393525,-1.558076
6277,-0.6533403544\O,4.8966835334,-1.9186569569,0.7017061819\S,-4.1848
410537,0.1681907539,0.237940899\O,-3.4879703301,-0.1915157278,1.672446
3007\H,-2.5033140323,-0.2949487639,1.5898308506\O,-4.5565879202,-1.310
9972014,-0.3365339692\H,-3.7265129559,-1.79861633,-0.5977743236\O,-3.0
603767379,0.7651464159,-0.6625042783\O,-5.49658914,0.9512041219,0.4916
731116\\Version=x86-Linux-G98RevA.7\HF=-2776.75746\RMSD=4.429e-09\RMSF
=9.484e-06\Dipole=0.4498769,-0.9716953,0.0922015\PG=C01 [X(H7O16S4)]\\
@

Appendix B: GAUSSIAN archive entries for AM1, HF/3-21G, HF/6-31+G(d), B3-LYP/6-31+G(d) and B3-LYP/6-311+G(d,p) optimized geometries

(Nitric Acid)

NO_3^- AM1

1\1\GINC-MS1\FOpt\RAM1\ZDO\N1O3(1-)\DAN\24-Apr-2003\0\\# OPT FREQ=NORA
MAN RAM1\\NO3-\\-1,1\N,0.0000062564,0.0000108364,0.0000044239\O,-0.204
2080854,-0.3536991025,1.155164561\O,1.0210301978,-0.3536988365,-0.5775
843043\O,-0.8168275867,0.7073884572,-0.5775841277\\Version=x86-Linux-G
98RevA.7\State=1-A1\HF=-0.1416946\RMSD=0.000e+00\RMSF=2.239e-05\Dipole
=0.0000151,0.0000262,0.0000107\PG=C03V [C3(N1),3SGV(O1)]\\@

NO_3^- HF/3-21G

1\1\GINC-MS1\FOpt\RHF\3-21G\N1O3(1-)\DAN\24-Apr-2003\0\\# OPT FREQ=NOR
AMAN RHF/3-21G\\NO3-\\-1,1\N,-0.0000162664,-0.0000002075,-0.0000094014
\O,-0.0000137753,0.0000184275,1.2832777876\O,1.1113445678,0.0000184275
,-0.6416503783\O,-1.1113165591,-0.0000366734,-0.6416191836\\Version=x8
6-Linux-G98RevA.7\HF=-277.2876468\RMSD=6.142e-09\RMSF=1.489e-05\Dipole
=-0.0001179,-0.0000004,-0.0000681\PG=C01 [X(N1O3)]\\@

NO_3^- HF/6-31+G(d)

1\1\GINC-MS1\FOpt\RHF\6-31+G(d)\N1O3(1-)\DAN\24-Apr-2003\0\\# OPT FREQ
=NORAMAN RHF/6-31+G(D)\\NO3-\\-1,1\N,-0.0000102931,0.,-0.0000059268\O,
-0.000003113,0.,1.2268669365\O,1.0624993011,0.,-0.6134310282\O,-1.0624
871818,0.,-0.6134307223\\Version=x86-Linux-G98RevA.7\State=1-A'\HF=-27
8.938158\RMSD=4.514e-09\RMSF=1.889e-05\Dipole=-0.0000838,0.,-0.0000484
\PG=CS [SG(N1O3)]\\@

NO_3^- B3-LYP/6-31+G(d)

1\1\GINC-MS1\FOpt\RB3LYP\6-31+G(d)\N1O3(1-)\DAN\24-Apr-2003\0\\# OPT F
REQ=NORAMAN RB3LYP/6-31+G(D)\\NO3-\\-1,1\N,0.0000126481,0.,0.000000818
1\O,-0.0000414585,0.,1.2652247106\O,1.0957032636,0.,-0.6326272679\O,-1
.0956728722,0.,-0.6325981586\\Version=x86-Linux-G98RevA.7\State=1-A'\H
F=-280.380753\RMSD=3.066e-09\RMSF=1.501e-05\Dipole=0.0001048,0.,-0.000
0084\PG=CS [SG(N1O3)]\\@

NO_3^- B3-LYP/6-311+G(d,p)

1\1\GINC-MS1\FOpt\RB3LYP\6-311+G(d,p)\N1O3(1-)\DAN\27-Apr-2003\0\\# OP

T FREQ=NORAMAN RB3LYP/6-311+G(D,P)\\NO3-\\-1,1\N,0.0000258942,0.,-0.00
00209777\O,-0.0000030424,0.,1.2600858708\O,1.0912771734,0.,-0.63010496
94\O,-1.0912967885,0.,-0.6299625459\\Version=x86-Linux-G98RevA.7\State
=1-A'\HF=-280.4575523\RMSD=4.963e-09\RMSF=3.002e-05\Dipole=-0.0000365,
0.,-0.0000398\PG=CS [SG(N1O3)]\\@

HNO_3 AM1

1\1\GINC-MS1\FOpt\RAM1\ZDO\H1N1O3\DAN\27-Apr-2003\0\\# OPT FREQ=NORAMA
N RAM1\\HNO3\\0,1\H,0.0895086407,-0.0000218838,-1.7761435894\N,0.03562
42093,0.0000181284,0.126996513\O,1.2308003292,-0.0000548563,0.10481789
76\O,-0.6947893674,0.0000218152,1.0619503345\O,-0.578370725,0.00001991
42,-1.0558722323\\Version=x86-Linux-G98RevA.7\HF=-0.0598163\RMSD=0.000
e+00\RMSF=8.601e-05\Dipole=0.0764098,0.0000208,-1.0091071\PG=C01 [X(H1
N1O3)]\\@

HNO_3 HF/3-21G

1\1\GINC-MS1\FOpt\RHF\3-21G\H1N1O3\DAN\27-Apr-2003\0\\# OPT FREQ=NORAM
AN RHF/3-21G\\HNO3\\0,1\H,0.070121121,0.0000229534,-1.7509563036\N,0.0
404588766,-0.0000249474,0.1458571229\O,1.2740079517,0.0000283854,0.057
6700571\O,-0.6715049189,-0.0000117221,1.1235901502\O,-0.64666969,0.000
0022965,-1.0900156519\\Version=x86-Linux-G98RevA.7\HF=-277.8308616\RMS
D=4.499e-09\RMSF=1.258e-04\Dipole=0.1755707,-0.0000207,-1.0552216\PG=C
01 [X(H1N1O3)]\\@

HNO_3 HF/6-31+G(d)

1\1\GINC-MS1\FOpt\RHF\6-31+G(d)\H1N1O3\DAN\27-Apr-2003\0\\# OPT FREQ=N
ORAMAN RHF/6-31+G(D)\\HNO3\\0,1\H,0.0599436875,0.0000297228,-1.7117434
506\N,0.0374345764,-0.0000072734,0.1270480836\O,1.2247682177,-0.000052
6493,0.0610430845\O,-0.6494178971,-0.0000047955,1.0776080908\O,-0.6155
985359,0.0000600937,-1.0358503172\\Version=x86-Linux-G98RevA.7\HF=-279
.4536979\RMSD=9.899e-09\RMSF=1.088e-04\Dipole=0.0814806,0.0000118,-1.1
546214\PG=C01 [X(H1N1O3)]\\@

HNO_3 B3-LYP/6-31+G(d)

1\1\GINC-MS1\FOpt\RB3LYP\6-31+G(d)\H1N1O3\DAN\27-Apr-2003\0\\# OPT FRE
Q=NORAMAN RB3LYP/6-31+G(D)\\HNO3\\0,1\H,0.0446663784,0.0000059445,-1.7
533560523\N,0.0505097676,0.0000067203,0.1436676465\O,1.2649862427,-0.0
000085396,0.0496508108\O,-0.6529211765,-0.000003089,1.1190633455\O,-0.
6618444101,0.0000050053,-1.0752538404\\Version=x86-Linux-G98RevA.7\HF=
-280.8952546\RMSD=1.981e-09\RMSF=1.158e-04\Dipole=0.1639426,0.0000095,
-0.9568332\PG=C01 [X(H1N1O3)]\\@

HNO_3 B3-LYP/6-311+G(d,p)

1\1\GINC-MS1\FOpt\RB3LYP\6-311+G(d,p)\H1N1O3\DAN\27-Apr-2003\0\\# OPT
FREQ=NORAMAN RB3LYP/6-311+G(D,P)\\HNO3\\0,1\H,0.0414358418,-0.00000108
27,-1.7495523336\N,0.0522102452,0.0000353802,0.1475330037\O,1.25837942
13,-0.000017175,0.0527171961\O,-0.6484477276,-0.0000178074,1.114098311
\O,-0.6607951385,0.0000041602,-1.0772128437\\Version=x86-Linux-G98RevA
.7\HF=-280.978558\RMSD=9.232e-09\RMSF=8.289e-05\Dipole=0.1702732,0.000
0286,-0.9200061\PG=C01 [X(H1N1O3)]\\@

$NO_3^-(HNO_3)$ AM1

1\1\GINC-MS1\FOpt\RAM1\ZDO\H1N2O6(1-)\DAN\29-Apr-2003\0\\# OPT FREQ=NO
RAMAN RAM1 GUESS=CHECK GEOM=CHECK\\HNO3\\-1,1\H,0.249970273,0.24986576
78,-0.1950359363\N,2.1261407211,-0.0037938469,0.0962767608\O,1.8754087
722,-0.9152542889,0.8317064632\O,3.2212042065,0.3969772567,-0.18307809
74\O,1.1380604112,0.6369391173,-0.4728532459\N,-2.1125250432,-0.040073
1301,-0.0596307485\O,-1.4441431696,-0.6345732921,-0.9042849917\O,-1.51
44967779,0.6981835394,0.7220007033\O,-3.3191934447,-0.1751219485,-0.00
11766002\\Version=x86-Linux-G98RevA.7\HF=-0.2320766\RMSD=0.000e+00\RMS
F=2.110e-05\Dipole=2.0196567,0.1587301,-0.0424945\PG=C01 [X(H1N2O6)]\\
@

$NO_3^-(HNO_3)$ HF/3-21G

1\1\GINC-MS1\FOpt\RHF\3-21G\H1N2O6(1-)\DAN\23-Jan-2003\0\\# OPT FREQ=N
ORAMAN RHF/3-21G GEOM=CHECK GUESS=CHECK\\nitric_dimer\\-1,1\N,2.101099
4897,-0.1523365927,-0.0052399943\O,1.0182317694,0.6493530662,0.0203365
463\H,-0.0000566345,-0.0000954802,0.0002169047\O,3.2186254265,0.397617
7868,0.0116772159\O,1.9266166951,-1.3893470869,-0.0441795084\N,-2.1010
966368,0.1523417612,0.0052523167\O,-1.9265002305,1.3893478201,0.043600
1417\O,-3.2186755096,-0.3974947042,-0.0116597209\O,-1.0182935677,-0.64
94694693,-0.0198125698\\Version=x86-Linux-G98RevA.7\HF=-555.1869223\RM
SD=5.516e-09\RMSF=2.989e-05\Dipole=-0.0002193,-0.0000346,0.000138\PG=C
01 [X(H1N2O6)]\\@

$NO_3^-(HNO_3)$ HF/6-31+G(d)

1\1\GINC-MS1\FOpt\RHF\6-31+G(d)\H1N2O6(1-)\DAN\29-Apr-2003\0\\# OPT FR
EQ=NORAMAN RHF/6-31+G(D)\\Nitric dimer\\-1,1\N,-1.1441804677,0.0002976
371,-1.8057362578\O,-1.1665456154,0.0002877885,-0.5557438431\H,0.25420
21741,-0.000287805,0.1447739941\O,-2.1892597288,0.0008560106,-2.415053
8377\O,-0.0681036372,-0.0007097222,-2.3742361338\N,1.1236149526,-0.000
3907027,1.8383046461\O,0.0544165661,0.0005515348,2.3637215373\O,2.1760

859,-0.0002341255,2.396117523\O,1.1796260693,-0.0006340781,0.538600665
2\\Version=x86-Linux-G98RevA.7\HF=-558.4345248\RMSD=2.899e-09\RMSF=1.0
44e-04\Dipole=0.811129,-0.0004701,1.1703445\PG=C01 [X(H1N2O6)]\\@

$NO_3^-(HNO_3)$ B3-LYP/6-31+G(d)

1\1\GINC-MS1\FOpt\RB3LYP\6-31+G(d)\H1N2O6(1-)\DAN\24-Jan-2003\0\\# OPT
=RCFC RB3LYP/6-31+G(D)\\Nitric dimer\\-1,1\N,-1.1489778752,0.000165484
8,-1.7859977459\O,-1.1411444511,-0.0001507361,-0.4832696\H,0.142447313
1,-0.0000702551,0.0621656908\O,-2.2486315801,0.000099081,-2.3634048373
\O,-0.0615060226,0.000520674,-2.3965937605\N,1.1368242252,-0.000160967
7,1.8084733555\O,0.0460558876,-0.0002337342,2.3790703716\O,2.232792735
,-0.0001738639,2.3662455008\O,1.1652619607,-0.0000565915,0.4705154557\
\Version=x86-Linux-G98RevA.7\HF=-561.321981\RMSD=3.424e-09\RMSF=2.112e
-05\Dipole=0.4440144,-0.0000847,0.6541079\PG=C01 [X(H1N2O6)]\\@

$NO_3^-(HNO_3)$ B3-LYP/6-311+G(d,p)

1\1\GINC-MS4\FOpt\RB3LYP\6-311+G(d,p)\H1N2O6(1-)\DAN\28-Feb-2003\0\\#
OPT FREQ=NORAMAN RB3LYP/6-311+G(D,P)\\Nitric dimer\\-1,1\N,-1.12732606
55,-0.0001508988,-1.7950863996\O,-1.1123378731,-0.0000559513,-0.489687
8992\H,0.0980398462,-0.0000597094,0.0442241745\O,-2.2263364282,-0.0000
046936,-2.3548759608\O,-0.05085498,-0.0001266236,-2.4071158261\N,1.118
7850668,0.0001059949,1.810730501\O,0.0353713067,0.0002718588,2.3861608
352\O,2.2101430398,0.0000519832,2.3662254755\O,1.1392333279,-0.0000898
19,0.4800767649\\Version=x86-Linux-G98RevA.7\HF=-561.4819139\RMSD=8.85
3e-09\RMSF=4.231e-05\Dipole=0.3013201,-0.0000478,0.4509761\PG=C01 [X(H
1N2O6)]\\@

$NO_3^-(HNO_3)_2$ AM1

1\1\GINC-MS2\FOpt\RAM1\ZDO\H2N3O9(1-)\DAN\16-Apr-2003\0\\# OPT FREQ=NO
RAMAN RAM1 GEOM=CHECK GUESS=CHECK\\Nitric trimer\\-1,1\N,0.0092215252,
1.3772781105,-0.0117879656\O,0.0034024495,0.1421184125,-0.000795909\H,
2.0358854393,0.1041550499,0.344822136\O,-1.0445843045,1.9678814209,-0.
1846582141\O,1.068633941,1.9608570458,0.150619503\N,3.71305731,-0.7240
641259,-0.0508252599\O,3.5163030014,-0.5257294237,-1.2149273418\O,4.67
46747794,-1.2527920241,0.4282238001\O,2.8032374982,-0.3400905829,0.812
2302236\O,-2.8031380324,-0.3236917243,-0.805636981\H,-2.0282851506,0.1
150611175,-0.3455051772\N,-3.7229532941,-0.6702703313,0.0626563667\O,-
3.5238673156,-0.4538851177,1.2231410476\O,-4.6950219016,-1.1871457241,
-0.4081484969\\Version=x86-Linux-G98RevA.7\HF=-0.317693\RMSD=0.000e+00
\RMSF=1.051e-05\Dipole=-0.0025527,-0.9282308,0.0087325\PG=C01 [X(H2N3O
9)]\\@

$NO_3^-(HNO_3)_2$ HF/3-21G

1\1\GINC-MS1\FOpt\RHF\3-21G\H2N3O9(1-)\DAN\26-Mar-2003\0\\# OPT FREQ=N
ORAMAN RHF/3-21G GUESS=CHECK GEOM=CHECK\\Nitric trimer\\-1,1\N,-0.2634
923232,2.0103810483,-0.1014432316\O,0.0952872838,0.714692223,-0.251890
5647\H,1.5186703201,0.4997912383,0.0631903879\O,-1.4530759853,2.301924
048,-0.3201321843\O,0.6235103933,2.8155056827,0.2367219369\N,2.8258818
719,-0.9622122802,-0.0051454763\O,1.919980218,-1.6767936463,-0.4583358
53\O,3.9894882297,-1.3026323856,0.2123321799\O,2.5224899827,0.34650968
15,0.2886626377\O,-1.8515438799,-0.7390904965,-0.9151059791\H,-1.08757
81409,-0.1252097354,-0.5846486369\N,-2.6157230686,-1.0883437207,0.1724
084523\O,-2.2505316278,-0.6875880129,1.2858066334\O,-3.6028243071,-1.7
841966983,-0.070468802\\Version=x86-Linux-G98RevA.7\HF=-833.0657877\RM
SD=9.582e-09\RMSF=6.614e-06\Dipole=0.1810093,-0.1505346,-0.1690025\PG=
C01 [X(H2N3O9)]\\@

$NO_3^-(HNO_3)_2$ HF/6-31+G(d)

1\1\GINC-MS1\FOpt\RHF\6-31+G(d)\H2N3O9(1-)\DAN\29-Mar-2003\0\\# OPT FR
EQ=NORAMAN RHF/6-31+G(D)\\Nitric trimer\\-1,1\N,0.2573864778,-0.437250
2863,-2.0743714089\O,0.1894779278,-0.3710630114,-0.8129898738\H,1.6685
550791,-0.4496454483,-0.0383840784\O,-0.7664356207,-0.3799277307,-2.70
78210471\O,1.3445599237,-0.557406798,-2.5834566877\N,2.4291017448,-0.4
796737971,1.6818497838\O,1.3291050612,-0.4157251491,2.1327217799\O,3.4
434750109,-0.5316098751,2.2970154776\O,2.5621529894,-0.4975082985,0.38
12720951\O,-2.2436879405,-0.2044898151,0.2454818086\H,-1.3685151159,-0
.1411735473,-0.2033697812\N,-2.7246877917,0.9959144083,0.435718975\O,-
2.0678236205,1.9253242398,0.0904236381\O,-3.7949041038,1.0371422782,0.
9497743605\\Version=x86-Linux-G98RevA.7\HF=-837.9226686\RMSD=9.471e-09
\RMSF=2.128e-05\Dipole=0.0443206,-0.106739,0.7702133\PG=C01 [X(H2N3O9)
]\\@

$NO_3^-(HNO_3)_2$ B3-LYP/6-31+G(d)

1\1\GINC-MS1\FOpt\RB3LYP\6-31+G(d)\H2N3O9(1-)\DAN\02-Apr-2003\0\\# OPT
FREQ=NORAMAN RB3LYP/6-31+G(D)\\Nitric trimer\\-1,1\N,0.156201624,-0.3
081657645,-2.1050059219\O,0.1699123058,-0.3190708562,-0.7885748756\H,1
.6286961235,-0.3003238965,-0.1768573628\O,-0.9423640373,-0.3203438729,
-2.673913994\O,1.2453138127,-0.2895974328,-2.6945280275\N,2.5490988707
,-0.3799522703,1.5349052876\O,1.4501331662,-0.4637104691,2.0699558269\
O,3.6368608614,-0.3727977099,2.0914799826\O,2.598018301,-0.2850146997,
0.180561017\O,-2.1614171488,-0.4349016347,0.3860263209\H,-1.282815394,
-0.2736521445,-0.1232479795\N,-2.7513342566,0.7676781674,0.6141088247\
O,-2.1713993459,1.7778823732,0.2386828988\O,-3.8280134646,0.7096861912
,1.1893168522\\Version=x86-Linux-G98RevA.7\HF=-842.2503941\RMSD=3.311e

-09\RMSF=5.109e-06\Dipole=0.0706468,-0.1147502,0.526063\PG=C01 [X(H2N3
O9)]\\@

$NO_3^-(HNO_3)_2$ B3-LYP/6-311+G(d,p)

1\1\GINC-MS4\FOpt\RB3LYP\6-311+G(d,p)\H2N3O9(1-)\DAN\17-Apr-2003\0\\#
OPT FREQ=NORAMAN RB3LYP/6-311+G(D,P)\\Nitric trimer\\-1,1\N,0.16282320
18,-0.3979056044,-2.1247031944\O,0.1624142882,-0.4062915976,-0.8070922
667\H,1.5646180315,-0.386194667,-0.153828428\O,-0.9242939004,-0.377293
6292,-2.6989661841\O,1.2518869793,-0.4156939183,-2.6978265921\N,2.4257
767789,-0.431227536,1.5934115599\O,1.3155743094,-0.4930986504,2.091435
612\O,3.4884714336,-0.4181932071,2.1817631581\O,2.5185534387,-0.371115
5542,0.2402000696\O,-2.131125045,-0.3318392645,0.3767162389\H,-1.24720
60863,-0.2554723253,-0.1385941842\N,-2.6308359705,0.9157900894,0.57174
32434\O,-1.9841885826,1.8644073471,0.1676056255\O,-3.7000129233,0.9535
020178,1.1473220076\\Version=x86-Linux-G98RevA.7\HF=-842.4929389\RMSD=
6.573e-09\RMSF=3.105e-05\Dipole=0.055128,-0.119917,0.4741074\PG=C01 [X
(H2N3O9)]\\@

$NO_3^-(HNO_3)_3$ HF/3-21G

1\1\GINC-MS4\FOpt\RHF\3-21G\H3N4O12(1-)\DAN\24-Apr-2003\0\\# OPT FREQ=
NORAMAN RHF/3-21G\\tetramer\\-1,1\N,0.0704522049,-0.0107599727,-0.5845
577667\O,-0.2004965406,-0.1698071758,0.703406416\H,1.0819131099,-0.189
3765975,1.5829202542\O,-0.8413722667,0.0667027435,-1.3985193881\O,1.31
16440362,0.0544199889,-0.9110458537\N,1.4534970486,-0.3023667388,3.483
7666222\O,0.2283334397,-0.3500271964,3.6598986288\O,2.3285194135,-0.33
24828947,4.3435692406\O,1.9044274518,-0.2060243198,2.1803466773\O,-2.7
210250813,-0.1064368639,1.2067990601\H,-1.7302461676,-0.0791128181,0.9
874257461\N,-3.1769684088,1.1973454557,1.1805141101\O,-2.3496384347,2.
0818575551,0.9231405005\O,-4.3712692163,1.3441199143,1.4201241306\N,1.
5517640667,-0.8762827593,-4.0890044758\O,1.7009177893,0.3291440167,-3.
4303881465\H,1.4981204387,0.1626519696,-2.4471886982\O,1.2347716706,-1
.8591005826,-3.4063208241\O,1.7575625185,-0.8460794912,-5.2982837829\\
Version=x86-Linux-G98RevA.7\HF=-1110.9350474\RMSD=5.814e-09\RMSF=2.876
e-05\Dipole=0.2293486,-0.0575386,0.0271209\PG=C01 [X(H3N4O12)]\\@

$NO_3^-(HNO_3)_3$ HF/6-31+G(d)

1\1\GINC-MS4\FOpt\RHF\6-31+G(d)\H3N4O12(1-)\DAN\29-Apr-2003\0\\# OPT F
REQ=NORAMAN RHF/6-31+G(D)\\nitric tetramer\\-1,1\N,-0.1779668715,-0.02
86167532,-0.6293510244\O,-0.1715656117,-0.0307866725,0.6180975757\H,1.
3991930547,-0.0335373479,1.3406184317\O,-1.2172682115,-0.0051479675,-1
.2251941291\O,0.9022751123,-0.0508755208,-1.2079579311\N,2.2313444281,
-0.0387139225,3.0169376164\O,1.1481420424,-0.0518883756,3.510138568\O,

3.271824744,-0.0332163837,3.5838917481\O,2.3078409175,-0.0301564424,1.
707564454\O,-2.5510509978,-0.0052815701,1.9032517263\H,-1.7237677921,0
.1070586065,1.3931627503\N,-3.0471837398,1.1782501174,2.171982793\O,-2
.4468619988,2.1320045918,1.7921557399\O,-4.0647035066,1.1721259021,2.7
801556873\N,0.9297978463,-1.107664149,-4.523915751\O,0.9911412876,0.03
78591621,-3.8888137313\H,0.8801838708,-0.1218492626,-2.9278270973\O,0.
7826157156,-2.0948084282,-3.8774457581\O,1.0341666602,-1.0366356758,-5
.70278514\\Version=x86-Linux-G98RevA.7\HF=-1117.4050496\RMSD=5.781e-09
\RMSF=1.883e-05\Dipole=0.3014142,-0.021772,0.0859884\PG=C01 [X(H3N4O12
)]\\@

$NO_3^-(HNO_3)_3$ B3-LYP/6-31+G(d)

1\1\GINC-MS4\FOpt\RB3LYP\6-31+G(d)\H3N4O12(1-)\DAN\03-May-2003\0\\# OP
T FREQ=NORAMAN RB3LYP/6-31+G(D)\\nitric tetramer\\-1,1\N,-0.1679013424
,-0.0282058217,-0.6236772044\O,-0.1549458906,-0.0372380248,0.666898622
5\H,1.3676971839,-0.0188628334,1.325683826\O,-1.2382694777,-0.03006393
58,-1.2310870962\O,0.9502884151,-0.01773437,-1.2096891814\N,2.23891262
,-0.047075813,3.0479553302\O,1.1257199027,-0.0937699787,3.5538938739\O
,3.3136288203,-0.0342109882,3.6215085418\O,2.318868936,-0.0045292636,1
.6836884874\O,-2.5300851256,-0.0580354007,1.8845841741\H,-1.6625577102
,0.0606957619,1.3727496265\N,-3.0606718034,1.1859458297,2.0847028856\O
,-2.4357686618,2.1485224084,1.6630108414\O,-4.1246682339,1.1945993151,
2.6784878465\N,0.914615735,-1.1102074435,-4.4763599261\O,0.9915221343,
0.1008167842,-3.848010751\H,0.8876899621,-0.0615860343,-2.8472840222\O
,0.7679294224,-2.1063275144,-3.7825271185\O,1.0073402713,-1.0599595509
,-5.6906953688\\Version=x86-Linux-G98RevA.7\HF=-1123.1734125\RMSD=7.78
9e-09\RMSF=1.245e-05\Dipole=0.2216411,-0.0054595,0.1148756\PG=C01 [X(H
3N4O12)]\\@

$NO_3^-(HNO_3)_3$ B3-LYP/6-311+G(d,p)

1\1\GINC-MS4\FOpt\RB3LYP\6-311+G(d,p)\H3N4O12(1-)\DAN\07-May-2003\0\\#
OPT FREQ=NORAMAN RB3LYP/6-311+G(D,P)\\nitric tetramer\\-1,1\N,-0.2386
387653,-0.6438371117,-0.0753985957\O,0.1462784181,0.5610322708,-0.3201
266122\H,0.0362780464,1.6068182113,0.9258569248\O,-0.1355226083,-1.507
3819241,-0.9354692533\O,-0.713656092,-0.8710292866,1.065979295\N,0.410
211643,3.4554936919,1.3422144509\O,0.79730644,3.5862177431,0.196386529
\O,0.3753499486,4.3000062964,2.2089929532\O,-0.0456094939,2.2241055191
,1.7248995697\O,1.2709663507,1.0521814001,-2.6610714616\H,0.9262371378
,0.7907311847,-1.7484913077\N,2.6148124295,0.8000986862,-2.6841706443\
O,3.1258025227,0.3541243436,-1.675325103\O,3.1589391067,1.0570352173,-
3.7348983701\N,-2.7498747319,-3.6045999646,1.344202734\O,-1.4741617932
,-3.2865135721,1.7192382879\H,-1.2613801752,-2.3634446139,1.354980684\
O,-3.3783262784,-2.7784504974,0.7115684873\O,-3.1219551505,-4.70185149

71,1.6972904386\\Version=x86-Linux-G98RevA.7\HF=-1123.498327\RMSD=7.19
8e-09\RMSF=1.719e-05\Dipole=0.1940998,-0.0477967,0.0957509\PG=C01 [X(H
3N4O12)]\\@

Appendix C: Breakdown diagrams of $HSO_4^-(H_2SO_4)_n$ at various gas pressures

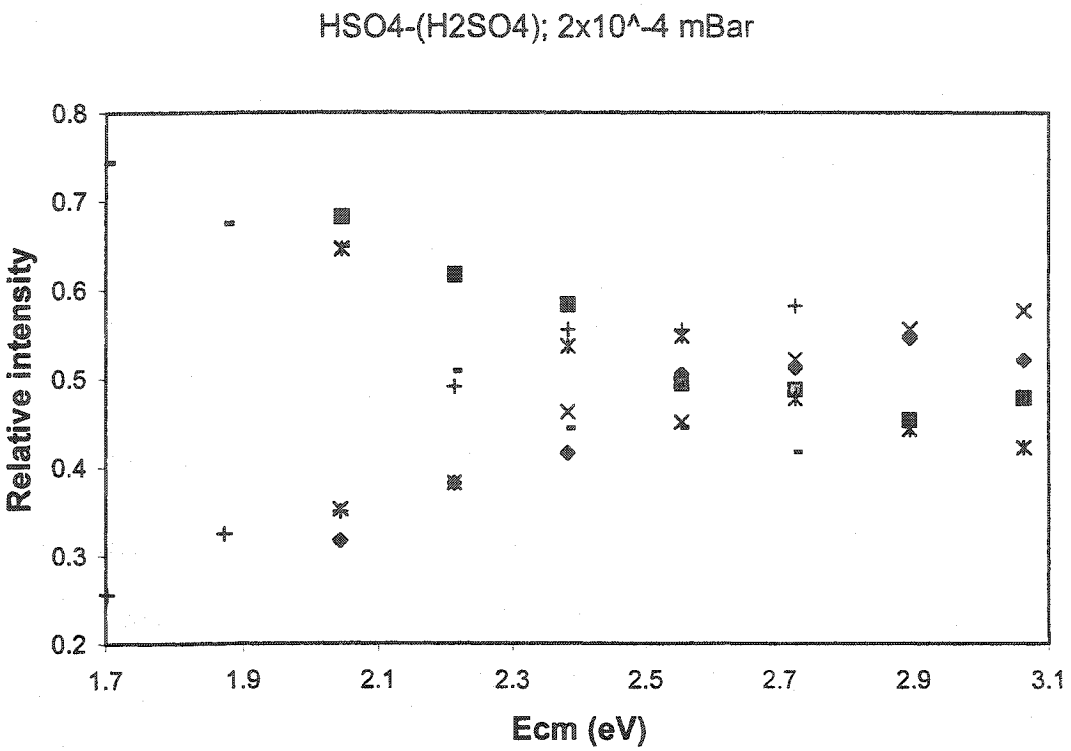

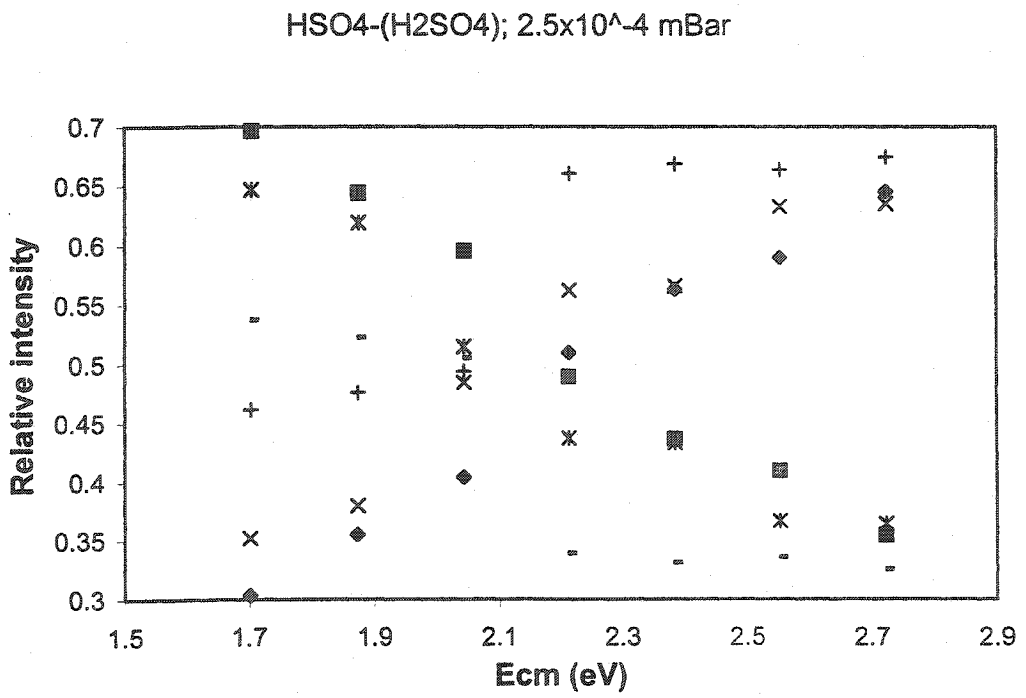

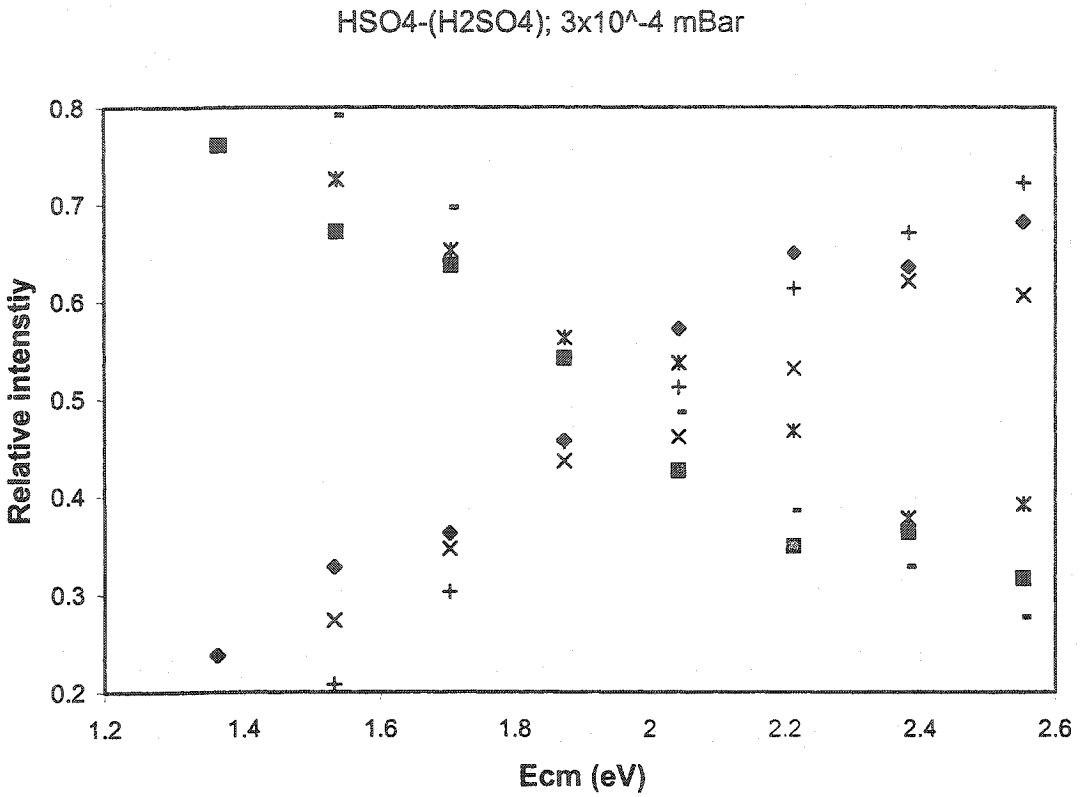
HSO4-(H2SO4); 3x10^-4 mBar
Relative intenstiy
0.8
0.7
0.6
0.5
0.4
0.3
0.2
1.2
1.4
1.6
1.8
2
2.2
2.4
2.6
Ecm (eV)

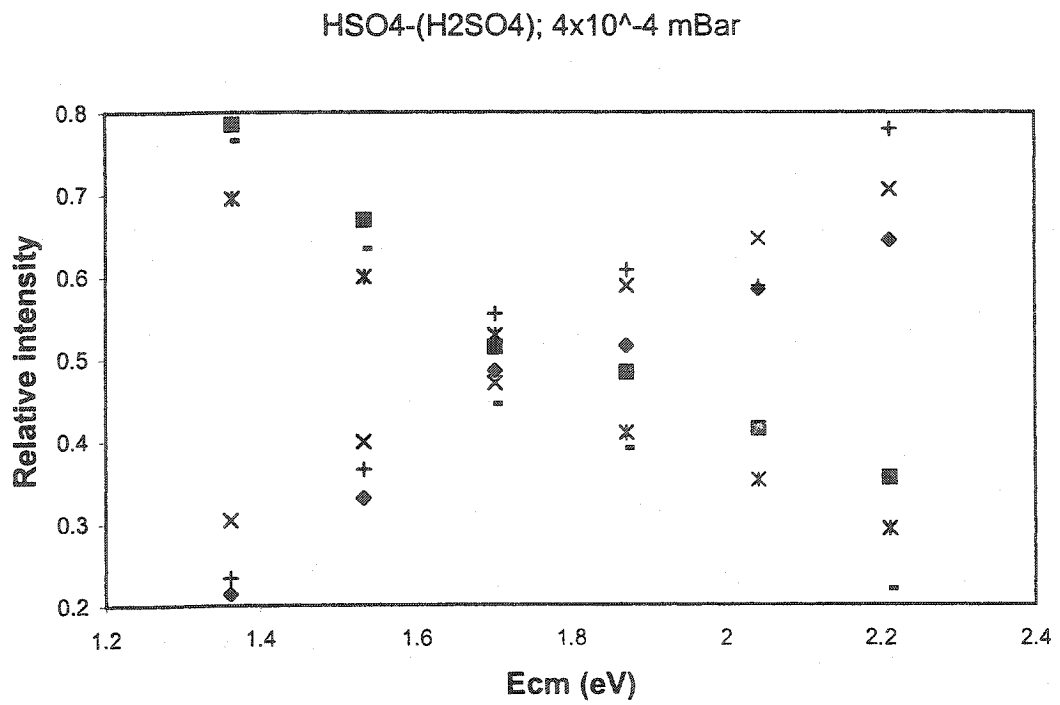
HSO4-(H2SO4); 4x10^-4 mBar
Relative intensity
0.8
0.7
0.6
0.5
0.4
0.3
0.2
1.2
1.4
1.6
1.8
2
2.2
2.4
Ecm (eV)

HSO4-(H2SO4); 8x10^-4 mBar

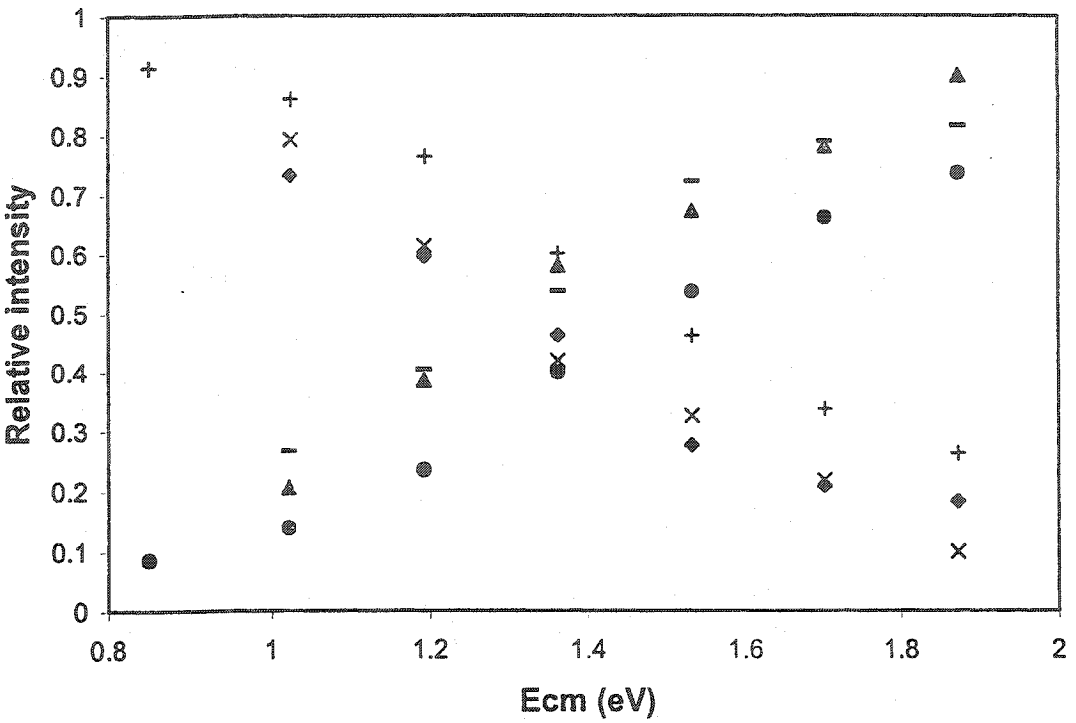

HSO4-(H2SO4)2; 2x10^-4 mBar

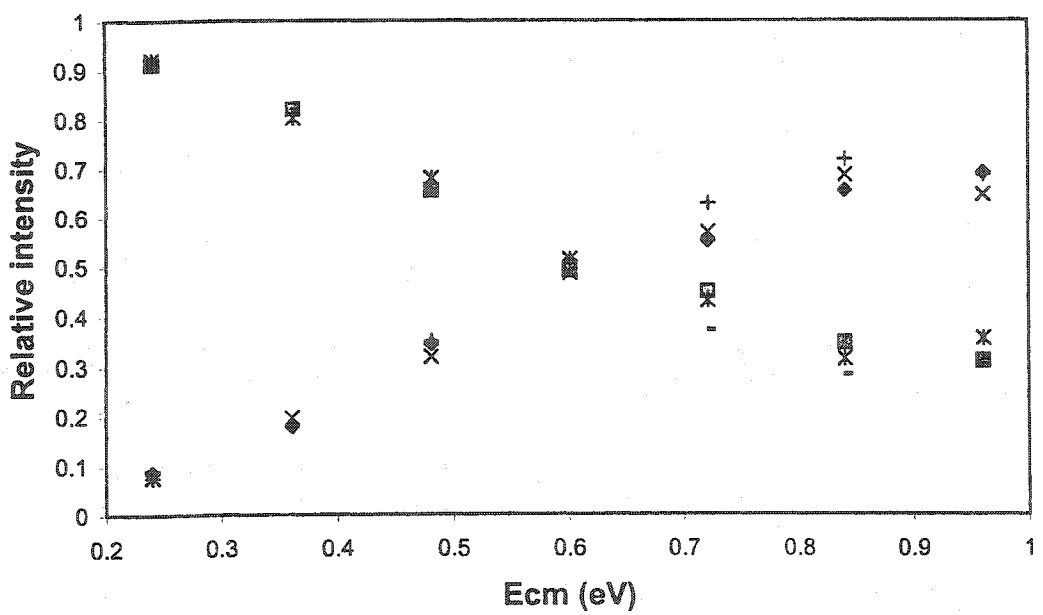

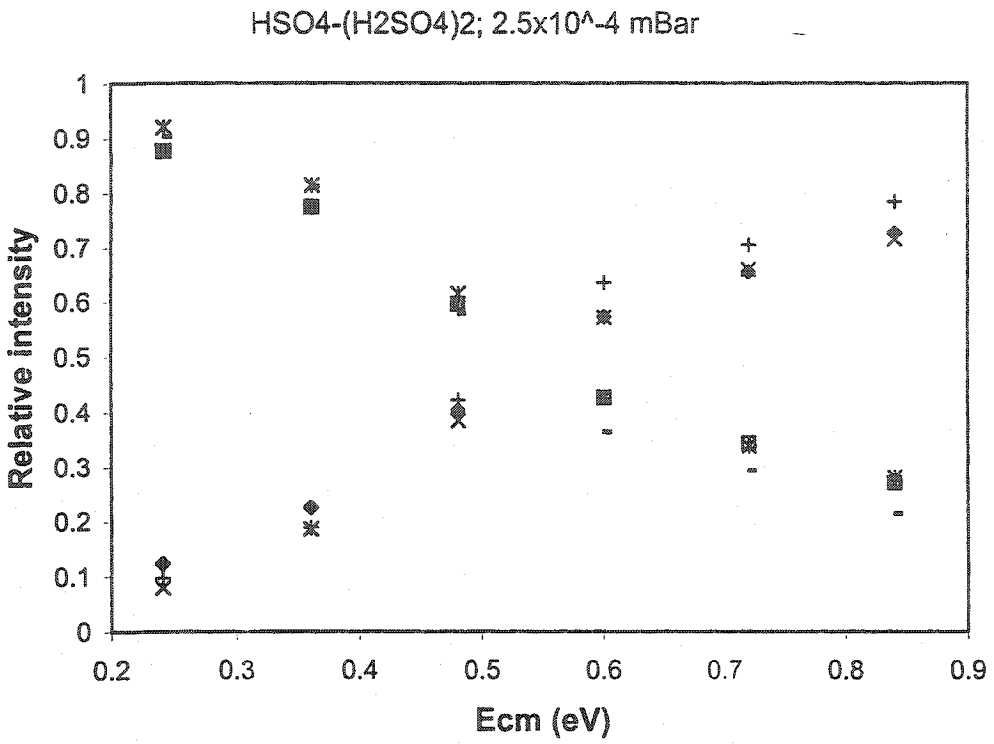
HSO4-(H2SO4)2; 2.5x10^-4 mBar
Relative intensity
Ecm (eV)
0
0.1
0.2
0.3
0.4
0.5
0.6
0.7
0.8
0.9
1
0.2
0.3
0.4
0.5
0.6
0.7
0.8
0.9

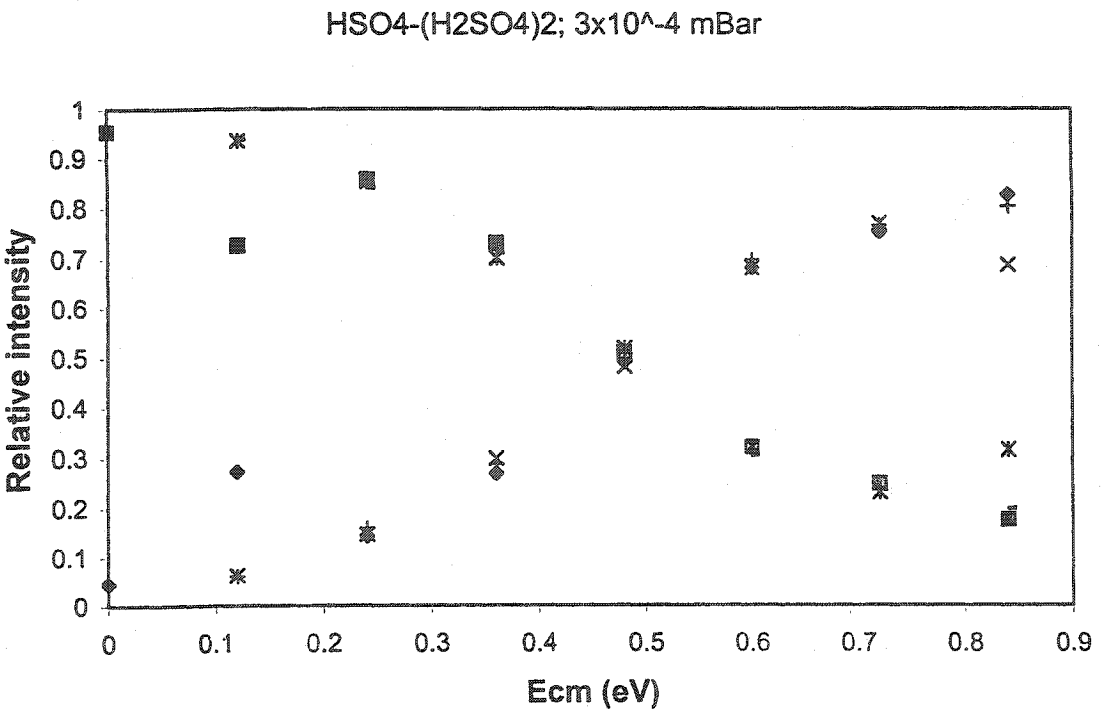
HSO4-(H2SO4)2; 3x10^-4 mBar
Relative intensity
Ecm (eV)
0
0.1
0.2
0.3
0.4
0.5
0.6
0.7
0.8
0.9
1
0
0.1
0.2
0.3
0.4
0.5
0.6
0.7
0.8
0.9

HSO4-(H2SO4)2; 4x10^-4 mBar

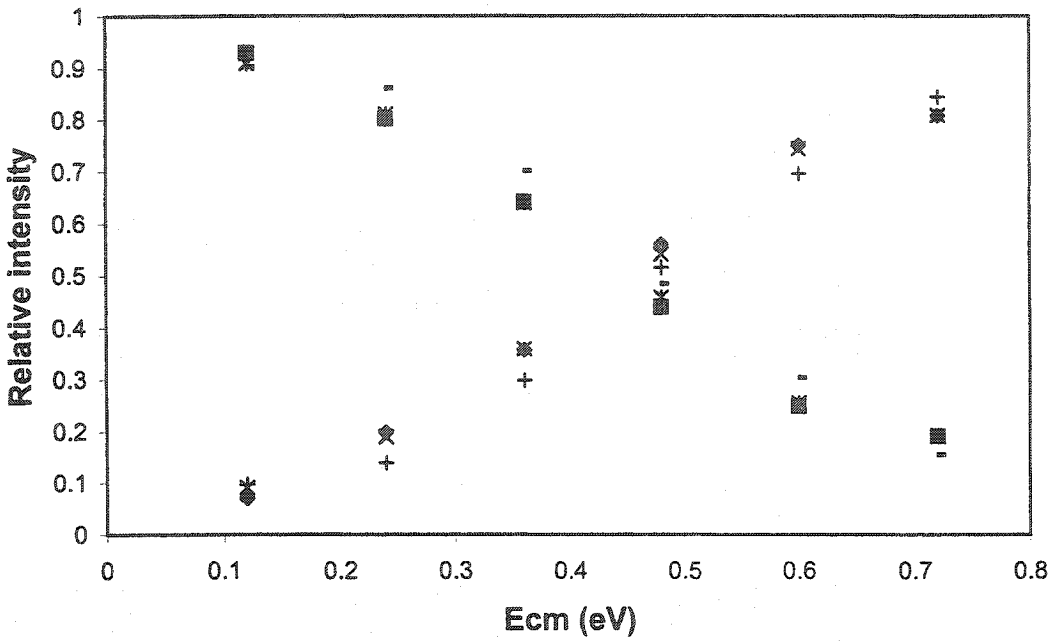

HSO4-(H2SO4)2; 8x10^-4 mBar

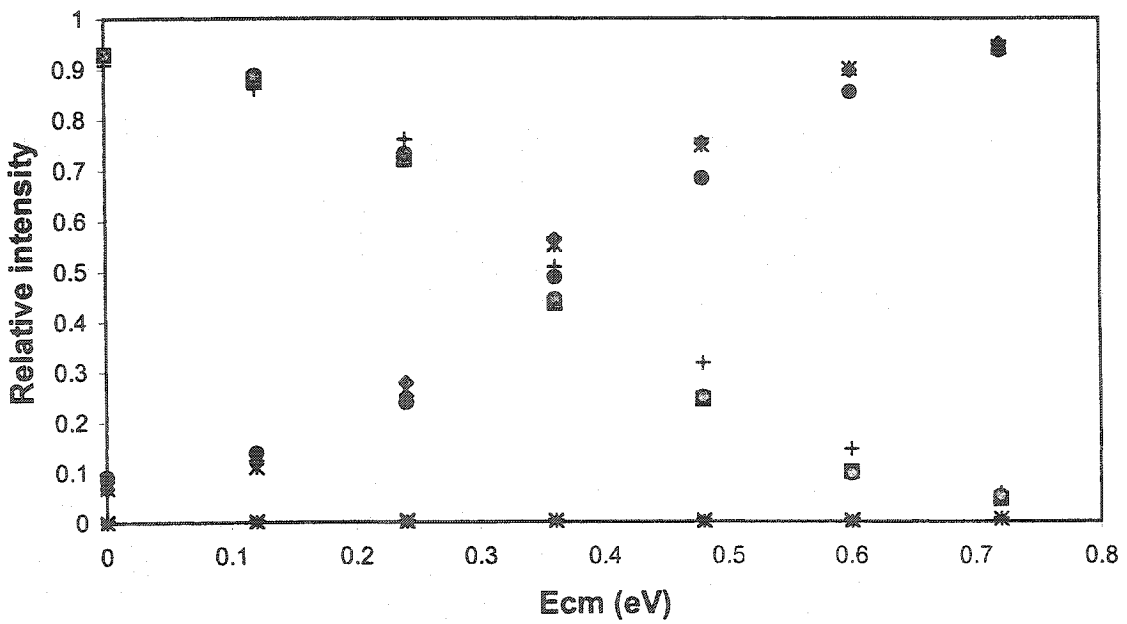

HSO4-(H2SO4)3; 2x10^-4 mBar

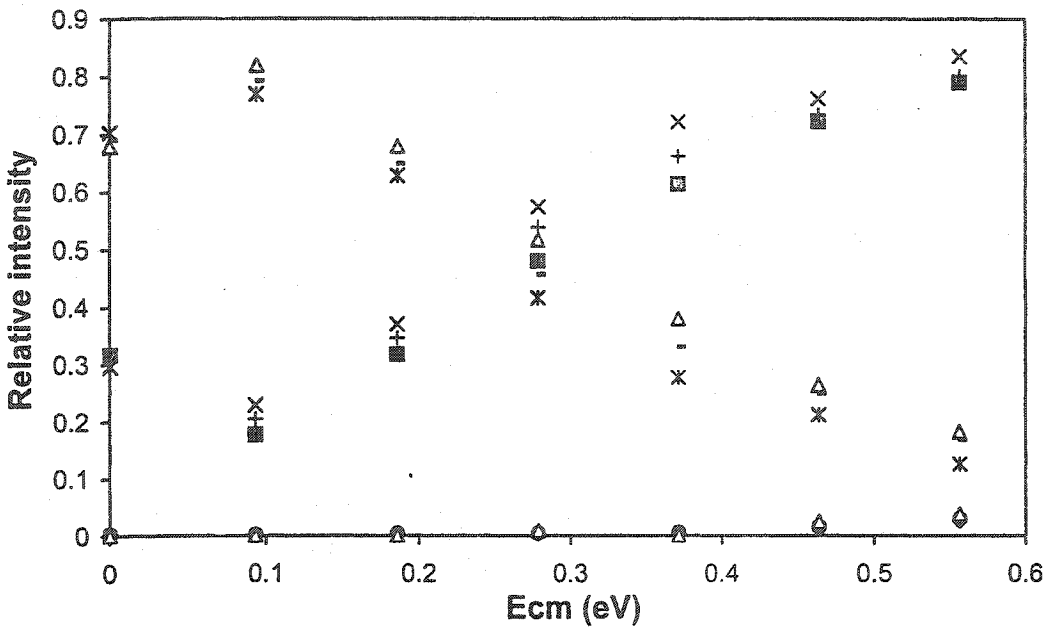

HSO4-(H2SO4)3; 2.5x10^-4 mBar

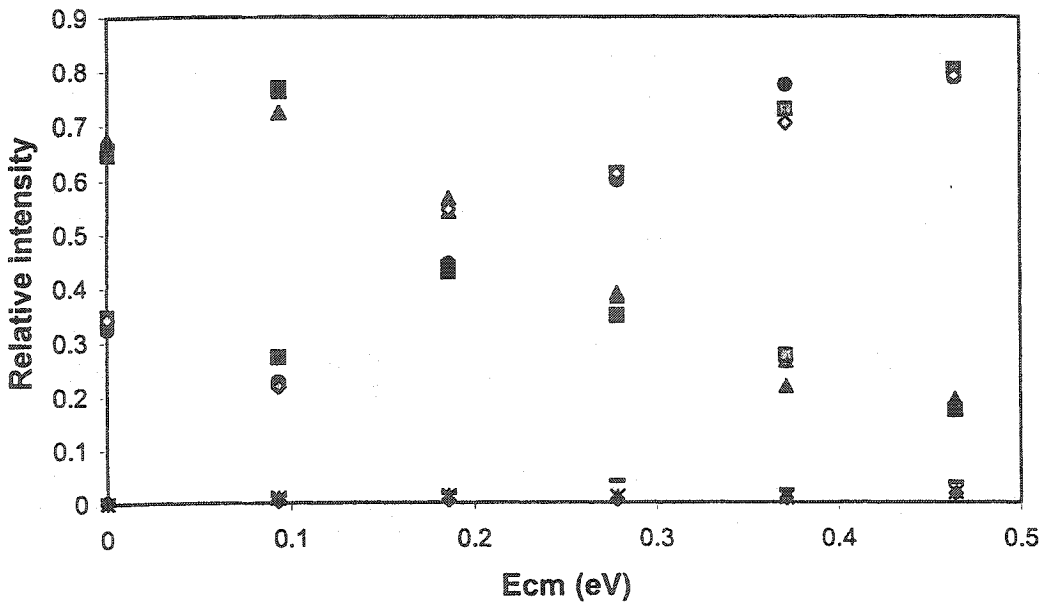

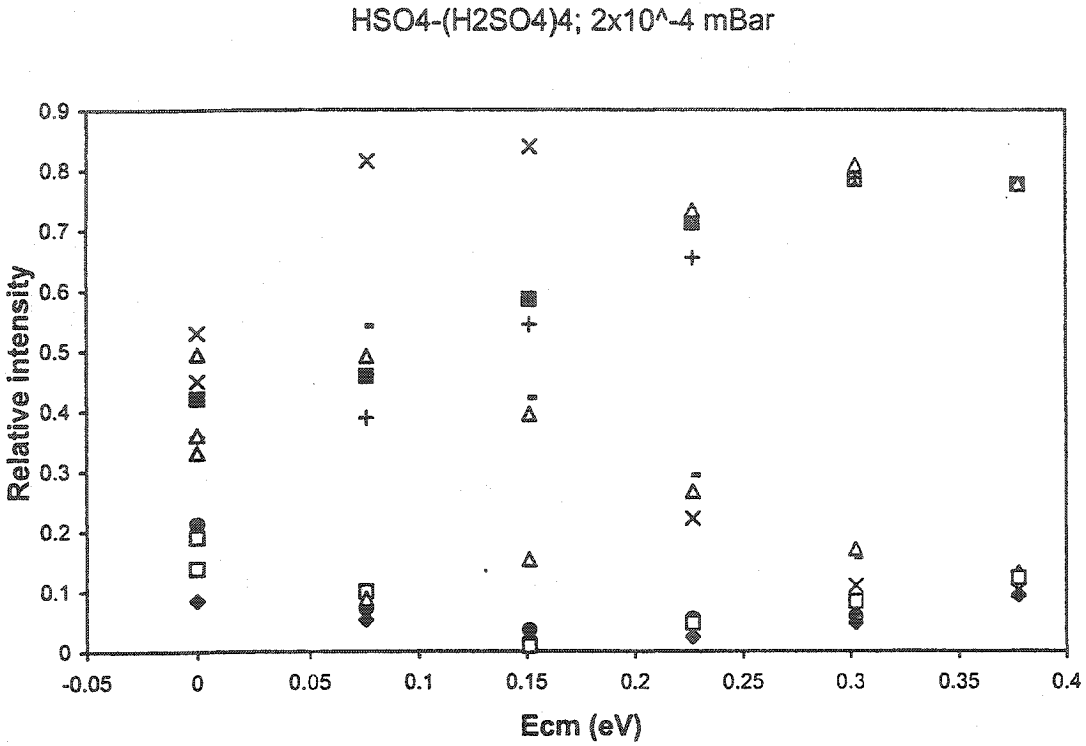
HSO4-(H2SO4)4; 2x10^-4 mBar
Relative intensity
0.9
0.8
0.7
0.6
0.5
0.4
0.3
0.2
0.1
0
-0.05
0
0.05
0.1
0.15
0.2
0.25
0.3
0.35
0.4
Ecm (eV)

Appendix D: Breakdown diagrams of $NO_3^-(HNO_3)_n$ at various gas pressures

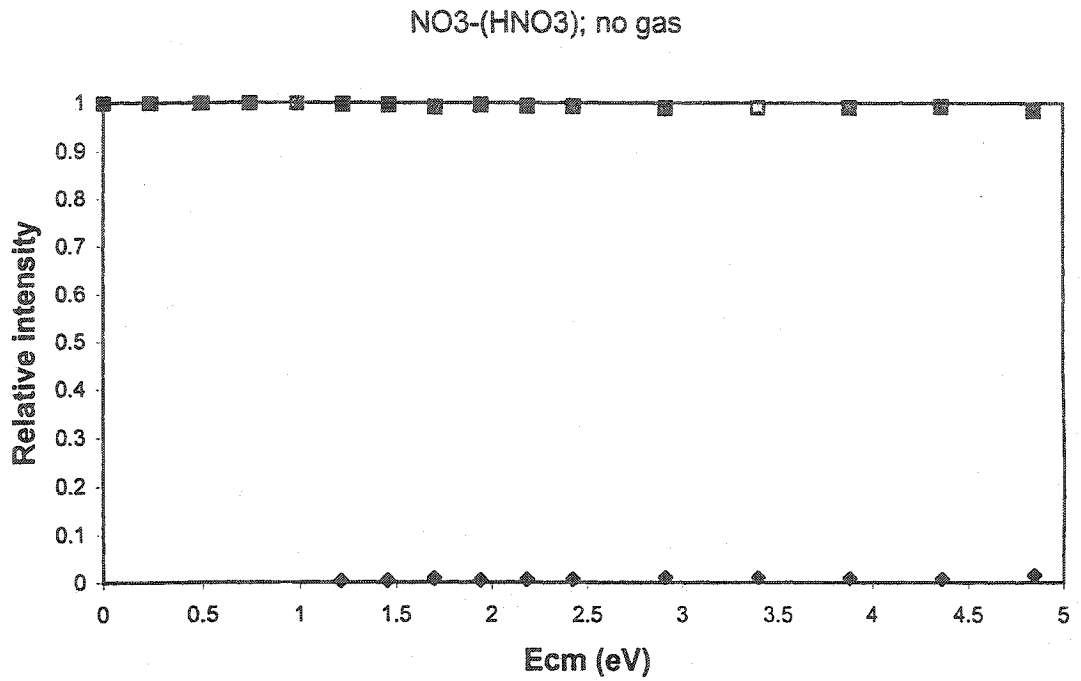

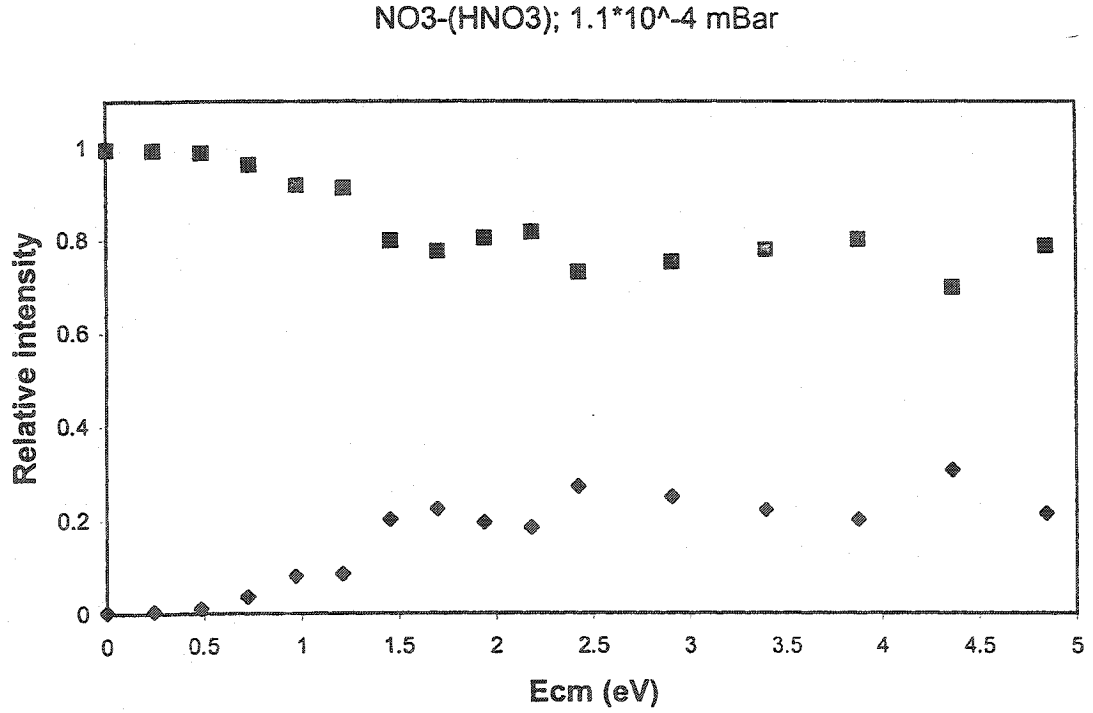

NO3-(HNO3);2*10^-4 mBar

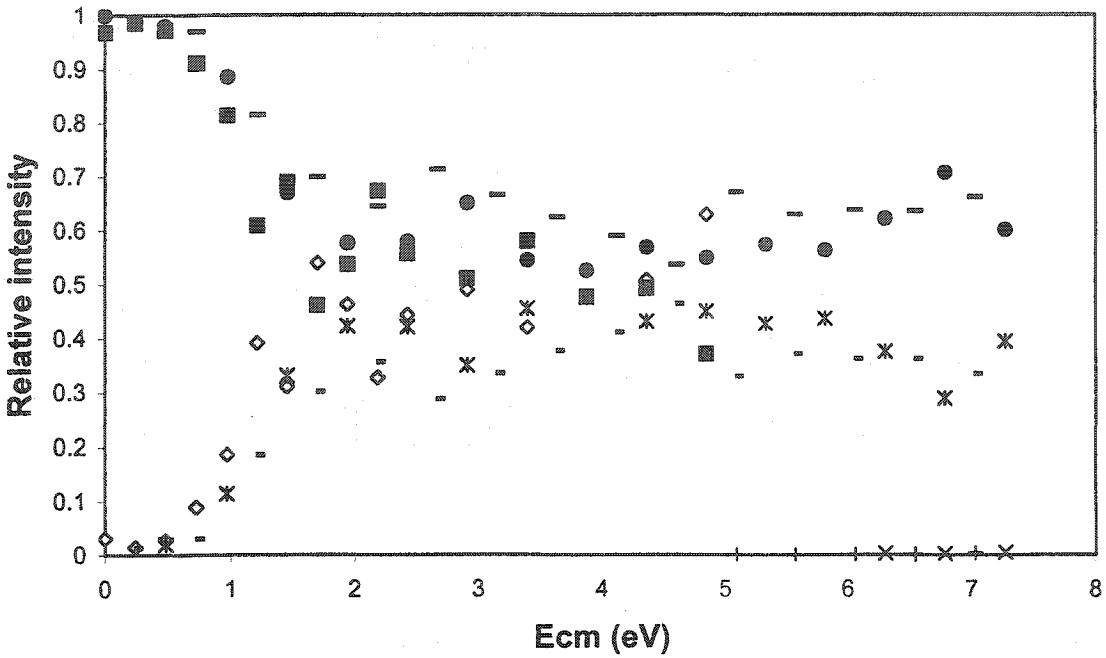

NO3-(HNO3)2; 3* 10^-4 mBar

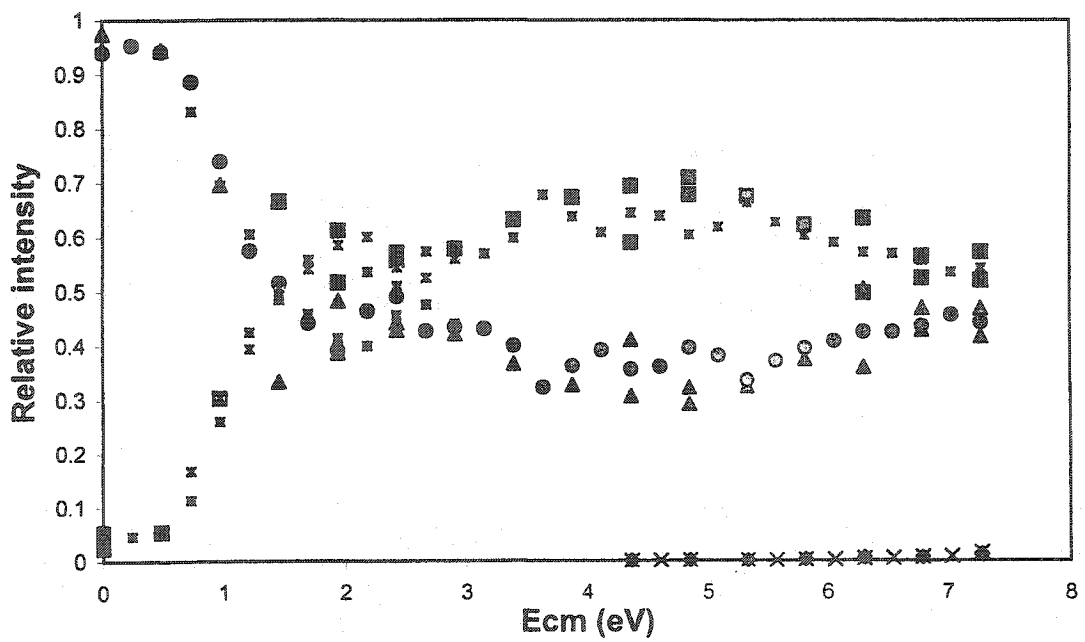

NO3-(HNO3); 4*10^-4 mBar

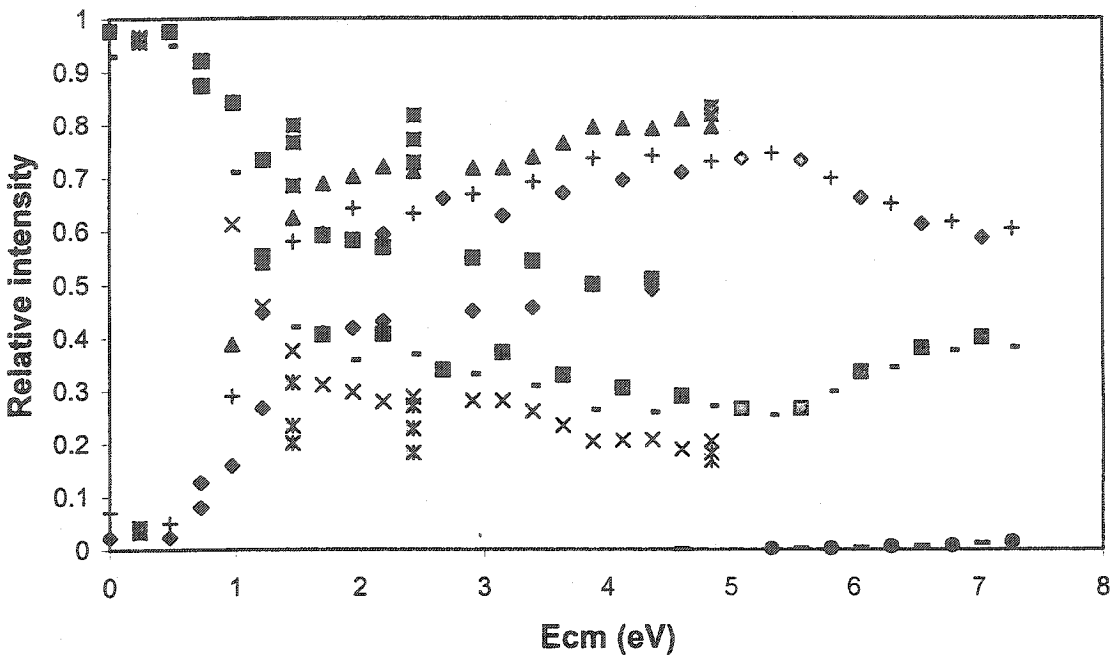

NO3-(HNO3); 8*10^-4 mBar

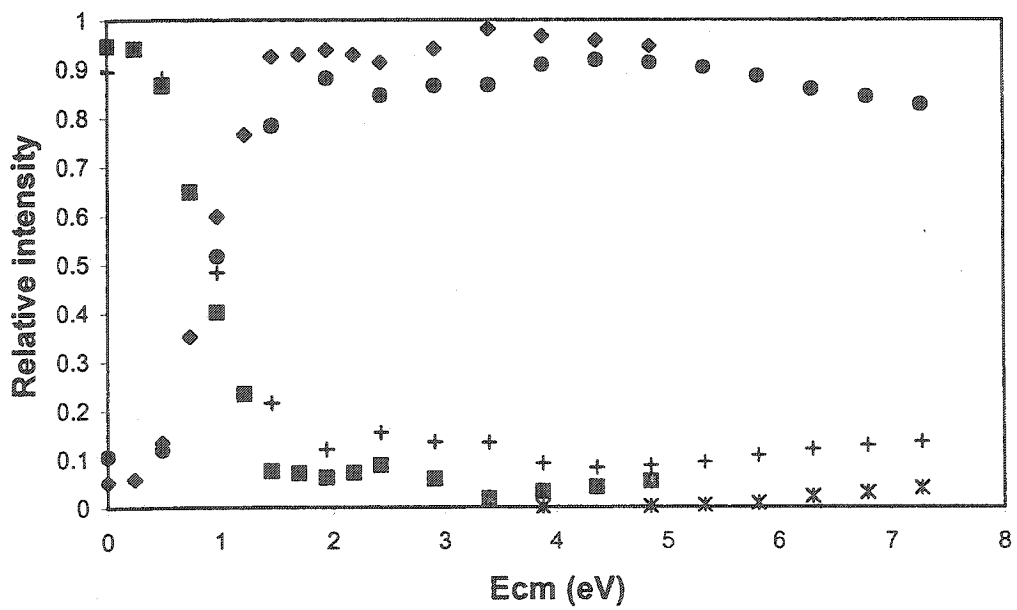

NO3-(HNO3)2; no gas

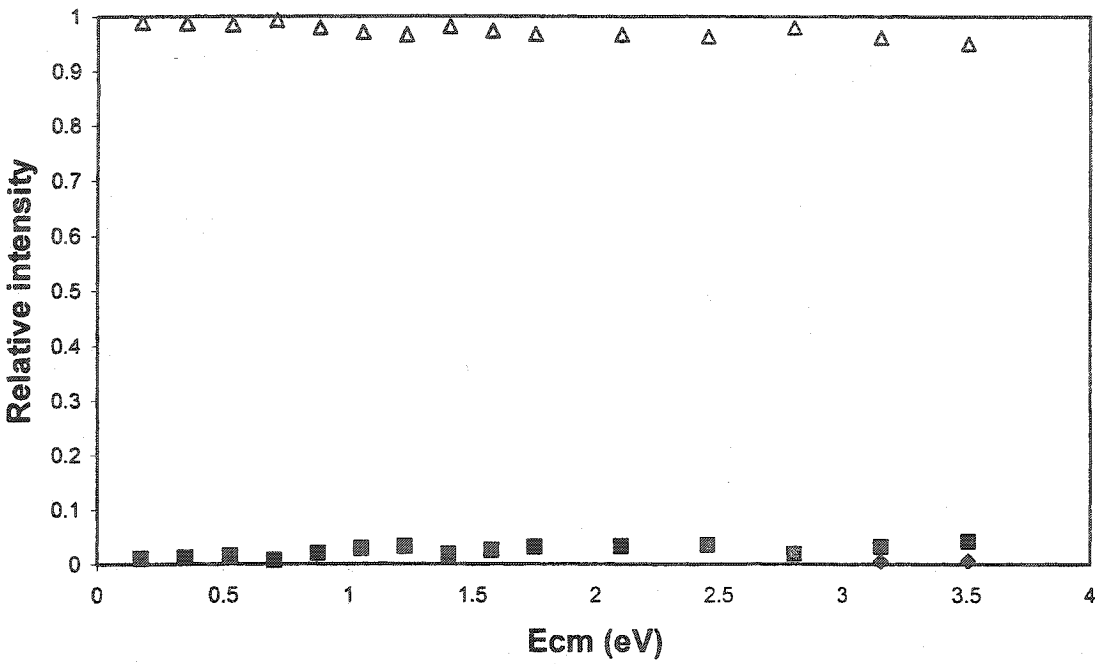

NO3-(HNO3)2; 1.1*10-4 mBar

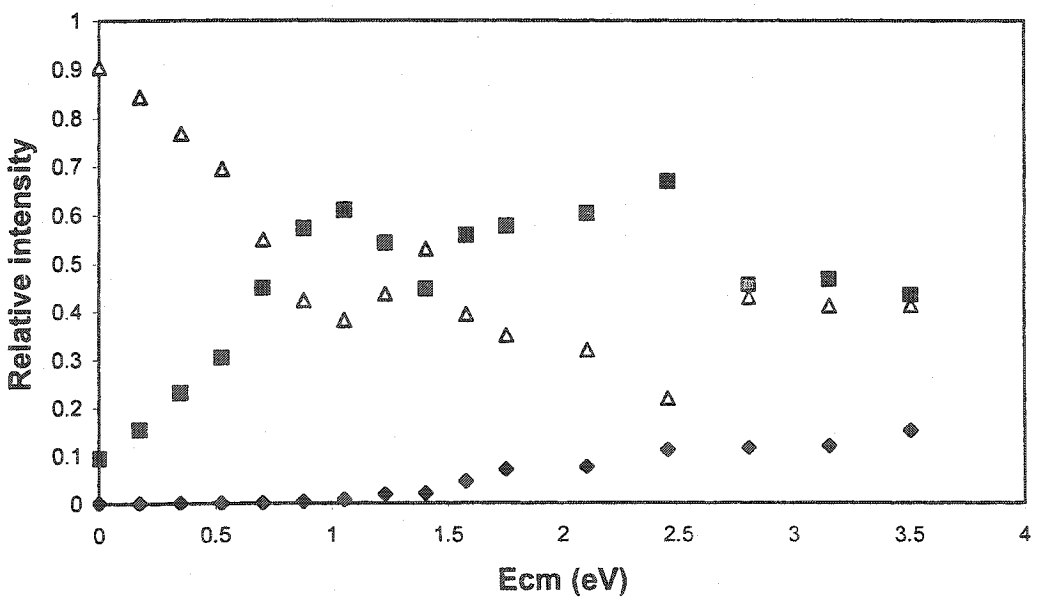

NO3-(HNO3)2; 2*10-4 mBar

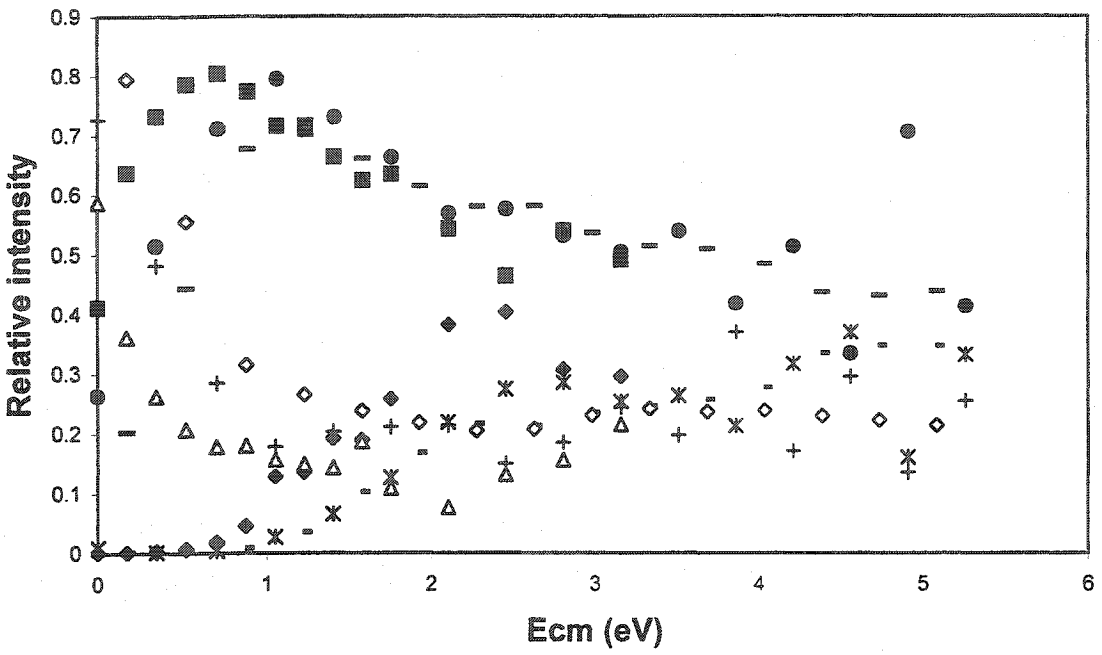

NO3-(HNO3)2; 2.5*10-4 mBar

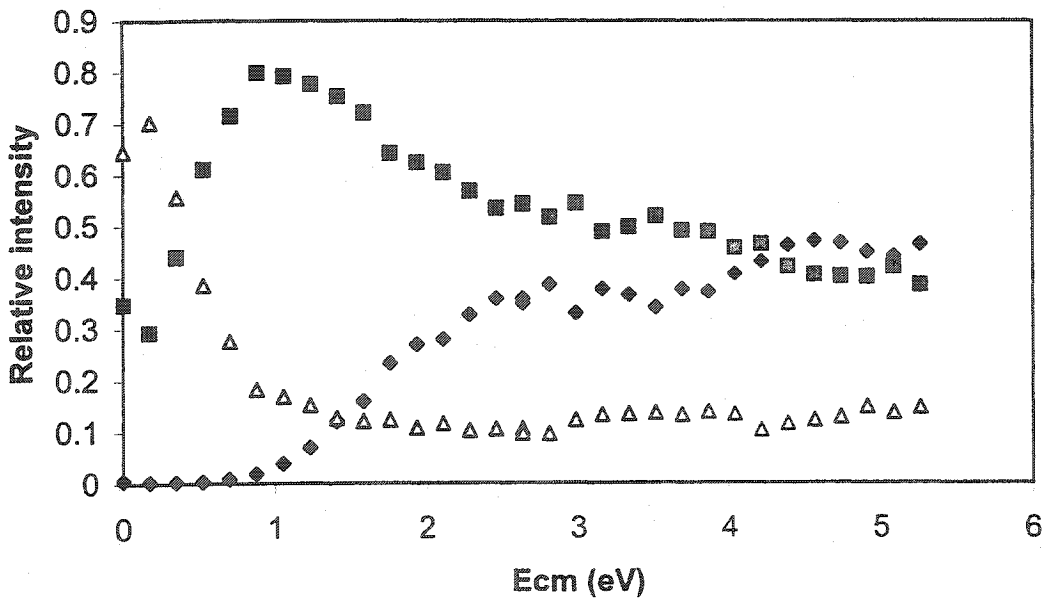

NO3-(HNO3)2; 3.0 e-3 mBar

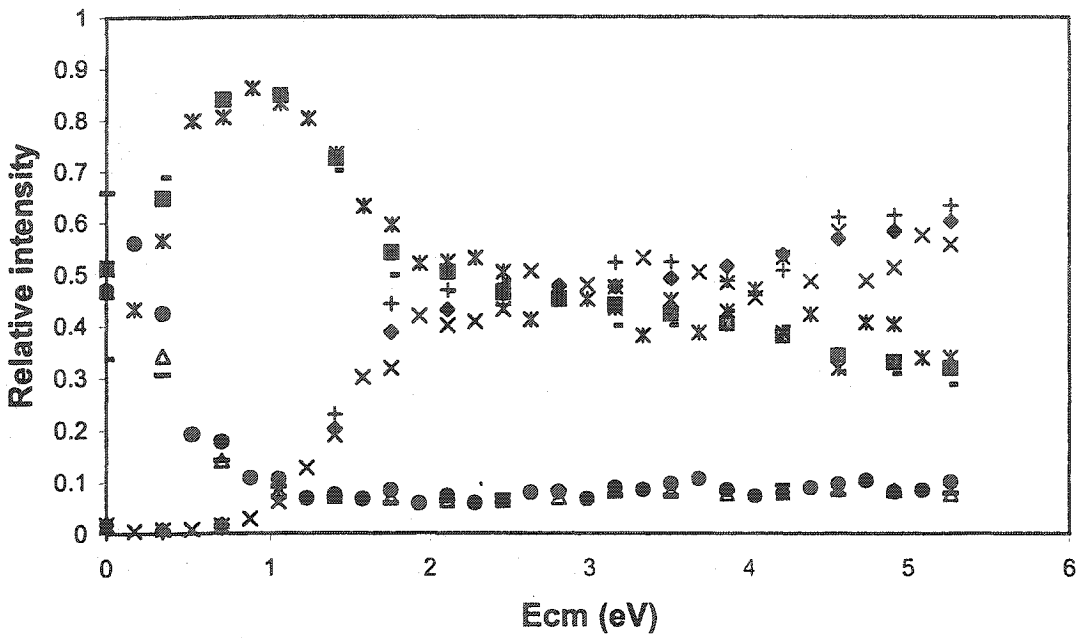

NO3-(HNO3)2; 4*10^-4 mBar

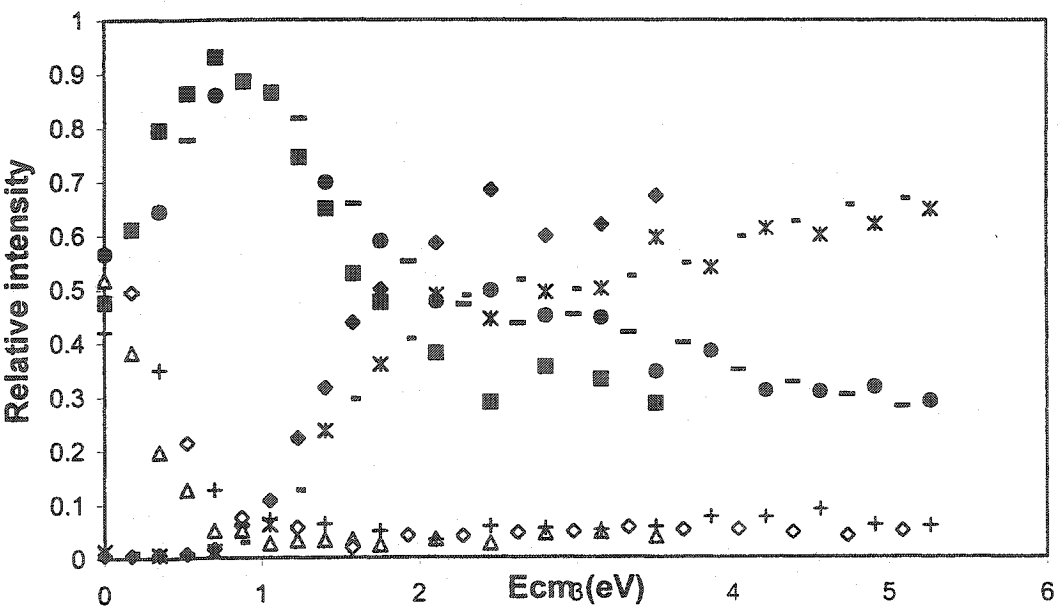

NO3-(HNO3)2; 2*10^-4 mBar

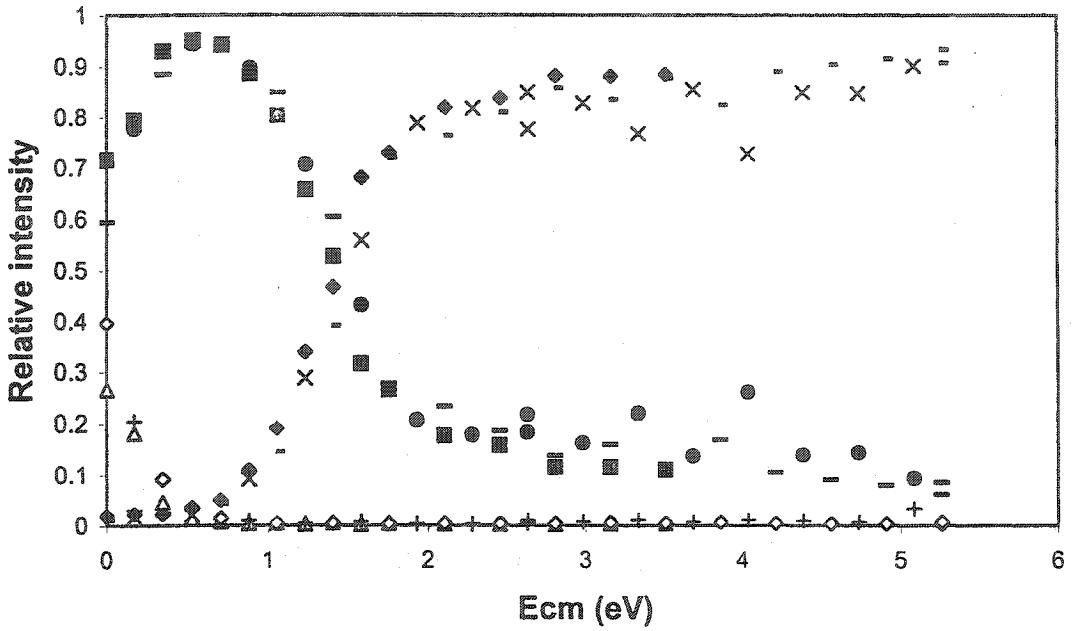

15NO3-(H15NO3)2; 2*10^-4 mBar

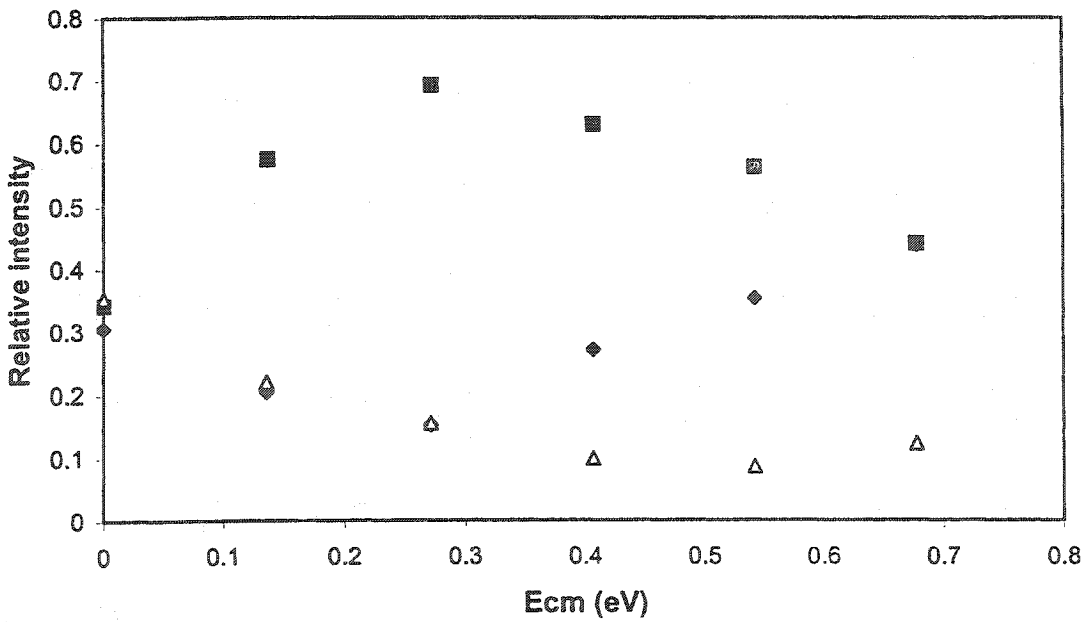

Claims to Original Research

1. The cross over point method involving electrospray-mass spectrometry was used to determine the binding energy of $HSO_4^-(H_2SO_4)_n$ and $NO_3^-(HNO_3)_n$ clusters. This represents the first time this approach has been employed for the determination of binding energies of gas phase ions.

2. Optimized geometries of $HSO_4^-(H_2SO_4)_n$ and $NO_3^-(HNO_3)_n$ were obtained using AM1, HF/3-21G, HF/6-31,+G(d), B3-LYP/6-31+G(d), and B3-LYP/6-311+G(d,p). The energies obtained were used to calculate binding energies of the clusters. These represent the best theoretical estimates of these values to date.